

8. SITE 910¹

Shipboard Scientific Party²

HOLE 910A

Date occupied: 17 August 1993
Date departed: 17 August 1993
Time on hole: 8 hr, 58 min
Position: 80°15.882'N, 6°35.405'E
Bottom felt (drill pipe measurement from rig floor, m): 567.4
Distance between rig floor and sea level (m): 11.02
Water depth (drill pipe measurement from sea level, m): 556.4
Total depth (from rig floor, m): 601.4
Penetration (m): 34.0
Number of cores (including cores with no recovery): 5
Total length of cored section (m): 34.0
Total core recovered (m): 24.26
Core recovery (%): 71
Oldest sediment cored:
Depth (mbsf): 34.0
Nature: silty clay
Earliest age: Quaternary

HOLE 910B

Date occupied: 17 August 1993
Date departed: 18 August 1993
Time on hole: 3 hr, 45 min
Position: 80°15.876'N, 6°35.451'E
Bottom felt (drill pipe measurement from rig floor, m): 568.0
Distance between rig floor and sea level (m): 11.02
Water depth (drill pipe measurement from sea level, m): 557.0
Total depth (from rig floor, m): 583.6
Penetration (m): 15.6
Number of cores (including cores with no recovery): 2
Total length of cored section (m): 15.6
Total core recovered (m): 15.37
Core recovery (%): 98
Oldest sediment cored:
Depth (mbsf): 15.6
Nature: silty clay
Earliest age: Quaternary

HOLE 910C

Date occupied: 18 August 1993
Date departed: 22 August 1993
Time on hole: 3 days, 21 hr, 23 min
Position: 80°15.896'N, 6°35.430'E
Bottom felt (drill pipe measurement from rig floor, m): 567.4
Distance between rig floor and sea level (m): 11.02
Water depth (drill pipe measurement from sea level, m): 556.4
Total depth (from rig floor, m): 1074.8
Penetration (m): 507.4
Number of cores (including cores with no recovery): 53
Total length of cored section (m): 507.4
Total core recovered (m): 293.49
Core recovery (%): 57
Oldest sediment cored:
Depth (mbsf): 507.4
Nature: silty clay
Earliest age: Pliocene

HOLE 910D

Date occupied: 28 August 1993
Date departed: 29 August 1993
Time on hole: 1 day, 4 hr, 15 min
Position: 80°15.881'N, 6°35.424'E
Bottom felt (drill pipe measurement from rig floor, m): 567.7
Distance between rig floor and sea level (m): 11.02
Water depth (drill pipe measurement from sea level, m): 556.7
Total depth (from rig floor, m): 728.3
Penetration (m): 160.6
Number of cores (including cores with no recovery): 18
Total length of cored section (m): 160.6
Total core recovered (m): 103.46
Core recovery (%): 64
Oldest sediment cored:
Depth (mbsf): 160.6
Nature: silty clay
Earliest age: Pliocene

¹Myhre, A.M., Thiede, J., Firth, J.V., et al., 1995. *Proc. ODP, Init. Repts.*, 151: College Station, TX (Ocean Drilling Program).

²Shipboard Scientific Party is as given in the list of participants preceding the Table of Contents.

Principal results: Site 910 (proposed Site YERM-4) is located in 556 m of water on the central inner Yermak Plateau. Its objectives were to study the Neogene evolution and glacial history of the Arctic, to investigate the his-

tory of influx of North Atlantic waters into the Arctic Ocean, and to form the shallow member of a bathymetric transect of depth gradients of sediment properties and accumulation. Owing to stiff and sticky surface sediments, attempts at advanced hydraulic piston coring (APC) and extended core barrel (XCB) coring did not result in satisfactory recovery, so we were forced to switch to the rotary core barrel (RCB) mode relatively early, with a marked improvement in the recovery below 150 mbsf.

The 507.4-m-thick sequence recovered at Site 910 consists of very firm, nearly homogeneous, silty clays and clayey silts, predominantly very dark gray. The sequence is highly consolidated in the surface layers. Sediment texture and mineral components exhibit variations of 20%–30% throughout the sequence, but few major trends. Dropstone frequency, however, reaches 1–3 dropstones per meter recovered in Cores 151-910C-1R to -22R (0–208.7 mbsf), whereas frequencies are less than 1 per meter in Cores 151-910C-23R to -53R (208.7–507.4 mbsf). The drilled sequence comprises a single silica-rich lithologic unit that is subdivided into three subunits, based on dropstone frequency and variations in siliciclastic abundance. Reworked siliceous microfossils, episodic occurrences of mollusc fragments, and wood fragments have been observed at a number of intervals. In general, carbonate values are low, varying between 1.5% and 6.0%. Organic carbon values are relatively high throughout (0.7%–1.4%). The recovered sequence suggests variations in the siliciclastic influx to the Yermak Plateau throughout the time interval documented in these cores, and an increase of ice-rafting at ~208.7 mbsf, possibly an indicator of the intensification of Northern Hemisphere glaciation.

The sediments are glacial-marine throughout and mostly devoid of siliceous microfossils, except for Cores 151-910C-17R through -20R, which contain reworked diatoms, silicoflagellates, and radiolarians. Silica in the interstitial waters is substantially lower than at other sites, which appears to reflect equilibrium with diagenetic opal phases.

The biostratigraphy of this site is based on calcareous nannofossils and planktonic foraminifers. The upper part of Hole 910C, down to 64.2 mbsf, contains Quaternary fossils, but the position of the Pliocene/Quaternary boundary is not clear because of the poor recovery in the upper part of the hole. The occurrences of small specimens of the calcareous nannofossil *Gephyrocapsa* and the foraminifer *Neogloboquadrina* dex. in Sample 151-910C-11R-CC indicate that the Pliocene/Quaternary boundary may be situated close to this horizon. Below 112.4 mbsf the nannofossil assemblages change abruptly and are dominated by Pliocene species. The unusually consistent occurrence of benthic foraminifers in the entire sequence provides a basis for ecologic and oceanographic interpretations of the bottom conditions. Benthic foraminifers indicate a Pacific Ocean influence below Core 151-910C-38R. Terrestrial plant material and palynomorphs are common throughout the section. Dinoflagellates are only represented by rare reworked Cretaceous taxa.

The shipboard paleomagnetic studies of Site 910 cores did not yield accurate temporal constraints for the stratigraphic section, although APC-coring in Holes 910A and 910B allowed us to locate the upper 25 mbsf of the sedimentary column in the Brunhes Chron. In Hole 910C, drilled with the RCB, poor recovery in the upper 150 mbsf prevented any useful interpretation of the magnetostratigraphy for that interval. When *JOIDES Resolution* was driven off location at Site 912 by encroaching ice, Hole 910D was drilled to enable further high-resolution shore-based research of physical properties to address the observed overconsolidation of these glacial Quaternary and Pliocene sediments. Recovery of the upper 150 m was markedly improved in this hole.

Methane contents were high throughout (10,000–100,000 ppm, based on headspace). Significant amounts of ethane and propane occurred below 300 mbsf. C_1/C_2 ratios show a consistent but “normal” decrease with increasing depth (i.e., temperature), reaching values of ~500 at 500 mbsf (at temperatures of ~50°C).

The outstanding geotechnical properties of this site, with its highly overconsolidated upper part of the penetrated sequence, resulted in our decision to devote a dedicated D-hole to an in-depth post-cruise study of the physical properties. The drilled sequence could be subdivided into two geotechnical units determined by the marked increase in shear strength

observed at 19 mbsf in Hole 910A and between 9 and 18 mbsf in Hole 910C. Sharp increases in sediment strength (from <100 kPa to >300 kPa) and wet-bulk density (from 1.7 to 2.2 g/cm³), and a sharp decrease in porosity (from 50% to 35%) between 0 and 20 mbsf indicate that the shallow sediments are overconsolidated. Below 150 mbsf, where core recovery is better, the sediments show more normal distributions of index properties and strength. The overconsolidation of shallow sediments of this site may result from ice-loading.

BACKGROUND AND OBJECTIVES

Physiography, Plate Tectonic, and Volcanic History of Yermak Plateau

The marginal Yermak Plateau is attached to the continental margin Northwest of the Svalbard archipelago. It extends from the shelf off Spitsbergen Island and into the Arctic Ocean almost to 83°N in water depths between 600 and 2000 m (see Fig. 7 of “Introduction” chapter, this volume). Most of the plateau is under waters permanently covered with ice; however, in good ice years the ice retreats to North of 81°N, and in late summer/early autumn the southern part of the Yermak Plateau can be accessible (see Figs. 12 and 13 of “Introduction” chapter, this volume). An extensive grid of seismic reflection and refraction data has been collected in this area through the years, but so far only shallow sediment cores have been obtained.

Physiographically the northern Svalbard Margin is divided into two different regions, the Yermak Margin including the Yermak Plateau to the Northwest and the Hinlopen Margin between the plateau and 20°E (see Frontispiece and Fig. 7 of “Introduction” chapter, this volume). The Yermak Margin is characterized by a narrow shelf with a wide slope having an irregular slope gradient. The Yermak Plateau is a prominent arcuate marginal plateau extending for almost 400 km in a North-northwestward direction from the continental shelf of Svalbard. The plateau defined by the 1000-m contour is elevated more than 2000 m with respect to the Arctic Basin to the North and East. The southern part of the plateau extends to approximately 82°N and is enclosed by the 700-m isobath with a series of shallow banks along the crest with water depths of about 500 m (Sundvor et al., 1978). To the Southwest the plateau dips gently toward the Spitsbergen Transform consisting of the Molloy and Spitsbergen fracture zones and the Molloy Ridge segment. The topography of the eastern part, however, is more blocky and rough, reflecting the outcrop of basement and major faulting down toward the East into the deep basin, together with canyons cutting into the eastern flank of the plateau. The northernmost part of the plateau strikes Northeast with minimum depths of 700 m and is parallel to the Gakkel spreading axis.

The morphological division of the plateau into two parts is also reflected in the magnetic field, which is subdued over the southern part; the northernmost part North of 82°N is characterized by high amplitude magnetic anomalies, 700–900 nT, parallel to the seafloor magnetic spreading anomalies in the Eurasia Basin (Fig. 1). Depth estimates to magnetic basement over the northern part by Kovacs and Vogt (1982) suggest magnetic source depths of less than 2 km.

A limited amount of heat flow measurements has been collected at the southwestern part of the plateau, giving high heat-flow values. Crane et al. (1982) interpreted this as the westernmost part of the Yermak Plateau, which was underlain by young oceanic crust not older than 13 Ma, considerably younger than the northeastern segment of the plateau. They implied that a thermal boundary exists between the warm western segment and the cold margin off the Nordaustlandet.

The northern margin of the Barents Sea and Svalbard archipelago developed in early Tertiary times, between late Paleocene and the earliest Eocene, when seafloor spreading started in the Eurasian Basin, and the Lomonosov Ridge microcontinent was rifted off from the northern Eurasian Margin. The oldest observed magnetic seafloor

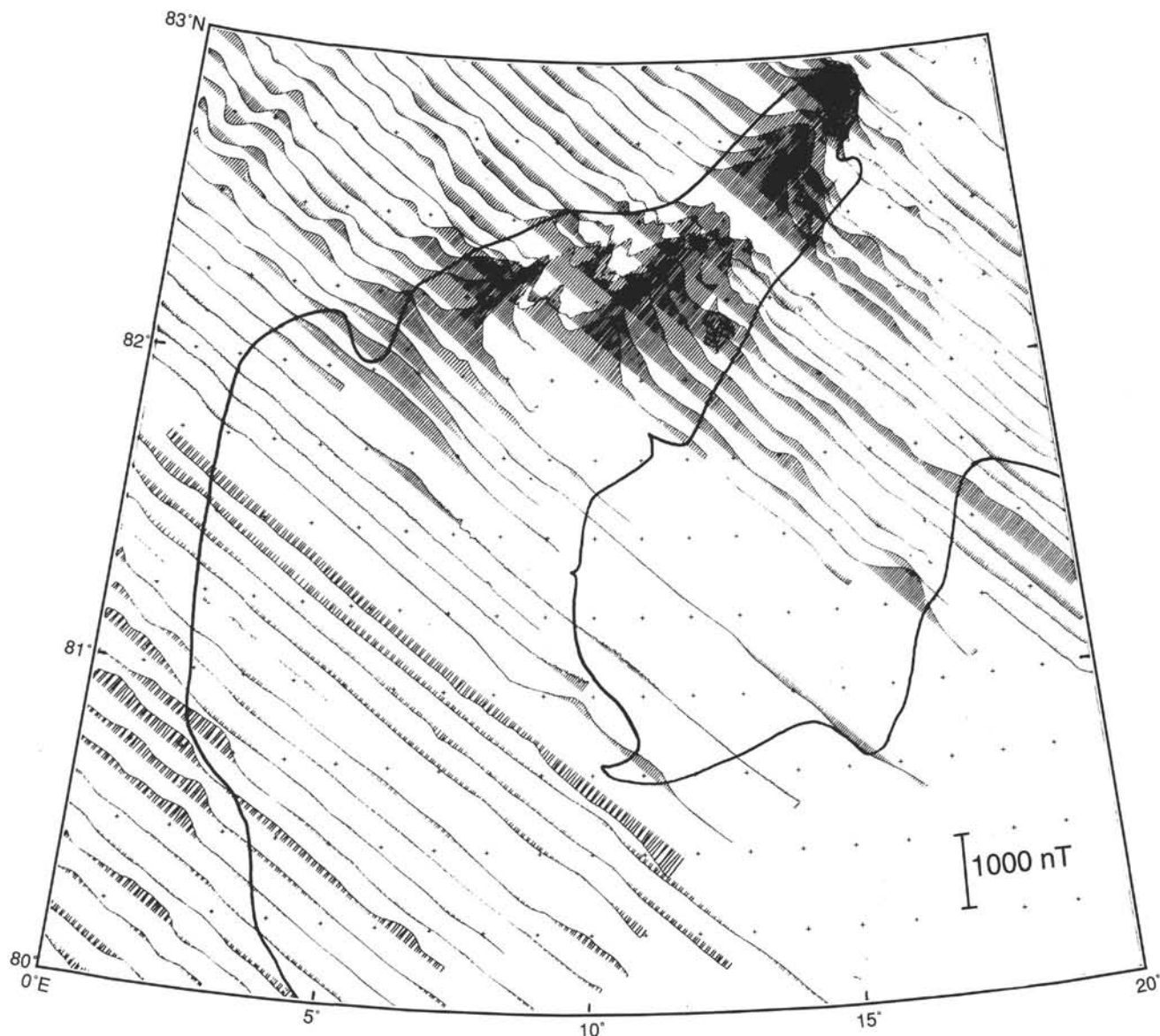


Figure 1. Aeromagnetic profiles across the Yermak Plateau. The 1500-m isobath is shown (Feden et al., 1979).

spreading anomaly in the Eurasia Basin is Anomaly 24; seafloor spreading started between 56 and 53 Ma.

Sundvor et al. (1982a) suggested that the magnetically quiet southern part of the Yermak Plateau is a downfaulted part of the northern Svalbard Margin and underlain by continental crust. Crane et al. (1982) suggest an oceanic origin for the western part. However, there is still no conclusive evidence with respect to the nature and origin of the crust underlying southern parts of the plateau. The northern, highly magnetically disturbed part has been suggested to be a volcanic feature created together with its counterpart, the Morris Jesup Rise, situated adjacent to the North Greenland Margin. A hot spot, probably active from Anomaly 18–13 time (middle Eocene to earliest Oligocene), has been suggested as the source for the excessive volcanism (Feden et al., 1979). The volcanic activity abated in early Oligocene time, and normal seafloor spreading commenced in the area, splitting a continuous volcanic structure then consisting both of the Morris Jesup Rise and Yermak Plateau.

The present-day plate boundary between the Knipovich Ridge in the Greenland Sea and the Gakkel Ridge in the Eurasian Basin is as-

sumed to be a complicated system of short spreading axis elements and transform faults (see Fig. 5 of "Introduction" chapter, this volume) (Perry et al., 1986; Eldholm et al., 1990; Thiede et al., 1990b). Although the present plate boundary is partly known, the evolution of the northernmost Greenland Sea and the earlier transformation of the plate boundary into the Arctic Ocean is not well documented. To understand the paleoceanographic evolution of the northern Atlantic-Arctic Gateway, both the evolution of the plate boundary and the evolution and subsidence of the volcanic Yermak Plateau and Morris Jesup Rise have to be unraveled. The timing of the subsidence of the Yermak and the Morris Jesup volcanic features, in addition to the oblique opening of the deep-water passage in the Fram Strait, has had a profound influence on the exchange of the shallow and deep-water masses of the Arctic Ocean.

Oceanography

Because of its specific morphologic and tectonic setting, the Yermak Plateau is particularly well suited to study the impact of the in-

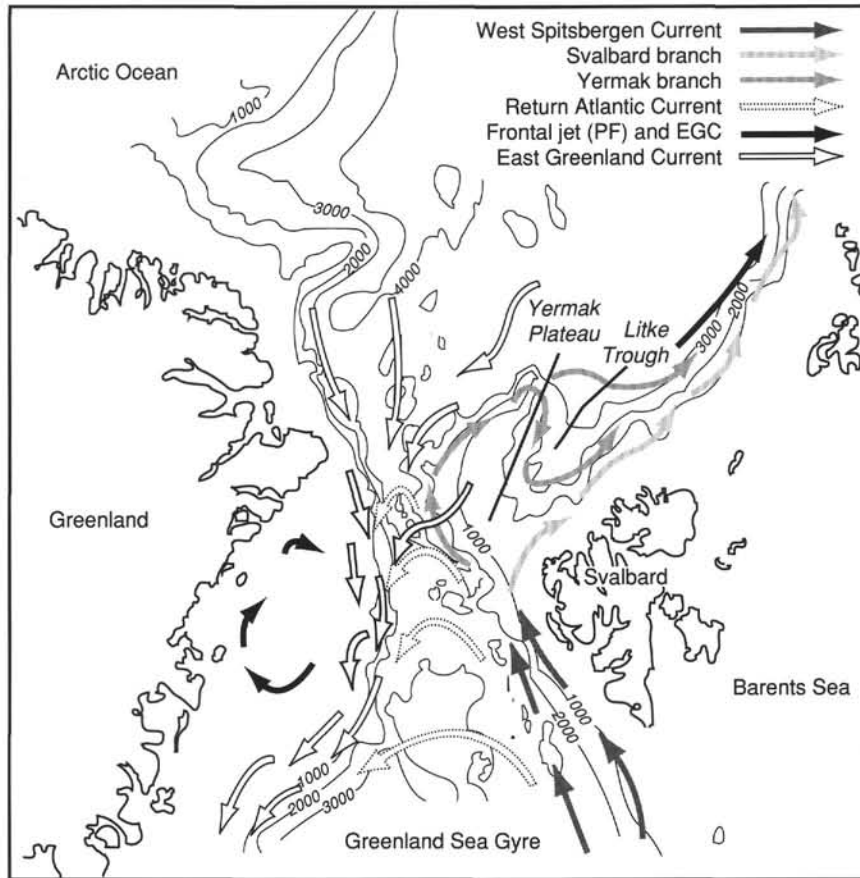


Figure 2. Upper-layer circulation patterns of the various currents in northern Greenland Sea, Yermak Plateau, and surrounding areas (Manley et al., 1992).

flux of Atlantic waters, the response of the modern system (oceanography, sea-ice cover, Barents Sea ice shield) to the glacial/interglacial fluctuations, the paleoceanographic transition of the temperate to the ice-covered Arctic Ocean, and the properties of the preglacial Paleogene Arctic.

The modern oceanography over the Yermak Plateau and its surroundings has been studied in considerable detail since the days of Nansen (1928), more recently through the efforts of MIZEX (Gascard et al., 1988; Johannessen, J.A. et al., 1987; Johannessen, O.M. et al., 1987; Quadfasel et al., 1987). The Fram Strait and its surroundings were recognized early as some of the most dynamically unstable parts of the gateways between the Arctic and North Atlantic oceans. The West Spitsbergen Current, as a continuation of the Norwegian Current, is transporting temperate Atlantic waters through Fram Strait to the edge of the Arctic sea-ice cover. In the northern Fram Strait, these waters are either recirculated into the East Greenland Current or they continue on their path into the Arctic under the sea-ice cover and a relatively thin layer of cold Arctic surface waters (see Fig. 14 of "Introduction" chapter, this volume).

Bourke et al. (1988) and Manley et al. (1992) described in detail how a branch of the Atlantic waters turns East immediately North of Svalbard (Svalbard Branch), and another branch continues along the outer Yermak Plateau (Yermak Branch) to return into the Litke Trough (Fig. 2). The marginal ice zone at the same time experiences extensive mesoscale (10–30 km in diameter) eddy formation. The East Greenland Polar Front (see Fig. 14 of "Introduction" chapter, this volume), which is marked by the sea surface outcrop of the 0°C isotherm and usually coincides with the ice edge (Manley et al., 1992), also follows the highly turbulent water mass boundary between the Arctic waters of the East Greenland Current and the rela-

tively warm West Spitsbergen Current with geostrophic velocities of 30–80 cm/s.

Whereas the modern oceanography can be taken as an interglacial scenario, reconstructions of the glacial situation of the sea-ice cover, as well as of the northern extension of the Barents Sea Ice Sheet, are much more difficult to find. Most of the presently available reconstructions are not supported by sufficient data from the Yermak Plateau. This applies to reconstructions of the time of transition from the preglacial to the glacial Arctic and of the temperate Paleogene Arctic Ocean to an even higher degree (Thiede and NAD Science Committee, 1992).

Scientific Objectives

Site 910 (proposed Site YERM-4) (see Figs. 7 and 17 of "Introduction" chapter, this volume) is located at the southwestern Yermak Plateau in 556 m of water on a thick, draping, sediment sequence blanketing the western flank of the plateau (Fig. 3). A strong seafloor multiple is masking the deeper part of the section. Sequences of continuous, strong amplitude are alternating with more transparent sequences with weak but mostly continuous reflectors. The site is the most shallow end member of a depth transect across the plateau. The transect was proposed to study the environmental response pre- and postdating the opening of the deep gateway into the Arctic Ocean, the timing of this event, the physical and chemical nature of the water masses associated with the gateway opening, and its influence on ocean circulation and climate, in the Neogene variations in Atlantic water influx to the Arctic Ocean. Furthermore, a transect in this area could provide a continuous high-quality upper Neogene and Quaternary record from the Arctic Ocean, making the identification of the

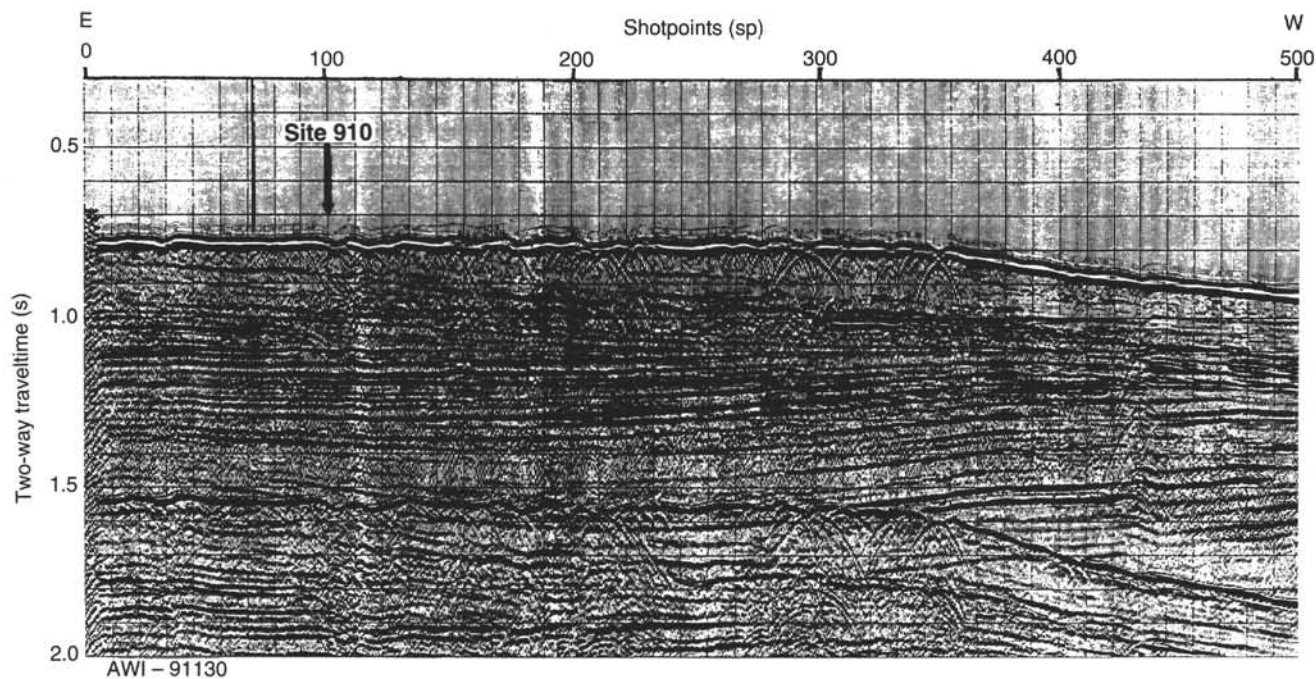


Figure 3. Seismic line AWI-91130, Site 910 at shotpoint 100.

onset of permanent ice cover in the Arctic Ocean possible. The site also would be part of the northernmost tie points in a North-South transect into the Norwegian-Greenland Sea.

OPERATIONS

Transit to Site 910 (YERM-4)

The 113-nmi transit required 10.1 hr at an average speed of 11.2 kt. The seismic survey at Site 910 started at 1248 hr, 17 August, and covered 18 nmi in 2.7 hr at 6.4 kt. A Datasonics 354B beacon (S/N 779, 14.5 kHz, 205 dB) was dropped at 1446 hr, the seismic gear was retrieved, and the ship returned to location. A backup Datasonics 354B beacon (S/N 770, 16.0 kHz, 205 dB) was dropped at 1620 hr.

Hole 910A

An advanced hydraulic piston corer/extended core barrel (APC/XCB) bottom-hole assembly (BHA) was run. The precision depth recorder (PDR) indicated a water depth of 567.4 mbrf, and the first core only recovered 0.30 m, which was declared to be a "water core" and donated to the paleontologists. Core 151-910A-1H determined the water depth to be 556.4 mbsl, and the location as 80°15.882'N, 6°35.405'E. Cores 151-910A-1H through -4H were taken from 0.0 to 24.5 mbsf (Table 1), with 24.5 m cored and 24.05 m recovered (98.2% recovery). APC-coring was terminated after Core 4H because it was the third core with a partial stroke and blown liner in the extremely stiff clays. Cores were not oriented because of the high latitude. The Adara temperature shoe was run on Core 4H. The formation was extremely stiff, compacted, gray, silty clay with occasional ice-rafted debris (IRD).

The XCB coring assembly was run, and Core 151-910A-5X was taken from 24.5 to 34 mbsf, with 9.5 m cored and 0.21 m recovered (2.2% recovery). The 9.5-m core required 47 min to cut, and the soft formation XCB shoe was jammed with baked clay.

Negligible concentrations of biogenic methane (5 ppm) were encountered in headspace gas analyses at this depth.

An erratic current was fluctuating East to West for short periods (20 min up to 2 hr) and increasing to 1.0 kt for short periods. Sudden current shifts were noted at 12-hr intervals and caused some excursions to nearly 3% of water depth. These currents could be seen as a surface disturbance at times. The air was noticeably colder near the ice, and dense fog, drizzle, rain, and heavy overcast skies were persistent as low-pressure centers passed East to West over the area. When a high-pressure cell predominated on 19 to 20 August, the wind dropped and the sea surface was calm.

Hole 910B

The ship was moved 20 m South, and Hole 910B was spudded at 0003 hr, 18 August, to provide high-resolution sampling. Core 151-910B-1H determined the water depth to be 557.0 mbsl. Cores 151-910B-1H through -2H were taken from 0.0 to 15.4 mbsf, with 15.4 m cored and 15.37 m recovered (99.8% recovery). APC-coring was terminated after Core 2H was a partial stroke. Cores were not oriented, and heat flow measurements were not taken. Coring parameters and formation remained the same as in Hole 910A. The bit cleared the rotary table at 0332 hr, 18 August, ending Hole 910B.

Hole 910C

The ship was moved 40 m North. A rotary core barrel (RCB) BHA was run with a mechanical bit release. The water depth was 556.4 mbsl. Hole 910C was spudded at 0847 hr, 18 August. Cores 151-910C-1R through -53R were taken from 0.0 to 507.4 mbsf, with 507.4 m cored and 293.5 m recovered (57.8% recovery). Coring was terminated because we reached the approved depth for drilling at this site. A heat flow measurement was taken with a downhole water sampler and temperature probe (WSTP) after Cores 7R and 10R. The air temperature grew noticeably colder, and it snowed on 19 August.

The coring results at this site are strikingly similar to results at Prydz Bay Sites 739 and 742 on Leg 119. The clays near the seafloor were so compacted that they were similar to what is normal clay compaction at a depth of more than 500 mbsf. One suggestion is that the

Table 1. Coring summary, Site 910.

Core	Date (Aug. 1993)	Time (UTC)	Depth (mbsf)	Length cored (m)	Length recovered (m)	Recovery (%)
151-910A-						
1H	17	1920	0.0–5.5	5.5	5.50	100.0
2H	17	1935	5.5–15.0	9.5	8.97	94.4
3H	17	2005	15.0–19.5	4.5	4.53	100.0
4H	17	2105	19.5–24.5	5.0	5.05	101.0
5X	17	2305	24.5–34.0	9.5	0.21	2.2
Coring totals				34.0	24.26	71.4
151-910B-						
1H	18	0005	0.0–6.9	6.9	6.90	100.0
2H	18	0040	6.9–15.6	8.7	8.47	97.4
Coring totals				15.6	15.37	98.5
151-910C-						
1R	18	0900	0.0–8.5	8.5	1.82	21.4
2R	18	0945	8.5–17.4	8.9	1.16	13.0
3R	18	1125	17.4–26.4	9.0	2.89	32.1
4R	18	1435	26.4–35.3	8.9	6.30	70.8
5R	18	1630	35.3–44.9	9.6	2.06	21.4
6R	18	1830	44.9–54.5	9.6	0.75	7.8
7R	18	1935	54.5–64.2	9.7	0.12	1.2
8R	18	2145	64.2–73.8	9.6	2.35	24.5
9R	18	2225	73.8–83.4	9.6	0.00	0.0
10R	18	2255	83.4–93.1	9.7	0.00	0.0
11R	19	0120	93.1–102.8	9.7	0.19	2.0
12R	19	0235	102.8–112.4	9.6	0.87	9.1
13R	19	0330	112.4–122.0	9.6	2.08	21.7
14R	19	0425	122.0–131.6	9.6	2.16	22.5
15R	19	0500	131.6–141.2	9.6	2.00	20.8
16R	19	0600	141.2–150.9	9.7	3.34	34.4
17R	19	0655	150.9–160.5	9.6	4.47	46.6
18R	19	0745	160.5–170.2	9.7	0.65	6.7
19R	19	0900	170.2–179.8	9.6	7.79	81.1
20R	19	0955	179.8–189.4	9.6	8.04	83.8
21R	19	1055	189.4–199.0	9.6	0.61	6.4
22R	19	1150	199.0–208.7	9.7	6.94	71.5
23R	19	1240	208.7–218.3	9.6	7.65	79.7
24R	19	1335	218.3–228.0	9.7	4.17	43.0
25R	19	1425	228.0–237.6	9.6	8.54	88.9
26R	19	1505	237.6–247.2	9.6	9.52	99.2
27R	19	1555	247.2–256.9	9.7	7.75	79.9
28R	19	1700	256.9–266.5	9.6	5.96	62.1
29R	19	1810	266.5–276.2	9.7	6.39	65.9
30R	19	1925	276.2–285.8	9.6	0.24	2.5
31R	19	2030	285.8–295.5	9.7	0.02	0.2

Core	Date (Aug. 1993)	Time (UTC)	Depth (mbsf)	Length cored (m)	Length recovered (m)	Recovery (%)
32R	19	2130	295.5–305.1	9.6	9.35	97.4
33R	19	2235	305.1–314.8	9.7	5.30	54.6
34R	19	2355	314.8–324.4	9.6	9.47	98.6
35R	20	0100	324.4–334.1	9.7	8.91	91.8
36R	20	0225	334.1–343.8	9.7	7.33	75.5
37R	20	0350	343.8–353.4	9.6	9.78	102.5
38R	20	0430	353.4–362.9	9.5	8.85	93.1
39R	20	0525	362.9–372.4	9.5	5.99	63.0
40R	20	0640	372.4–381.9	9.5	8.93	94.0
41R	20	0750	381.9–391.5	9.6	9.84	102.0
42R	20	0835	391.5–401.2	9.7	8.86	91.3
43R	20	0915	401.2–410.8	9.6	8.74	91.0
44R	20	1025	410.8–420.5	9.7	8.93	92.0
45R	20	1125	420.5–430.1	9.6	8.80	91.6
46R	20	1235	430.1–439.7	9.6	6.91	72.0
47R	20	1330	439.7–449.4	9.7	9.58	98.8
48R	20	1440	449.4–459.0	9.6	8.69	90.5
49R	20	1605	459.0–468.7	9.7	9.50	97.9
50R	20	1700	468.7–478.4	9.7	9.87	102.0
51R	20	1820	478.4–488.0	9.6	6.31	65.7
52R	20	1925	488.0–497.7	9.7	9.75	100.0
53R	20	2035	497.7–507.4	9.7	6.97	71.9
Coring totals				507.4	293.49	57.8
151-910D-						
1H	29	0130	0.0–5.8	5.8	5.79	99.8
2H	29	0145	5.8–14.4	8.6	8.58	99.8
3H	29	0215	14.4–18.6	4.2	4.18	99.5
4X	29	0535	18.6–27.3	8.7	3.22	37.0
5X	29	0820	27.3–36.3	9.0	0.80	8.9
6X	29	1005	36.3–45.3	9.0	2.01	22.3
7X	29	1145	45.3–54.9	9.6	1.10	11.4
8X	29	1400	54.9–64.5	9.6	1.71	17.8
9X	29	1520	64.5–74.1	9.6	3.46	36.0
10X	29	1610	74.1–83.7	9.6	4.82	50.2
11X	29	1700	83.7–93.4	9.7	9.50	97.9
12X	29	1815	93.4–103.0	9.6	8.64	90.0
13X	29	1920	103.0–112.6	9.6	9.77	102.0
14X	29	2025	112.6–122.3	9.7	8.52	87.8
15X	29	2110	122.3–131.9	9.6	7.47	77.8
16X	29	2200	131.9–141.5	9.6	7.72	80.4
17X	29	2315	141.5–151.1	9.6	9.05	94.3
18X	30	0040	151.1–160.6	9.5	7.12	74.9
Coring totals				160.6	103.46	64.4

clays were compacted by ice loading during glacial periods. No better explanation has been found.

Capillary suction tests on clays at 122, 151, and 257 mbsf indicated that the clays were drastically affected by contact with fresh water, but had no noticeable reaction to a mixture of 50% fresh and 50% seawater, 1% or 2% KCl. Therefore, chemical inhibition of the clays during logging did not appear to be feasible.

First Ice

At 0050 hr, 20 August, an ice pack was spotted moving toward the Southwest, and the *JOIDES Resolution*, at up to 0.7 kt. The *Fennica* was recalled from YERM-1, with an estimated transit time of 12 hr back to the drill ship. The ice advanced on a 120-degree-wide front and was up to 5 m thick. A free fall funnel was prepared as a precaution. The ice had advanced to within 3.8 nmi by 0630 hr, but appeared to stall in a dead calm sea. The ship's X-band (3 cm) radar was able to detect thick bergy bits at 6-nmi range. The *Fennica* returned to the *Resolution* at 1200 hr and determined that the ice flow was a tongue of bergy bits (3-m-high old ice). The NDR TV crew came aboard the *Resolution* to start filming, and the *Fennica* took up ice patrol around the drill ship.

Return to Site 910

Drilling operations were halted at Site 912 because of ice floes that came over the site. Therefore, we decided to return to Site 910 to drill a special hole dedicated to geotechnical studies of the overcon-

solidated sequence that was discovered in Holes 910A, 910B, and 910C. The 23-nmi transit from Site 912 to Site 910 required 1.9 hr for an average speed of 12.1 kt. No seismic survey was conducted. A Datasonics 354B beacon was dropped at 2310 hr, 28 August, on the original Site 910 GPS position. Two ice fields were 3.65 nmi Northwest and 4 nmi North of the location, moving Northwest at 0.2 kt. Visibility was less than 1/2 nmi.

Hole 910D

An APC/XCB BHA was run. Core 151-910D-1H established the water depth as 556.7 mbsf. Cores 151-910D-1H through -3H were taken from 0.0 to 18.6 mbsf, with 18.6 m cored and 18.55 m recovered (99.7% recovery). No cores were oriented because of the high latitude, and a good temperature gradient was obtained in the A and B holes. The formation was extremely stiff, compacted, gray, silty clay with occasional IRD. The last two APC cores were partial strokes with advance by recovery; therefore, the XCB system was used next.

The XCB coring assembly was run, and Cores 151-910D-4X through -18X were taken from 18.6 to 160.6 mbsf, with 142.0 m cored and 84.91 m recovered (59.8% recovery).

Transit to YERM-1D

At 1730 hr, 29 August, the *Fennica* was sent to YERM-1 to survey the ice edge and reported that YERM-1 and -1C were in the hard pack ice again, but that newly proposed location YERM-1D (10 nmi

South of YERM-1) was in open water. The ODP safety panel had approved YERM-1D, but the NPD advised they would send their decision by telex to ODP on 30 August. Because YERM-2A also was covered by ice tongues (which were not discernible on even the SAR images), a decision was made to time the departure for YERM-1D so that we could start coring as soon as NPD approval was received.

The 34-nmi transit to YERM-1D required 3.3 hr for an average speed of 10.3 kt. The *Resolution* passed through several ice tongues on the way, and four seals were seen. A 21-nmi seismic survey was conducted in 3.3 hr at 6.4 kt. A Benthos 210 beacon was dropped at 0935 hr, 30 August, on the GPS position. YERM-1D was 6–7 nmi from the ice edge, with small brash ice rafts in the area.

YERM-1D

An RCB BHA was run to 880 mbrf, and we waited on approval for 2 hr. We were advised at 1530 hr, 30 August, that the NPD had refused permission to core at new proposed Site YERM-1D because “it lies within an area of possible closure within the sedimentary sequence, where the seismic events also exhibit a distinct brightening.” The drill string was pulled, and preparations were made to go back to Site 912 (or Site 909 as an alternate).

Transit to Site 912

The 61-nmi transit to Site 912 required 5.9 hr for an average speed of 10.3 kt. Two ice tongues were crossed on the way. The *Fennica* crossed through the ice tongues 15 nmi ahead of the *Resolution*, but the ice closed in before the *Resolution* arrived, forcing it to find a lead in the ice. *Fennica* reported that Site 912 was completely covered by heavy pack ice; therefore, a decision was made to go to Site 909 to core the deep RCB hole and allow the ice pack to reassemble.

LITHOSTRATIGRAPHY

Introduction

Sediments recovered at Site 910 (Holes 910A, 910B, and 910C) are predominantly very dark gray, very firm, nearly homogeneous silty clays and clayey silts. Lithostratigraphy is largely based on Hole 910C (0–507.4 mbsf) because Holes 910A and 910B reached 34.0 mbsf and 15.6 mbsf, respectively. The sequence exhibits only subtle variations in sediment texture and mineral abundances. Sediment texture (Fig. 4) and particle abundances (Fig. 5) exhibit variations of ~20%–30% throughout the sequence, but few major trends. Somewhat coarser intervals with >10% sand occur as minor lithologies throughout the sequence (Fig. 4), defined as silty muds and clayey muds. These layers are visually very similar in color and texture to the major lithologies, but are distinguished by a more brownish, very dark gray color and a slightly coarser texture on the split core surface (Fig. 6), as well as by smear slide analysis.

The sequence recovered at Site 910 comprises a single unit, based on the relative uniformity in sediment type, texture, and mineralogy (Table 2). However, changes in dropstone (>1 cm) abundance (Fig. 7) and in mineral abundances (Fig. 5) support the definition of three subunits. Normalizing dropstone abundance to core recovery allows useful comparison between the upper and lower parts of the sequence (see Fig. 7 and caption). Dropstone abundance forms the basis for delineating the boundary between lithologic Subunits IA and IB. The sharply defined boundary between Subunits IB and IC is based on an abrupt transition in siliciclastic mineral abundances (Fig. 5), which average ~20% in Subunit IB and ~30% in Subunit IC. Dropstones are dominantly sand- and siltstones (Fig. 8; Table 3), although igneous and metamorphic rocks also are observed.

Smear-slide data reveal only trace abundances of calcareous and biosiliceous microfossils, scattered throughout the sequence. Biosili-

ceous and calcareous microfossils reach maximum abundances of ~5% to 10%, respectively, in Cores 151-910C-16R through -22R (140.2–208.7 mbsf), but the majority may be reworked in this interval (see “Biostratigraphy” section, this chapter). Inorganic calcite particles are common at this site, exhibiting a background abundance of ~5%, upon which are superimposed distinctly high peaks reaching ~60% inorganic calcite (Fig. 9). Similar inorganic calcite-rich layers have been observed at Leg 151 Sites 908 and 909 (see “Lithostratigraphy” sections, “Site 908” and “Site 909” chapters, this volume). Variations in inorganic calcite abundance seen in smear slides are confirmed by percent carbonate data (see “Organic Geochemistry” section, this chapter).

Sediments are nearly homogeneous throughout the sequence and exhibit few sedimentary structures. Small pyritized burrows are fairly common (Fig. 10), but larger sediment-filled burrows are rare (Fig. 11). Other lithostratigraphic features of interest include episodic occurrences of mollusc shell fragments in Cores 151-910C-16R through -53R (141.2–507.4 mbsf; Figs. 12 and 13), and wood fragments in Core 151-910C-26R, CC (~247 mbsf).

Subunit IA:

Cores 151-910C-1R through -22R (0–208.7 mbsf)
Thickness: 208.7 m
Age: Pliocene to Quaternary

The upper subunit is composed of silty clays and clayey silts with ~20%–30% siliciclastic components, characteristics that typify the entirety of Unit I. The subunit is distinguished by high dropstone abundance (Fig. 7), which reaches 10–30 dropstones per core in Cores 151-910C-1R through -22R (0–208.7 mbsf), whereas abundances are less than 10 per core in Cores 151-910C-23R through -53R (208.7–507.4 mbsf). The lower boundary of this unit is well defined because of fairly good core recovery over the transitional interval from Cores 151-910C-19R through -27R. Because dropstone abundance is averaged over the length of a single core, the boundary between Subunits IA and IB occurs at a core break. No discernible differences exist in textural or particle composition between these subunits.

Sediments are marked by distinct color banding in the top 17 m of the sequence (best recorded in Hole 910A). Colors grade from brownish gray and dark olive gray to very dark gray on a 1–10 cm scale. As the sediments become more uniformly dark gray below 17 m, they also become distinctly firmer. Downhole sediments become “very firm” in Core 151-910A-4H (see also “Physical Properties” section, this chapter). This apparent increase in compaction is not clearly reflected in textural or mineralogical variations. However, it may partially account for poor recovery in Core 151-910A-5X, no recovery in Core 151-910B-3H, and poor recovery in the upper cores of Hole 910C.

Subunit IB:

Cores 151-910C-23R through -41R (208.7–391.5 mbsf)
Thickness: 182.8 m
Age: Pliocene

The middle subunit is composed of silty clays and clayey silts, with siliciclastic components that grade from ~10%–20% in the lower portion of the subunit (314.8–391.5 mbsf) to ~20%–30% in the upper portion (208.7–314.8 mbsf). The subunit is marked by low dropstone abundances throughout the sequence.

The lower boundary of this unit is based on a subtle difference of ~10% in average siliciclastic mineral abundance (quartz, feldspar, and accessory minerals) between sediments above and below Section 151-910C-41R-CC (391.5 mbsf). The boundary itself, however, is sharp, as it is based on an abrupt transition in siliciclastic mineral

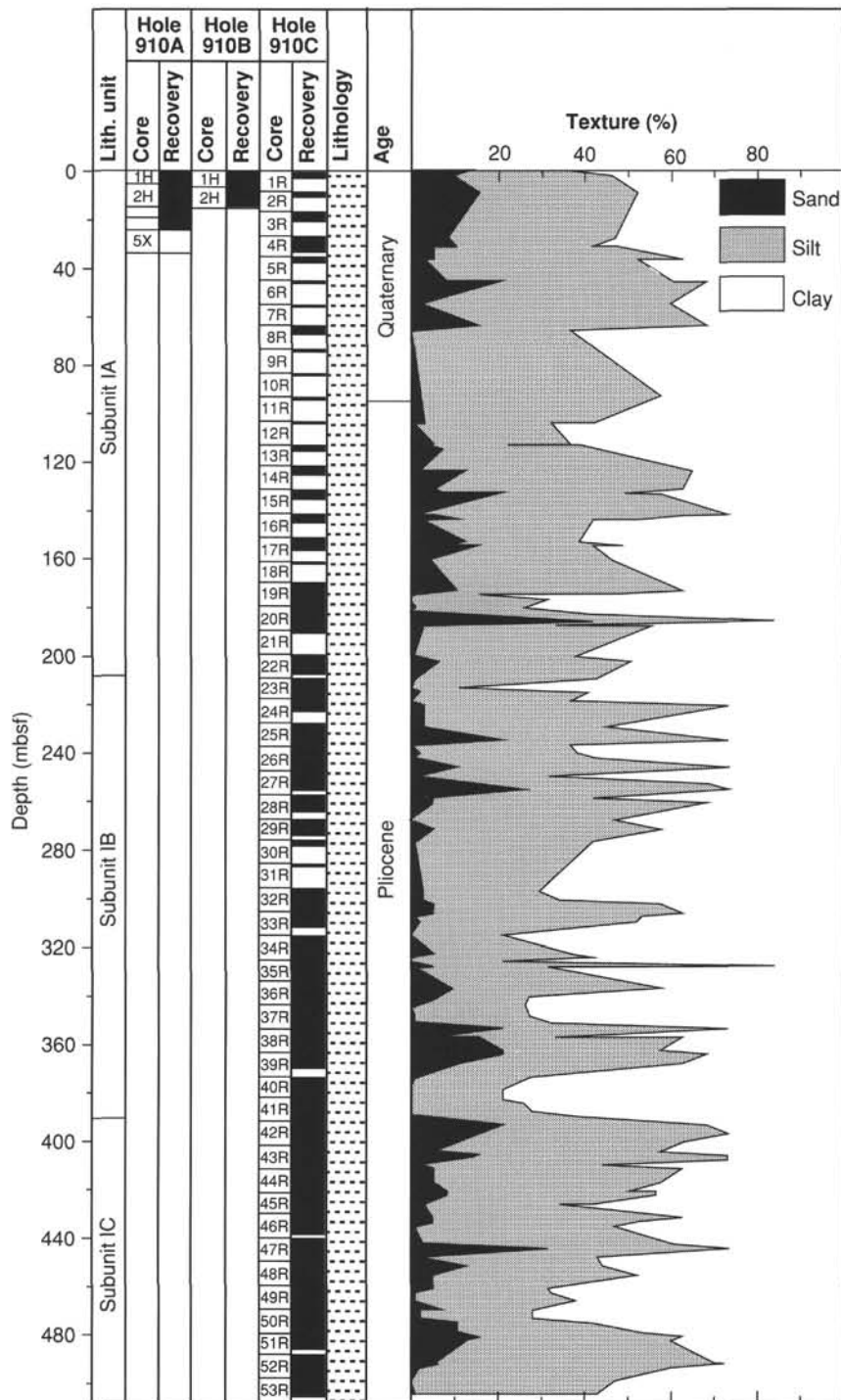


Figure 4. Core recovery, lithologic subunits, generalized lithology, and sediment texture (sand-, silt- and clay-sized) vs. depth for Holes 910A, 910B, and 910C. Note variations in texture throughout sequence, but lack of major trends.

abundances (Fig. 5). Distinctive changes in GRAPE bulk density and magnetic susceptibility values (see “Physical Properties” section, this chapter) and in sediment silica percentages (see “Inorganic Geochemistry” section, this chapter) at ~390–400 mbsf support the establishment of a subunit boundary at 391.5 mbsf.

Subunit IC:

Cores 151-910C-42R through -53R (391.5–507.4 mbsf)
 Thickness: 115.9 m
 Age: Pliocene

The lower subunit is composed of silty clays and clayey silts, with siliciclastic components that average ~20%–30%. This interval of relatively high siliciclastic mineral abundances could merely represent a continuation of siliciclastic variability seen in Subunit IB. Termination of drilling at 507.4 mbsf makes it difficult to evaluate the extent of this subunit. Dropstones are observed throughout this unit, although in low abundance. This unit contains the highest abundances of mollusc shell fragments (Fig. 13) and the greatest variability in silica percentages (see “Inorganic Geochemistry” section, this chapter) observed in the sequence.

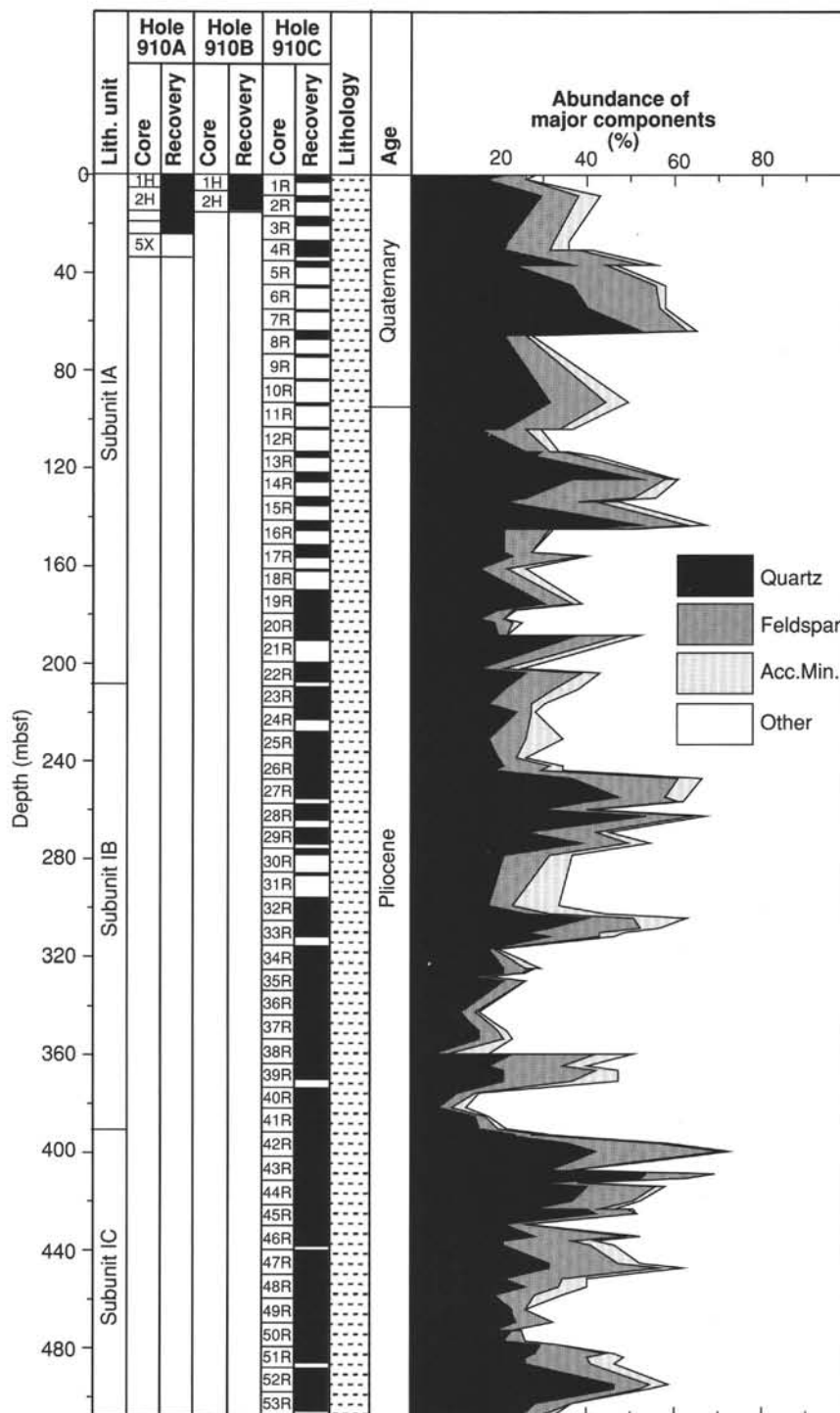


Figure 5. Core recovery, lithologic subunits, generalized lithology, and major particle composition (in the >4-μm fraction, expressed as percentage of bulk sediment) vs. depth for Holes 910A, 910B, and 910C. Note variations in mineral composition throughout sequence, and an abrupt decrease in quartz, feldspar, and accessory mineral abundance upsection at 391.5 mbsf from ~30% to ~20%. This difference is the basis for distinguishing subunits IB and IC. "Other" components include dominantly clay-sized material, plus minor amounts of mica, biogenic material, and opaque minerals.

Interpretation

The recovered sequence suggests variations in sediment deposition on the Yermak Plateau throughout the Pliocene to Quaternary, but few major changes in sediment type or composition. The silty clays that dominate the sediment in Subunits IC through IA are inter-

preted as terrigenous deposits with a small hemipelagic component. These predominantly clay- to silt-sized sediments, with relatively moderate siliciclastic abundances (~10%–30%), probably represent distal ice-rafted material. Sediments are generally finer-grained than correlative deposits closer to the surrounding ice sheets. The variations observed in sediment texture and siliciclastic abundance may

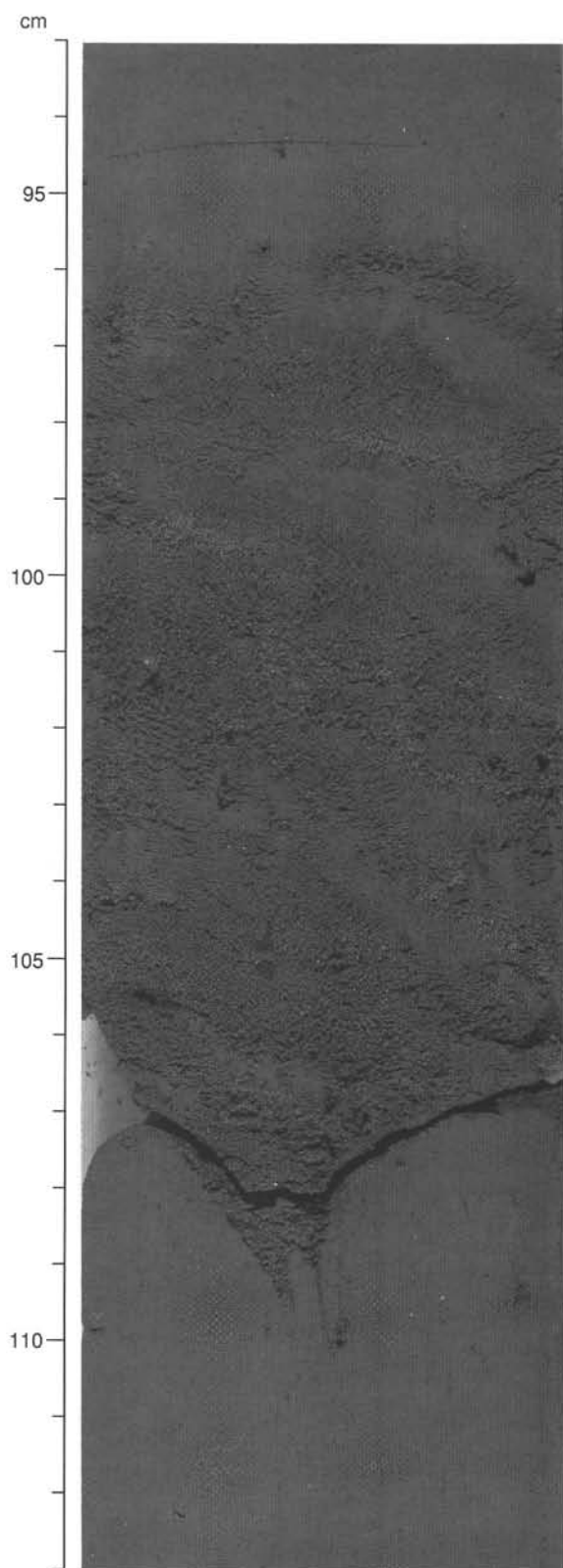


Figure 6. Close-up photograph showing a series of coarser layers within the fine-grained lithologies of Subunit IA (Interval 151-910A-4H-2, 93–113 cm).

reflect long-term cycles in the influx of ice-rafted material to the Yermak Plateau. Possible controlling factors include climatic variability, sedimentation rate changes, and source areas.

Interpretation of subtle differences in lithologic features and measured parameters that distinguish Subunits IC and IB is not straightforward. The high GRAPE bulk density and magnetic susceptibility values relative to Subunit IB might suggest greater clay contents. However, the smear slide textural data indicate that Subunit IC has lesser clay abundances relative to Subunit IB. One possible solution of this discrepancy is that the composition of clay-sized material may have changed significantly at this subunit boundary. Similarly, there is no sufficient explanation for the great variability in silica percentages observed in Subunits IC and IB relative to Subunit IA (see “Inorganic Geochemistry” section, this chapter), as it does not correspond with any discernible change in textural or mineralogical components.

On the other hand, the transition from Subunit IB to IA at ~208.7 mbsf is more easily interpreted. Based on a distinct increase in the number of dropstones, this transition is inferred to reflect increased ice-rafting of coarse material in the Pliocene. However, age control at this site is too premature (see “Paleomagnetism” section, this chapter) to compare the timing of this increase to expansion of Northern Hemisphere glaciation ~4.2–2.5 Ma (Shackleton et al., 1984; Krissek, 1989; Wolf and Thiede, 1991).

The remarkable decrease in compaction above ~17–19.5 mbsf deserves comment in the context of the regional glacial development. This sharp change in sediment firmness must have resulted from the termination of post-depositional processes that “overconsolidated” sediment below ~17–19.5 mbsf and/or from the removal of overburden at this depth. One possible mechanism involves the termination of episodic grounding of large marine-based ice sheets, which may have “overconsolidated” much of the sequence in the late Pliocene to late Quaternary (see also “Physical Properties” section, this chapter). Alternatively, increased erosion during the Quaternary may have reduced overburden and, therefore, compaction of the upper ~17 m of sediment. We note variations in the level of sediment compaction throughout the section, including distinctly firm sediments from Core 151-910C-4R through -16R and from Core 151-910C-33R through -43R. Sediment compaction also shows a generally positive relation to dropstone abundance. This relationship suggests a Pliocene to Quaternary history of glacial influence on sediment compaction through processes that may include direct episodic “overconsolidation” as well as erosional cycles.

Comparison of deeper sites on the Yermak Plateau should provide insights to this and other problems that relate to depth-dependent processes. At 556 m water depth, Site 910 is the shallow water end-member in a depth transect. Correlation of other sites in this transect will allow comparison of many processes that are related to deep-ocean circulation and climate interaction between the Arctic Ocean and North Atlantic Ocean basins, particularly during the Pliocene to Quaternary.

BIOSTRATIGRAPHY

Introduction

Site 910 was selected to provide the shallow member of the bathymetric transect with high stratigraphic resolution across the Yermak Plateau. At Site 910, 507.4 m of Pliocene and Quaternary glacial-marine sediments was drilled. These sediments are mostly devoid of siliceous microfossils but contain a relatively good record of calcareous benthic and planktonic microfossils (Fig. 14). Parts of the sequence contain microfossils reworked from older strata, probably by ice-rafting. Reworked lower Miocene and older diatoms and radiolarians are

Table 2. Summary of lithologic units, Site 910.

Subunit	Dominant lithologies	Interval, mbsf (thickness, m)	Age	Occurrence (hole-core-section)
IA	Nearly homogeneous silty clays and clayey muds, with dropstone abundances reaching 10–30 per core	0–208.7 (208.7)	Pliocene to Quaternary	910A-1H-1 to 910A-5X-CC 910B-1H-1 to 910B-2H-CC 910C-1R-1 to 910C-22R-CC
IB	Nearly homogeneous silty clays and clayey muds, with dropstone abundances <10 per core; ~10%–20% siliciclastic abundance	208.7–391.5 (182.8)	Pliocene	910C-23R-1 to 910C-41R-CC
IC	Nearly homogeneous silty clays and clayey muds, with dropstone abundances <10 per core; ~20%–30% siliciclastic abundance	391.5–507.4 (115.9)	Pliocene	910C-42R-1 to 910C-53R-CC

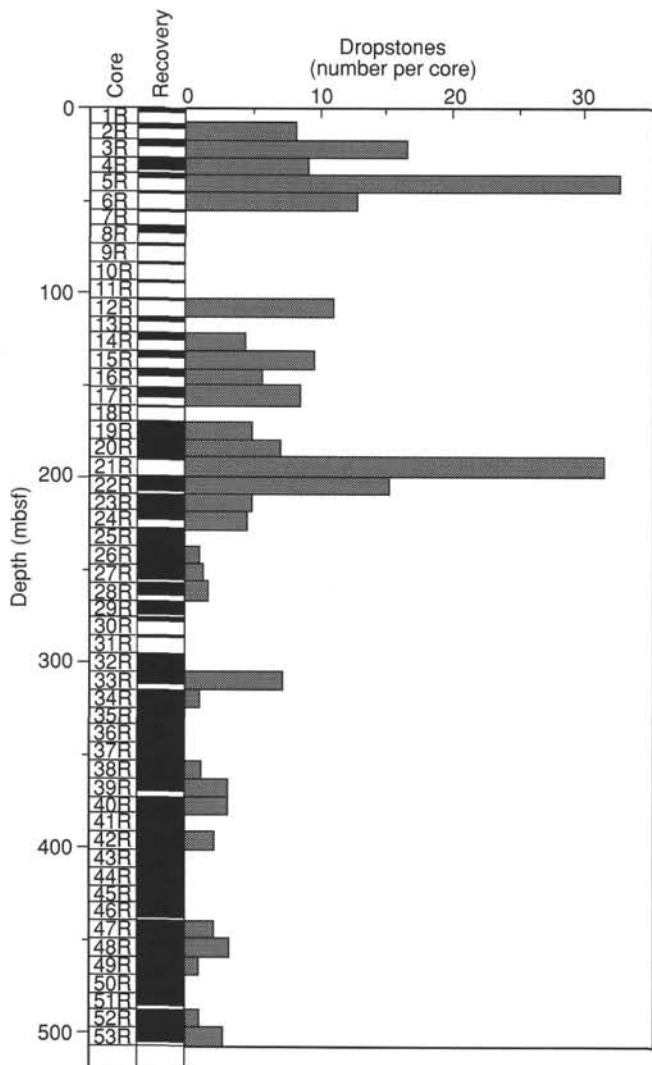


Figure 7. Core recovery and dropstones (>1 cm in diameter per core), normalized to recovery, vs. depth (mbsf) for Hole 910C. Normalization consisted of dividing the number of dropstones per core by the recovery fraction (e.g., in a given core, 5 dropstones/0.5 recovery = 10 dropstones per core). Increase upsection in dropstone abundances from <10 per core to 10–30 per core is the basis for distinguishing Subunits IA and IB.

present in Cores 151-910C-17R through -20R. Ice-rafted *Inoceramus* prisms (Cretaceous) occur in Samples 151-910C-3R-CC, -6R-CC, and -7R-CC in Quaternary sediments, as well as in Samples 151-910C-17R-CC through -19R-CC of the upper Pliocene.

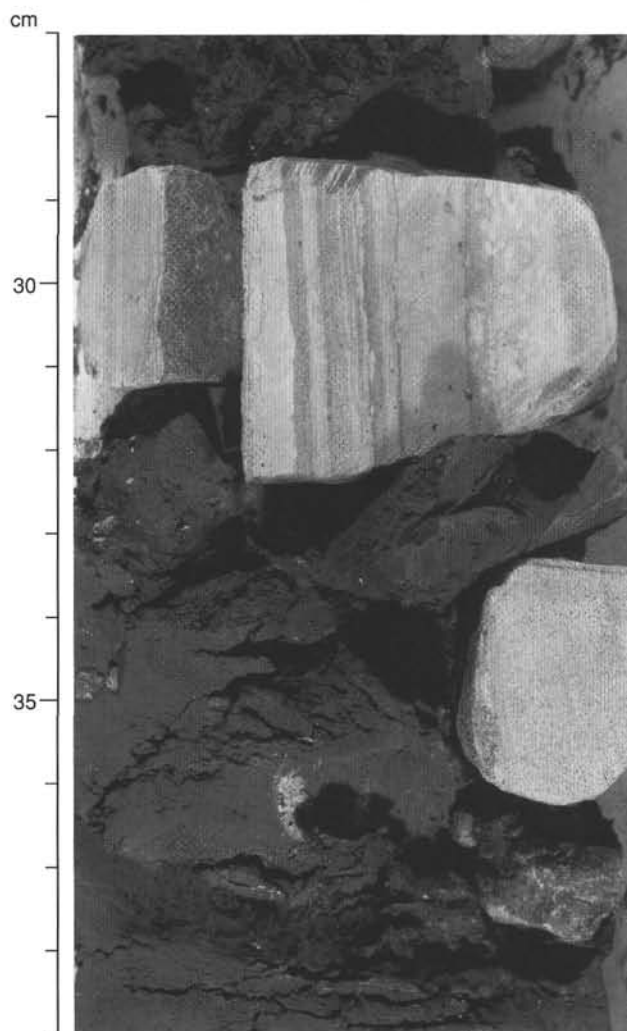


Figure 8. Close-up photograph showing a set of dropstones from Subunit IA, a coarse-grained sandstone, a laminated siltstone, and a large laminated dolostone (Interval 151-910C-5R-2, 27–39 cm).

Diatoms

Core-catcher samples from Holes 910A–C are barren of diatoms, with the exception of Cores 151-910C-17R through -20R. Core-catcher and shipboard samples from these cores contain rare and poorly preserved lower Miocene and older diatoms and non-age-diagnostic, heavily silicified species. No Pliocene or Quaternary diatoms are present.

Table 3. Occurrences of dropstones at Site 910.

Core, section, interval top (cm)	Depth (mbsf)	Size (cm)	Dropstone type	Core, section, interval top (cm)	Depth (mbsf)	Size (cm)	Dropstone type
151-910A-				15R-1, 40	132.00	3.0	Siltstone
1H-2, 1	1.51	1.0	Quartz sandstone	16R-1, 30	141.50	1.8	Sandstone
1H-3, 48	3.48	1.0	Sandstone	16R-2, 101	143.71	6.0	Calcite-cemented siltstone
1H-4, 20	4.70	1.0	Sandstone	17R-1, 40	151.30	2.1	Gray granite
1H-4, 45	4.95	1.5	Shale	17R-1, 116	152.06	5.2	Layered sandstone
1H-CC, 4	5.30	1.5	Shale	17R-2, 21	152.61	1.9	Black limestone
1H-CC, 12	5.38	1.5	Siltstone	17R-2, 41	152.81	1.2	Black slate
2H-3, 69	9.19	1.0	Gray siltstone with pyrite	19R-1, 3	170.23	1.0	Mudstone
2H-4, 37	10.37	1.2	Rock fragment	19R-1, 52	170.72	1.0	Mudstone
2H-4, 60	10.60	2.5	Sandstone	19R-3, 123	174.43	1.0	Conglomeratic limestone
3H-CC, 25	19.26	2.3	Sandstone	19R-4, 27	174.97	1.5	Shale
4H-1, 39	19.89	1.0	Siltstone (?)	20R-2, 33	181.63	1.5	Metamorphic rock
4H-1, 143	20.93	1.9	Siltstone	20R-2, 49	181.79	1.0	Carbonate
4H-1, 149	20.99	1.0	Sandstone	20R-3, 33	183.13	1.0	Pyrite
4H-2, 11	21.11	1.8	Anthracite	20R-3, 64	183.44	1.0	Dark gray siltstone
4H-2, 54	21.54	1.0	Basalt	20R-5, 44	186.24	2.3	Black quartzite
4H-2, 65	21.65	1.0	Coal	20R-5, 95	186.75	1.0	Black mudstone
4H-3, 67	23.17	3.0	Sandstone	21R-1, 20	189.60	1.0	Siltstone
				21R-1, 26	189.66	4.0	Siltstone
151-910B-				22R-1, 51	199.51	1.5	Dark gray siltstone
1H-1, 65	0.65	1.0	Sandstone	22R-1, 89	199.89	1.0	Siltstone (?)
1H-1, 80	0.80	3.0	Sandstone	22R-1, 117	200.17	1.0	Shale
1H-1, 87	0.87	1.5	Sandstone	22R-2, 98	201.48	1.5	Gray siltstone
1H-1, 144		1.5	Quartz	22R-2, 104	201.54	1.5	Black shale
1H-2, 17	1.67	3.0	Schist	22R-3, 2	202.02	1.5	Siltstone (?)
1H-4, 5	4.55	1.0	Sandstone	22R-3, 136	203.36	2.0	Siltstone
1H-4, 32	4.82	1.0	Sandstone	22R-4, 82	204.32	2.5	Siltstone (?)
1H-4, 63	5.13	1.0	Coal	22R-4, 87	204.37	1.0	Siltstone
2H-1, 50	7.40	1.0	Friable sandstone	22R-4, 110	204.60	2.5	Siltstone
2H-1, 62	7.52	1.4	Schist	22R-CC, 8	205.89	4.0	Siltstone
2H-1, 75	7.65	2.2	Greenschist	23R-1, 50	209.20	2.0	Metamorphic rock
2H-1, 131	8.21	2.6	Gneiss	23R-3, 64	212.34	5.5	Siltstone
2H-2, 110	9.50	1.1	Sandstone	23R-4, 149	214.69	1.0	Mudstone
2H-3, 55	10.45	3.1	Limestone	23R-5, 2	214.72	5.0	Sandstone
2H-4, 87	12.27	1.0	Schist	24R-3, 44	221.74	4.0	Gray limestone
2H-5, 2	12.92	1.1	Schist	24R-3, 94	222.24	5.8	Gray quartzite
				26R-6, 25	245.35	1.5	Sandstone
151-910C-				27R-1, 42	247.62	1.5	Quartz
2R-1, 40	8.90	1.0	Siltstone	28R-2, 103	259.43	4.0	Sandstone?
3R-1, 10	17.50	6.0	Siltstone	33R-1, 140	306.50	3.2	Sulfide-bearing propylite
3R-1, 13	17.53	3.0	Siltstone	33R-2, 4	306.64	4.1	Siltstone
3R-1, 46	17.86	2.5	Siltstone (?)	33R-2, 8	306.68	1.2	Mudstone
3R-1, 100	18.40	2.5	Siltstone	33R-2, 53	307.13	1.5	Quartz
3R-2, 67	19.57	3.0	Siltstone (?)	34R-6, 72	323.02	4.1	Siltstone
4R-1, 3	26.43	1.0	Sandstone	36R-5, 47	340.57	3.5	Siltstone
4R-1, 106	27.46	4.0	Conglomeratic limestone	38R-4, 74	358.64	2.6	Mudstone
4R-2, 54	28.44	2.0	Sandstone	39R-4, 120	368.60	1.5	Siltstone
4R-3, 58	29.98	3.0	Sandstone	39R-4, 134	368.74	2.5	Igneous rock?
4R-3, 59	29.99	1.0	Sandstone	40R-1, 69	373.09	3.0	Siltstone
4R-4, 52	31.42	2.5	Limestone	40R-1, 110	373.50	1.0	Siltstone
5R-1, 64	35.94	3.5	Siltstone	40R-6, 97	380.87	1.0	Pyrite
5R-1, 77	36.07	1.6	Siltstone	42R-1, 32	391.82	3.5	Sandstone
5R-2, 26	37.06	3.5	Sandstone	42R-5, 16	397.66	1.1	Shale
5R-2, 29	37.09	2.0	Siltstone	47R-3, 52	443.22	3.5	Siltstone
5R-2, 30	37.10	4.5	Siltstone with laminae, burrows	47R-6, 74	447.94	1.8	Claystone
5R-2, 34	37.14	2.5	Sandstone	48R-1, 143	450.83	1.5	Siltstone
5R-2, 37	37.17	1.5	Siltstone	48R-2, 86	451.76	1.5	Siltstone
6R-1, 18	45.08	2.0	Siltstone	48R-3, 42	452.82	1.5	Siltstone
8R-2, 78	66.48	2.5	Dark sandy shale	49R-4, 145	464.95	1.5	Metasediment
12R-1, 40	103.20	7.5	Sandstone	52R-1, 144	489.44	1.0	Siltstone (?)
14R-CC, 12	123.85	1.5	Siltstone	53R-5, 105	504.75	1.0	Siltstone
15R-1, 30	131.90	2.5	Sandstone	53R-5, 105	504.75	2.5	Siltstone

Silicoflagellates

No upper Neogene or Quaternary silicoflagellates were observed in Site 910 sediments. Very rare, reworked silicoflagellate specimens were noted in Cores 151-910C-17R through -20R.

Radiolarians

Core-catcher samples from Site 910 are barren of radiolarians with the exception of rare, mostly non-age-diagnostic, poorly preserved specimens of *Actinomma* and spongodiscids in Hole 910C (Cores 151-910C-4R through -42R). *Actinomma livae*, which ranges throughout the Miocene and Pliocene, is present in Sample 151-910C-13R-CC. Reworked Oligocene radiolarians (e.g., *Corythospyris jubata* and *Prunopyle* sp. C group of Lazarus and Pallant, 1989) occur in Sample 151-910C-18R-CC. A single specimen of *Cromyechinus borealis*, typical of glacial sediments in the Arctic Ocean,

Norwegian-Greenland Sea and in fjords of Norway and Svalbard (Hülsemann, 1963; Bjørklund, 1976), is present in Sample 151-910C-40R-CC.

Calcareous Nannofossils

All core-catcher samples from Holes 910A and 910B were examined for calcareous nannofossils. Nannofossils are rare to common, preservation is moderate to good, and species diversity is low. However, some marker species of Martini's (1971) zonation have been identified, as well as some datum planes described by Takayama and Sato (1987).

Emiliania huxleyi, an indicator for Zone NN21 of Martini's (1971) zonation, is found in Samples 151-910A-1H-CC, 151-910B-1H-CC, and 151-910C-1R-CC. Accordingly, these samples are assigned to the upper Quaternary. Samples 151-910A-2H-CC and 151-910B-2H-CC contain *Gephyrocapsa oceanica* and *Gephyrocapsa caribbeani*-

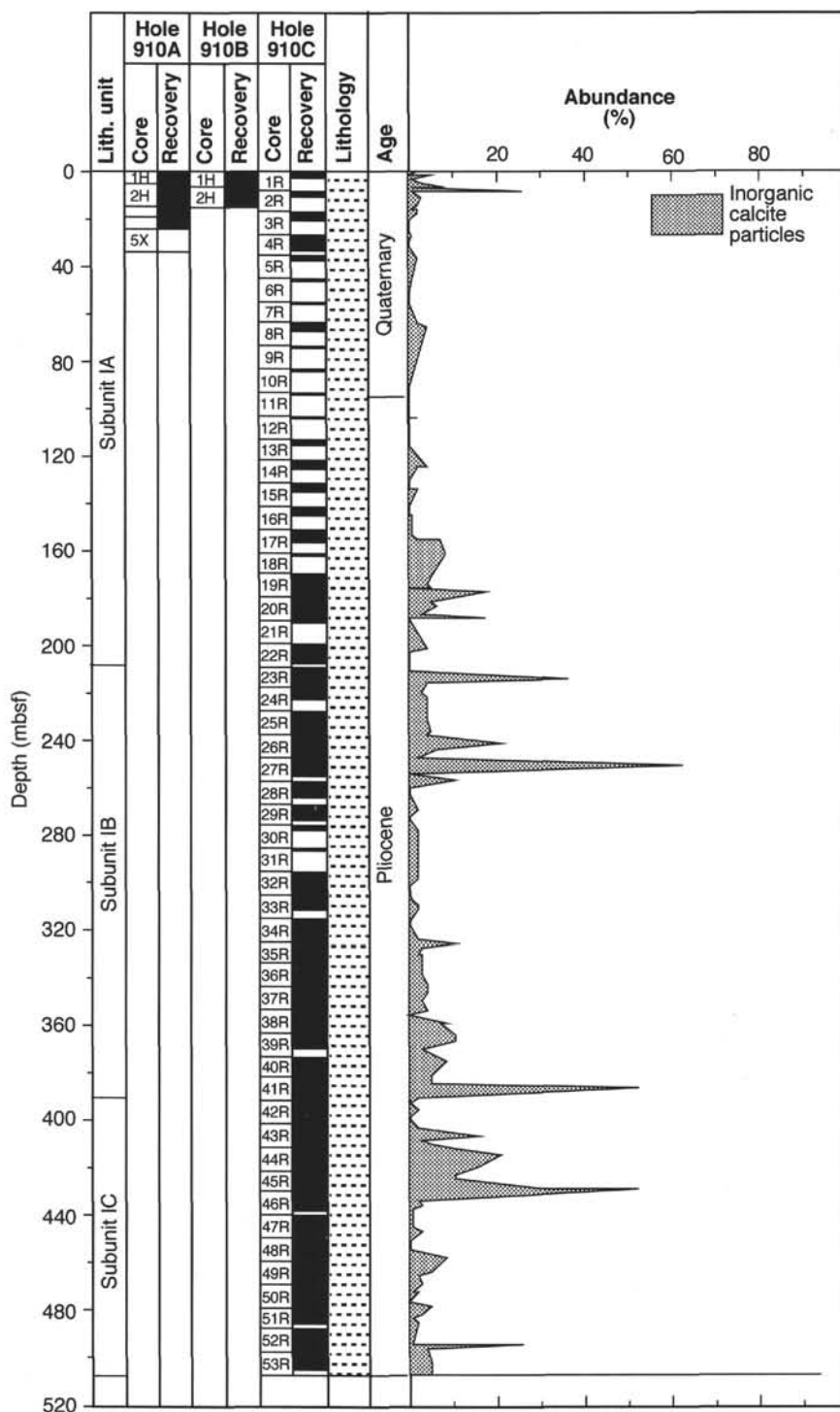


Figure 9. Core recovery, lithologic subunits, generalized lithology, and inorganic calcite particle abundance vs. depth for Holes 910A, 910B, and 910C. Note consistent background percentages of ~5% throughout sequence (see also percent carbonate in Figure 21 of "Organic Geochemistry" section, this chapter).

ca in the absence of both *E. huxleyi* and *Pseudoemiliania lacunosa*, indicating the upper Quaternary NN20 Zone.

The first-appearance datum (FAD) of *G. caribbeanica*, which occurs just above the Olduvai Event at all sites of Leg 94 in the North Atlantic (Takayama and Sato, 1987), is about 20 m above the Pliocene/Quaternary boundary at its stratotype, the Vrica section in Italy (Sato et al., 1988). This species occurs in Samples 151-910A-1H-CC through -5X-CC, and 151-910C-1R-CC through -7R-CC. *P.*

lacunosa, which first appears in latest early Pliocene time (uppermost NN15), has its last occurrence during the late Quaternary (NN19/NN20 boundary). *P. lacunosa* is present in Samples 151-910A-3H-CC through -4H-CC, and from 151-910C-2R-CC down to -41R-CC. Based on the co-occurrences of *G. caribbeanica* and *P. lacunosa*, the intervals from 151-910A-3H-CC through -5X-CC and from 151-910C-2R-CC through -7R-CC are correlated to the Quaternary NN19 Zone. Sample 151-910C-11R-CC contains a few speci-

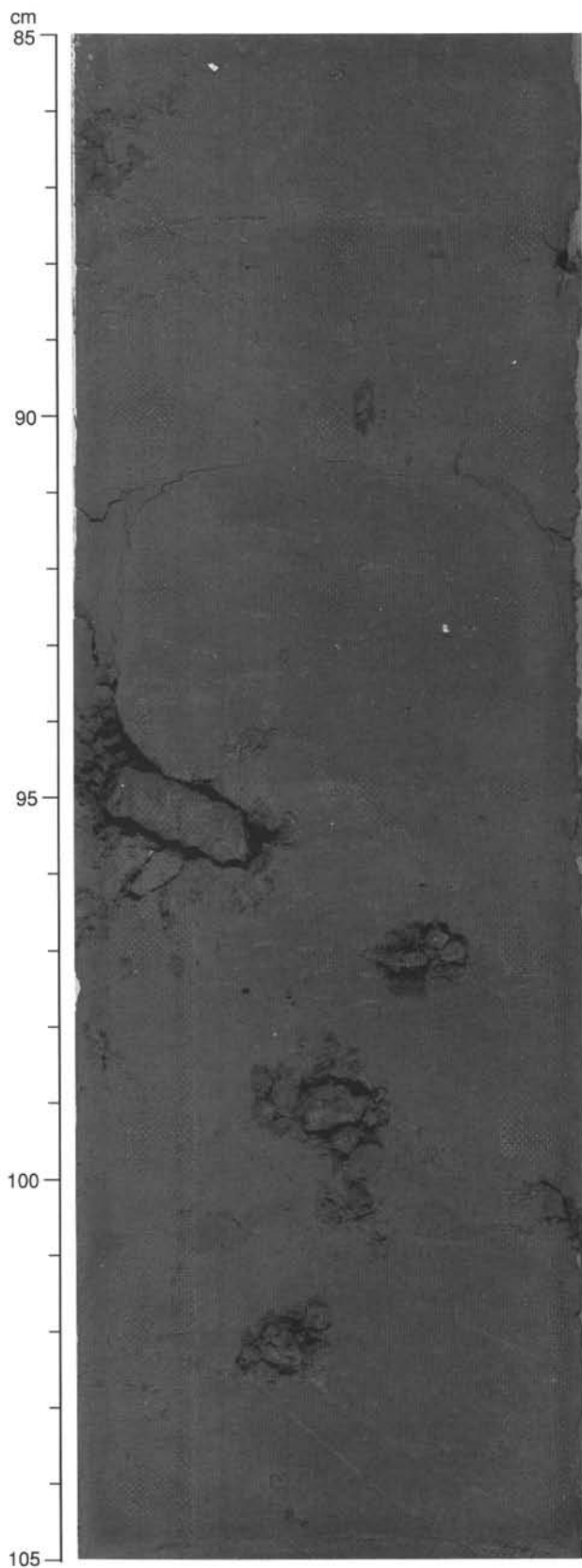


Figure 10. Close-up photograph of pyritized burrows and small, subhorizontal, sediment-filled burrows in Subunit IC (Interval 151-910C-48R-4, 85–105 cm).

mens of *Coccolithus pelagicus*, *Crenolithus daronicoides*, and *Gephyrocapsa* sp. (small), and may be correlated to upper NN18 or lower NN19 Zones, near the Pliocene/Quaternary boundary.

Below Sample 151-910C-12R-CC, and particularly in the interval from Samples 151-910C-25R-CC through -53R-CC (bottom of the hole), nannofossil assemblages are characterized by the relatively abundant occurrence of *C. daronicoides* co-occurring with *P. lacunosa* and *Helicosphaera sellii*. As warm-water species such as discoasters and ceratoliths are absent, it is difficult to correlate to Martini's (1971) zonation in detail. However, based on the lineages of both *H. sellii*, which ranges from uppermost NN15 to lower NN19 in the North Atlantic, Indian, and South Pacific oceans (Takayama and Sato, 1987; Sato et al., 1991; Takayama, 1993), and *P. lacunosa*, which ranges from upper NN15 to NN20 (Perch-Nielsen, 1985a), this sequence is correlated with upper lower Pliocene and/or upper Pliocene (upper NN15 Zone to NN18 Zone).

To summarize, all samples from Hole 910A and 910B, and core-catcher samples 151-910C-1R-CC through -7R-CC are Quaternary. Sample 151-910C-11R-CC is near the Pliocene/Quaternary boundary and Samples 151-910C-12R-CC through -53R-CC, are assigned to uppermost lower Pliocene and/or upper Pliocene.

Planktonic Foraminifers

All core-catcher samples from Holes 910A–C were examined for planktonic foraminifers. The preservation of planktonic foraminifers is good. They are abundant in the upper sequences of the Quaternary sediments and are mostly rare within the Pliocene sequences. The diversity is generally low.

Core-catcher samples from Cores 151-910A-1H through -5X, and 151-910B-1H and -2H, as well as Cores 151-910C-1R through -6R contain *Neogloboquadrina pachyderma* sin., with small amounts of *Globigerina bulloides* and *Neogloboquadrina* cf. *N. dutertrei*, indicating the Quaternary *N. pachyderma* sin. Zone. Samples 151-910C-7R-CC and -8R-CC are barren of planktonic foraminifers, and Cores 151-910C-9R and -10R had no recovery. Sample 151-910C-11R-CC contains only a few juvenile dextral coiling *Neogloboquadrina* specimens. Juvenile specimens of *N. pachyderma* and *N. atlantica* are indistinguishable, thus taxonomic assignment to the species level is not possible. This assemblage is similar to the uppermost Pliocene sequences observed at Site 644 on the Vøring Plateau (ODP Leg 104), where sequences containing dextral coiling *N. pachyderma* and *N. atlantica* overlie the Pliocene *N. atlantica* sin. Zone (Spiegler and Jansen, 1989). Core-catcher Samples 151-910C-12R-CC through -16R-CC are barren of planktonic foraminifers. The *N. atlantica* sin. Zone is recognized in Cores 151-910C-17R through -51R, although abundances of *N. atlantica* sin. are low in 75% of the examined core-catcher samples. Samples 151-910C-52R-CC and -53R-CC are barren of planktonic foraminifers.

Benthic Foraminifers

Every core catcher in Hole 910A, and at least every other core-catcher sample in Hole 910C, were analyzed for benthic foraminifers. At this time only a few trends are noted, and no zonation has been made of the site. Benthic foraminifers are unusually common at this site, but the diversity is low, with a few species found consistently throughout the entire sequence. Additional rare species will undoubtedly be recognized during shore-based analysis, providing better definition of the zonation.

Given the close proximity to Svalbard, this site experienced very high sedimentation rates throughout the Quaternary and Pliocene, and will provide a detailed record of benthic foraminifers during this interval. However, there may be a problem separating ice-rafted fauna from in-situ specimens. Hole 910A contains evidence for uppermost Quaternary glacial sediments throughout the upper five core-

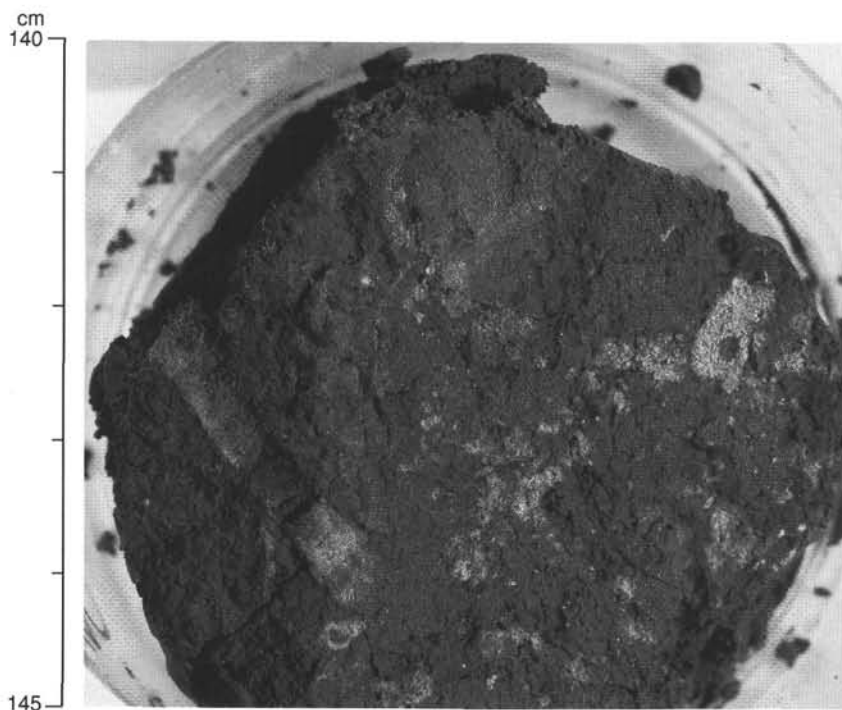


Figure 11. Cross-section close-up photograph of subhorizontal and high-angle sediment-infilled burrows in Subunit IC (Interval 151-910C-53R-5, 140–145 cm).

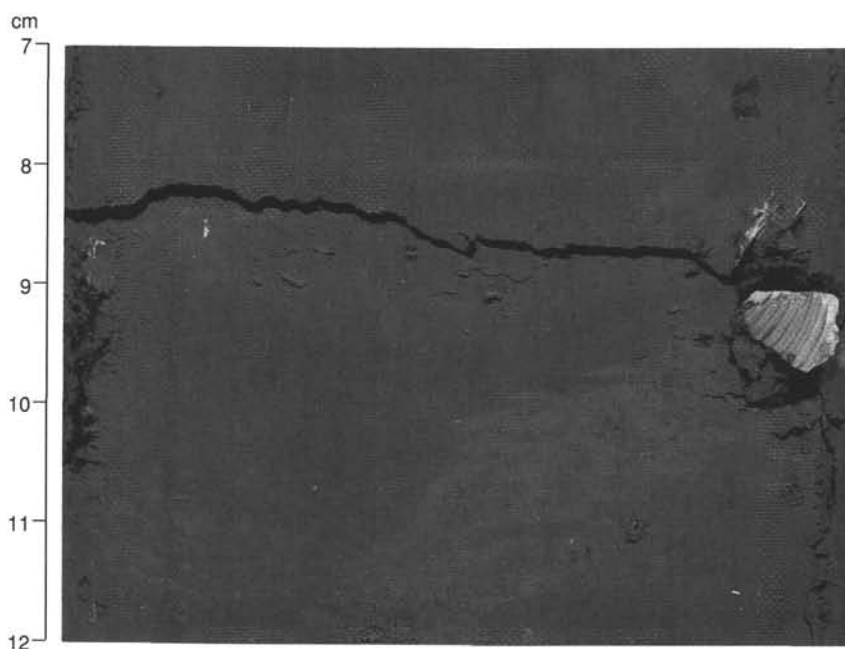


Figure 12. Close-up photograph of mollusc shell fragment in Subunit IA (151-910C-20R-5, 7–12 cm).

catcher samples. All of these samples contain *Eponides umbonatus*, which first appears on the Vøring Plateau at about Stage 18 (Osterman, 1992) and on the Alpha Ridge at Stage 8 (Scott et al., 1989).

The rotary-drilled Hole 910C appears to contain a shorter Quaternary record, with Pliocene species *Cassidulina teretis* and *Cibicides grossa* occurring below Sample 151-910C-3R-CC (Knudsen and Asbjørnsdottir, 1991; King, 1983). Drilling disturbance may be responsible for the very short Quaternary interval, although the presence of

well-preserved branching *Rhabdammina* sp. at the top of Core 151-910C-1R indicates minimal disturbance, at least of the top of Core 151-910C-1R. The two possibilities for the presence of Pliocene species in Sample 151-910C-5R-CC are: (1) ice rafting of older Pliocene sediments into Quaternary sediments or (2) these species may have extended ranges in this area.

From 151-910C-5R-CC through -23R-CC the benthic foraminifers consist of a Pliocene shallow-water continental shelf assem-

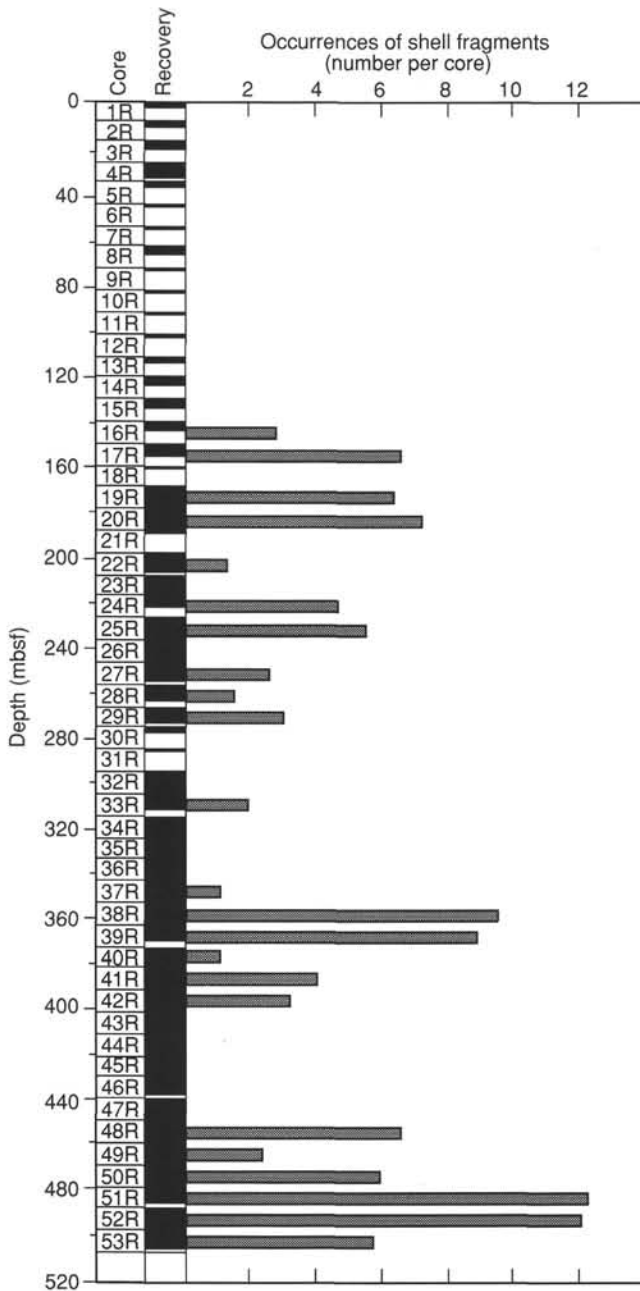


Figure 13. Mollusc shell fragments per core, normalized to recovery, vs. depth for Hole 910C. Normalization consisted of dividing the number of occurrences of shell fragments per core by the recovery fraction (e.g., in a given core, 5 occurrences of shell fragments/0.5 recovery = 10 shell fragments per core).

blage, including *C. teretis*, *C. grossa*, and various *Elphidium* species. Barren samples are rare in this interval, but recovery is poor, and the preservation of many specimens suggests ice transport.

From 151-910C-23R-CC through -32R-CC foraminiferal diversity improves with the appearance of numerous unilocular species, as well as an increase in *Cassidulina reniforme* and *Buccella frigida*. Increased diversity suggests slightly deeper water at this interval, possibly an outer shelf setting.

From 151-910C-33R-CC through -38R-CC, diversity and preservation declines and a mostly monospecific assemblage of *Melonis*

zaandamae with rare *C. reniforme* occurs. Several samples in this interval contain small concretions, which may indicate post-depositional reducing conditions that could have resulted in the dissolution of the foraminiferal tests. This interval also contains a small sand-sized fraction.

In the lowermost section of Hole 910C, from Sample 151-910C-39R-CC through -53R-CC, the benthic foraminiferal assemblage changes with the introduction of various cassidulinids including *Cassidulina carinata*, *Cassidulinoides porrecta*, and *Cassidulina* spp. These species could possibly represent Pacific influence, but it is unlikely that the interval spanning the opening of the Bering Straits was recovered at this site. The lowermost samples do not contain any evidence of pre-Pacific or Miocene sediments (McNeil, 1989).

Palynology

Core-catcher samples from Cores 151-910C-1R, -3R, -6R, -9R, -12R, -15R, -18R, -21R, -25R, -30R, -35R, and -40R were processed for palynomorphs, and all contain abundant amorphous organic matter, terrestrial plant debris, pollen, and spores. Dinoflagellates are very rare and mostly consist of reworked Cretaceous taxa. These include *Hystriochosphaeridium* sp., *Odontochitina* sp., *Gonyaulacysta* sp., and *Oligosphaeridium* sp. Taxa that are likely to be in situ include *Selenopemphix nephroides*, *Lejeunecysta* sp., and *Spiniferites* sp.

Biostratigraphic Synthesis

Biostratigraphic results reveal a 507.4-m succession of glacial-marine and hemipelagic muds reflecting very high sedimentation rates throughout the Quaternary and Pliocene (Fig. 14). Siliceous microfossils (diatoms, silicoflagellates, and radiolarians) are absent, with the exception of some reworked taxa, rare, non-age-diagnostic radiolarians, and a single specimen of the radiolarian *Cromyechinus borealis*, which is typical of glacial sediments in the Arctic Ocean and Norwegian-Greenland Sea (Sample 151-910C-40R-CC, 381.9 mbsf). Dinoflagellates also are very rare and mostly consist of reworked taxa. Consequently, the biostratigraphy of Site 910 is based on calcareous nannofossils and planktonic foraminifers. The unusually consistent occurrence of benthic foraminifers in the entire sequence provides a basis for ecologic and oceanographic interpretations of the bottom conditions.

The upper part of Site 910, from the top down to 64.2 mbsf, contains Quaternary fossils including nannofossils, *E. huxleyi*, *G. caribbeanica*, and *G. oceanica*, planktonic foraminifers *N. pachyderma* sin., and benthic foraminifers *E. umbonatus*. The position of the Pliocene/Quaternary boundary is not clear because of poor recovery in the upper part of the hole. However, the occurrences of small specimens of the calcareous nannofossil *Gephyrocapsa* and the foraminifers *N. pachyderma* dex. in Sample 151-910C-11R-CC indicate that the Pliocene/Quaternary boundary may be situated near this level. The Pliocene benthic foraminifer *C. grossa*, which is present in Samples 151-910C-5R-CC through -8R-CC, is presumed to be reworked.

Below Sample 151-910C-12R-CC (112.4 mbsf), the nannofossil assemblage changes abruptly and is dominated by Pliocene species, including *C. doronicoides*, *D. productus*, *P. lacunosa*, and *H. sellii*. This assemblage co-occurs with the Pliocene planktonic foraminifer *N. atlantica* sin., which is found below Sample 151-910C-16R-CC. Benthic foraminifers also suggest a Pliocene age to the bottom of the hole.

PALEOMAGNETICS

Shipboard paleomagnetic studies performed at Site 910 followed the methods described in the "Explanatory Notes" chapter (this volume). Paleomagnetic studies failed to provide significant temporal

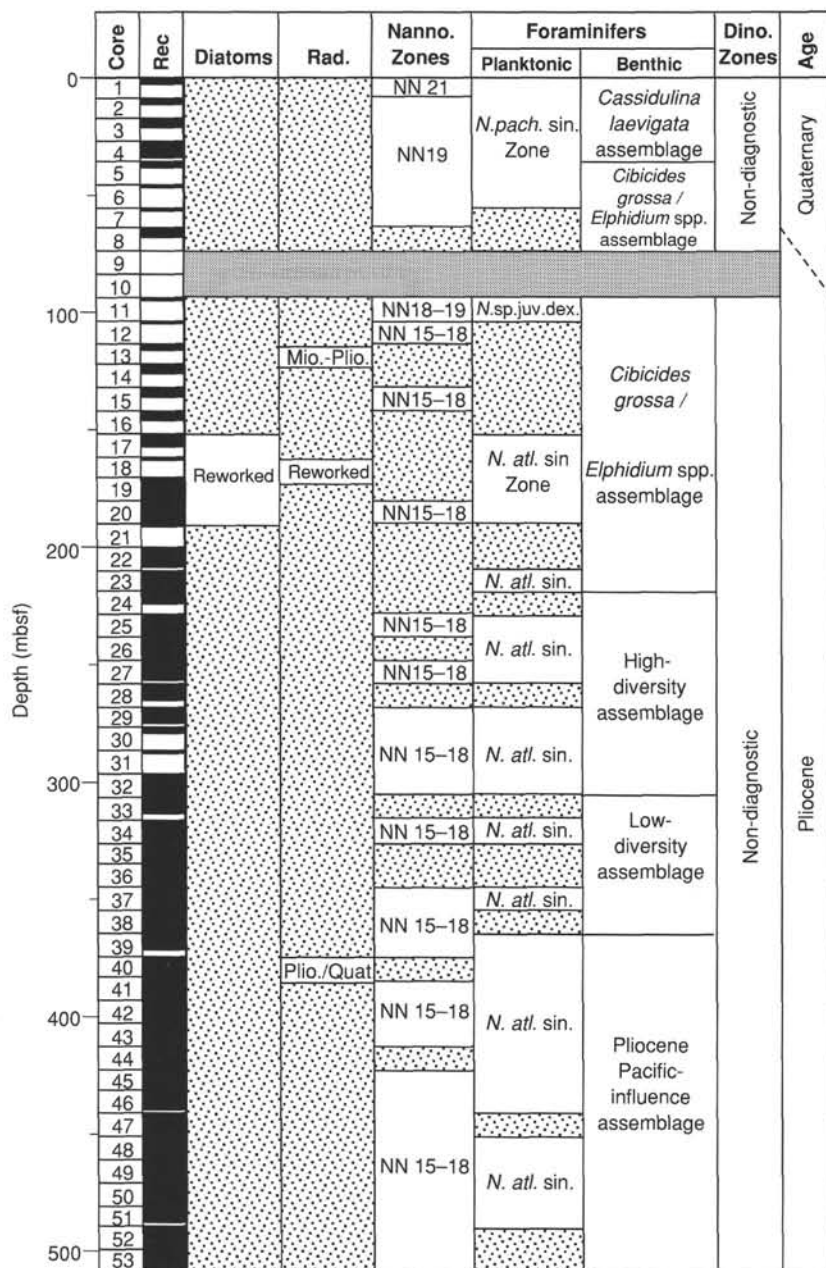


Figure 14. Biostratigraphic synthesis of Site 910.

constraints in this section primarily because of secondary magnetic minerals in the sediments. Additional rock magnetic investigations were undertaken at this site to explore the role played by iron sulfides in the sediments.

General Magnetic Character of the Site 910 Sediments

Demagnetization diagrams indicate that the difficulty in obtaining a coherent paleomagnetic signal arises from several possible sources (Fig. 15). The observation that the natural remanent magnetization (NRM) is reduced by less than half in many cases (Fig. 15B) and is still moving away from the origin in others (Figs. 15C and -D) indicates that the NRM of these sediments is carried, in large part, by minerals with coercivities greater than 30 mT. In addition, the tendency for the NRM to behave erratically above 40 or 60 mT suggests that spurious anhysteretic remanent magnetizations (ARMs) develop in these sediments at high demagnetizing fields. Alternating field

(AF) demagnetization of whole-core and discrete samples, in either the 2G or GSD-1 AF demagnetizers, revealed that these sediments have a strong tendency to acquire parasitic ARMs. As discussed in the explanatory notes, the field in the degauss region of the whole-core demagnetizer is variable in the range ± 100 nT and impossible to stabilize below that level; on sediments such as those recovered at Site 910, the quality of the paleomagnetic record would likely improve if it were possible to maintain a lower ambient demagnetization field.

In general, sediments recovered at Site 910 exhibit low NRM intensities; however, in Hole 910C there are many very high intensity spikes in NRM and magnetic susceptibility between ~200 mbsf and 507.4 mbsf (Fig. 16) that are observed to be related to the presence of iron sulfide concretions. In this interval, the NRM is dominated by the magnetizations of these secondary concretions and cannot be correlated to the geomagnetic polarity time scale (GPTS). Although they prevent the determination of a magneto-chronology, the common oc-

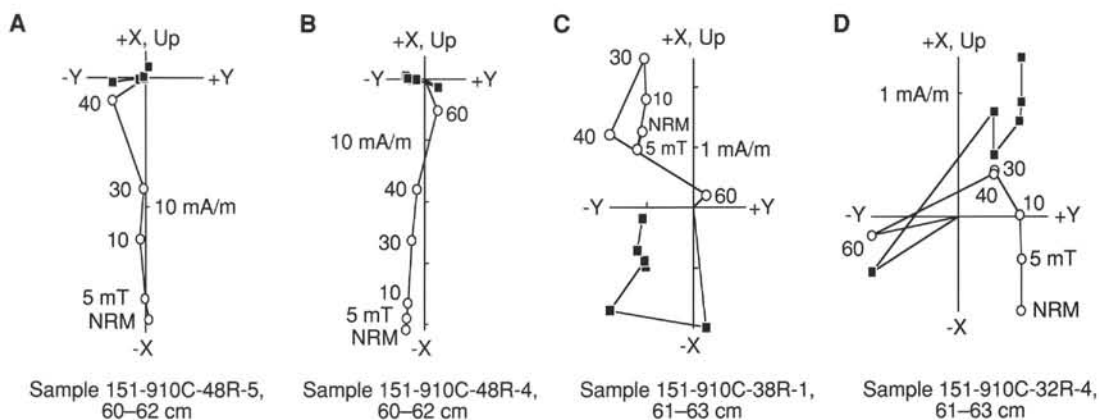


Figure 15. AF demagnetization diagrams for four discrete samples from Hole 910C. Black squares = projection onto the horizontal plane; white circles = projection onto the vertical plane parallel to the split face of the core.

currence of these highly magnetic concretions at this site might provide some constraints on the diagenesis and secondary alteration of these sediments; thus, further shipboard rock magnetic studies were undertaken to characterize the magnetic minerals in these sediments.

Rock Magnetic Investigations

The high geothermal gradients measured at Site 910 and elevated sulfur concentrations in the sediments (see "Inorganic Geochemistry" and "Organic Geochemistry" sections, this chapter) led us to suspect that early diagenetic processes such as iron oxide dissolution and the associated growth of iron sulfides were involved. To determine the nature of magnetic carriers, isothermal remanent magnetizations (IRM) were introduced in a group of nine pilot samples by subjecting discrete specimens to pulsed direct current fields in six steps ranging from 0.02 up to 1.2 T. In all cases, at least 98% of the saturation isothermal remanent magnetization (SIRM) was acquired in applied fields lower than 0.2 T (Fig. 17A), thus suggesting that highly coercive minerals such as pyrrhotite are volumetrically a small fraction of the sediment. On the other hand, the AF demagnetization of discrete samples indicates that magnetic minerals with coercivities in excess of 30–40 mT are important carriers of the NRM. Thus, pyrrhotite, greigite, or other iron sulfides may play a significant role in the NRM of these sediments, although these minerals represent only a small fraction of the remanence-carrying potential of the sediment. Further rock magnetic work should be able to characterize the various iron sulfide species present and thus shed some light on the diagenetic processes that affected the sediments of Site 910.

Comparison of the covariation of SIRM and susceptibility (k) yields some clues into the magnetic minerals responsible for the susceptibility spikes in Figure 16. SIRM/ k shows a near linear increase with increasing susceptibility (Fig. 17B). As SIRM is more dependent on coercivity changes than magnetic susceptibility (which mainly is affected by concentration changes), Figure 17B suggests that the high susceptibility peaks from Hole 910C mainly reflect increases in the concentration of higher coercivity minerals.

If one assumes that any SIRM remaining after the 300°C thermal treatment is carried by iron oxides (the Curie temperature of most iron sulfides is ~300°C [O'Reilly, 1984]), Figure 17C indicates that the iron oxides are proportionally of less importance in the sediments that have the largest SIRMs. Thus, the spikes in NRM intensity are not likely associated with iron oxides.

Inclination Record and Polarity Stratigraphy

The inclination records from the upper 25 m of Holes 910A and 910B are consistently shallower than the dipole (+85°) or present-day (+83°) geomagnetic fields at Site 910 and correlate poorly between

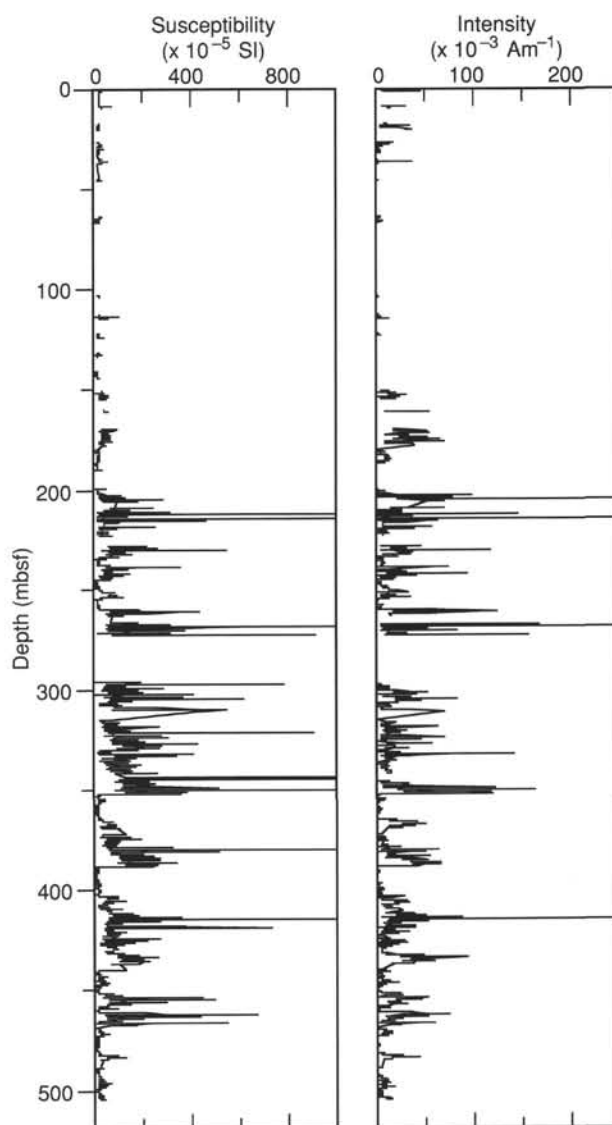


Figure 16. The variation of magnetic susceptibility (left) and NRM intensity (right) after 30-mT demagnetization treatment in Hole 910C. Scant recovery in the upper 200 m of the core indicates consistently low values for susceptibility and NRM intensity.

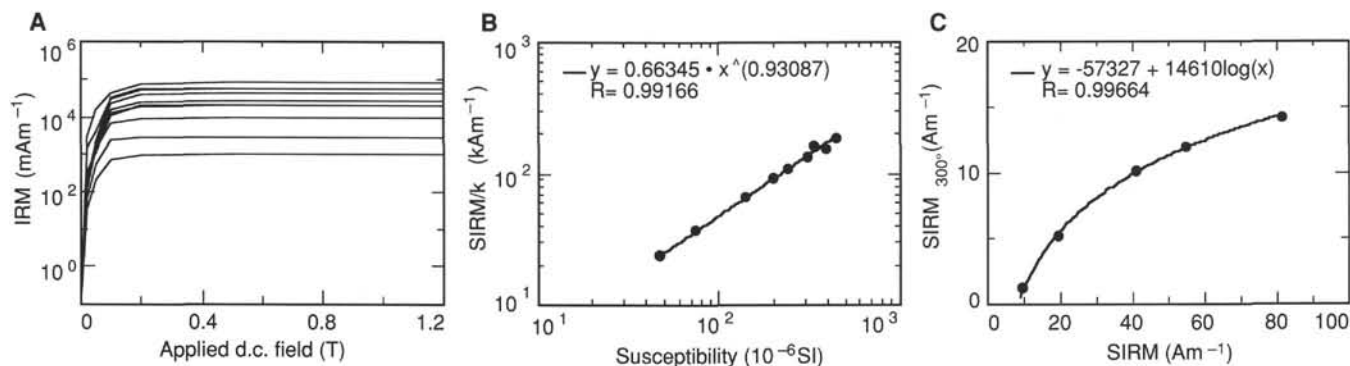


Figure 17. **A.** The acquisition of IRM for nine discrete samples from Hole 910C. The abscissa is logarithmic. **B.** The variation of SIRM/ k with susceptibility (k) in the same nine samples. Both scales are logarithmic. **C.** The relationship between the SIRM remaining after a 300°C thermal demagnetization treatment (SIRM_{300°}) and the original SIRM. Five results are shown; four samples disintegrated on heating.

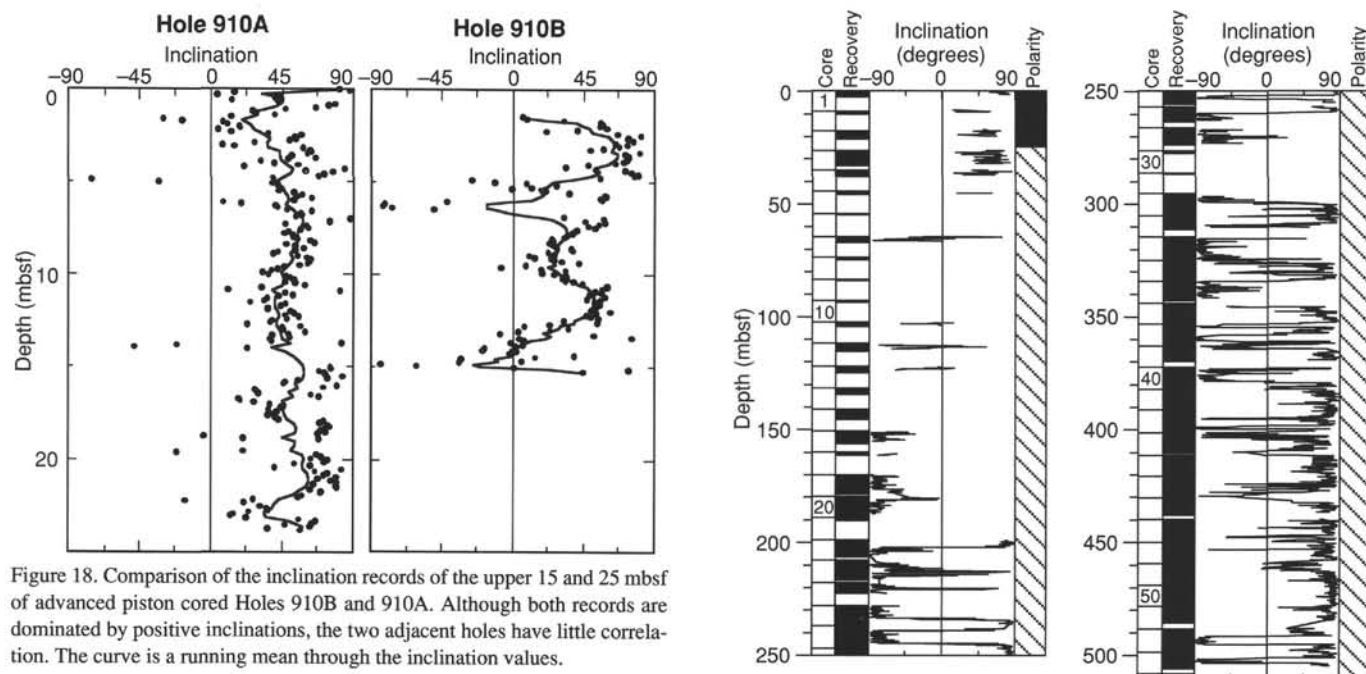


Figure 18. Comparison of the inclination records of the upper 15 and 25 mbsf of advanced piston cored Holes 910B and 910A. Although both records are dominated by positive inclinations, the two adjacent holes have little correlation. The curve is a running mean through the inclination values.

the two holes; however, they both yield predominantly positive inclinations (Fig. 18). This observation leads us to suggest that the upper 25 m of sediment was deposited during the Brunhes Chron. Below 25 mbsf the inclination record shows little stratigraphic coherency (Fig. 19). Occasionally the inclination record from Hole 910C shows intervals of bimodality with very steep positive and negative values (e.g., 230–260 mbsf in Hole 910C) but these intervals are not thick enough to correlate with the geomagnetic polarity time scale.

Conclusions

Through more extensive shore-based studies (such as thermal or detailed AF demagnetization), it may be possible to extract a characteristic magnetization more nearly contemporaneous with deposition. At present, we feel that no meaningful correlations to the geomagnetic polarity time scale, and thus no temporal constraints, are indicated with the available data set beyond the suggestion that the upper 25 m of sediment from Holes 910A and 910B was deposited during the Brunhes Chron. IRM acquisition and thermal demagnetization experiments indicate the spikes in susceptibility and NRM records are related to fairly high coercivity (30–40 mT) iron sulfides.

Figure 19. The paleomagnetic record from Hole 910C. The left two columns show the cored intervals; the length of the recovered core is shown in black. The center column is the inclination of the NRM after a 30-mT AF demagnetization treatment. On the right is the interpreted polarity; black = normal polarity; hatching = indeterminate polarity.

INORGANIC GEOCHEMISTRY

Interstitial Water

Table 4 shows the results of interstitial-water analyses in Holes 910A and 910C. Sodium (Fig. 20) shows a slight decrease with depth, probably caused by the release of interlayer water by clay minerals. Potassium (Fig. 20) shows a substantial decline with increasing depth reflecting its uptake by clay minerals. Magnesium and calcium (Fig. 20) show opposite trends, magnesium decreasing and calcium increasing with depth, although calcium shows a slight upward kick at the very top of the section. Magnesium declines rapidly near the seafloor but quite slowly with depth in the remainder of the section. Apparently, once again, interaction with basaltic basement rocks governs the Ca and Mg distributions.

Ammonia (Fig. 20) increases to very high values with depth, exceeding 8000 $\mu\text{mol/L}$ below 300 mbsf. Sulfate (Fig. 20) drops to essentially zero within the top 10 m of sediment column, confirming the

Table 4. Composition of interstitial waters in Holes 910A and 910C.

Core	Depth (mbsf)	Na (mmol/L)	K (mmol/L)	Mg (mmol/L)	Ca (mmol/L)	Cl (mmol/L)	SO ₄ (mmol/L)	SiO ₂ (μmol/L)	NH ₄ (μmol/L)	pH	Alkalinity (meq/L)
151-910A-1H	2.95	499.02	13.59	54.38	5.34	542	26.73	329	284	7.48	5.171
4H	22.40	482.98	13.01	41.16	3.88	548	0.23	362	823	nd	nd
151-910C-3R	18.83	503.38	10.81	42.73	3.74	543	0.32	312	832	7.76	17.538
8R	65.65	460.76	9.47	38.92	5.10	537	1.04	290	2578	7.84	12.332
13R	113.85	455.88	8.66	32.64	5.77	539	0.48	452	3521	7.79	9.333
16R	142.60	465.58	9.49	31.20	6.72	530	0.04	308	4640	7.79	9.753
19R	176.10	462.63	8.04	32.42	7.77	533	0.76	443	5746	7.63	11.087
22R	204.90	469.34	8.07	30.91	7.85	531	0.26	344	6814	7.62	12.723
25R	235.40	438.72	7.57	29.38	8.09	527	0.03	530	7092	7.65	13.668
28R	261.30	459.15	7.18	31.47	8.70	522	0.25	582	6494	7.88	13.642
32R	303.36	444.45	7.43	28.98	8.67	534	0.38	490	7856	7.56	12.473
35R	331.80	464.05	6.94	29.33	9.26	525	0.50	527	7131	7.87	10.856
38R	360.80	456.48	6.01	27.99	10.19	533	0.00	449	8569	7.51	12.120
41R	389.30	457.91	5.53	27.54	10.82	537	0.50	302	8000	7.52	11.710
44R	418.20	466.23	5.00	29.14	12.57	525	1.57	565	6362	7.57	10.506
47R	447.10	471.81	4.84	27.34	11.78	530	0.47	457	6877	7.71	10.011
50R	476.10	481.07	4.20	26.24	11.91	532	0.50	269	7033	7.55	10.351
53R	503.13	468.09	4.35	26.24	12.02	528	1.54	460	6693	7.62	10.113

Note: nd = not determined.

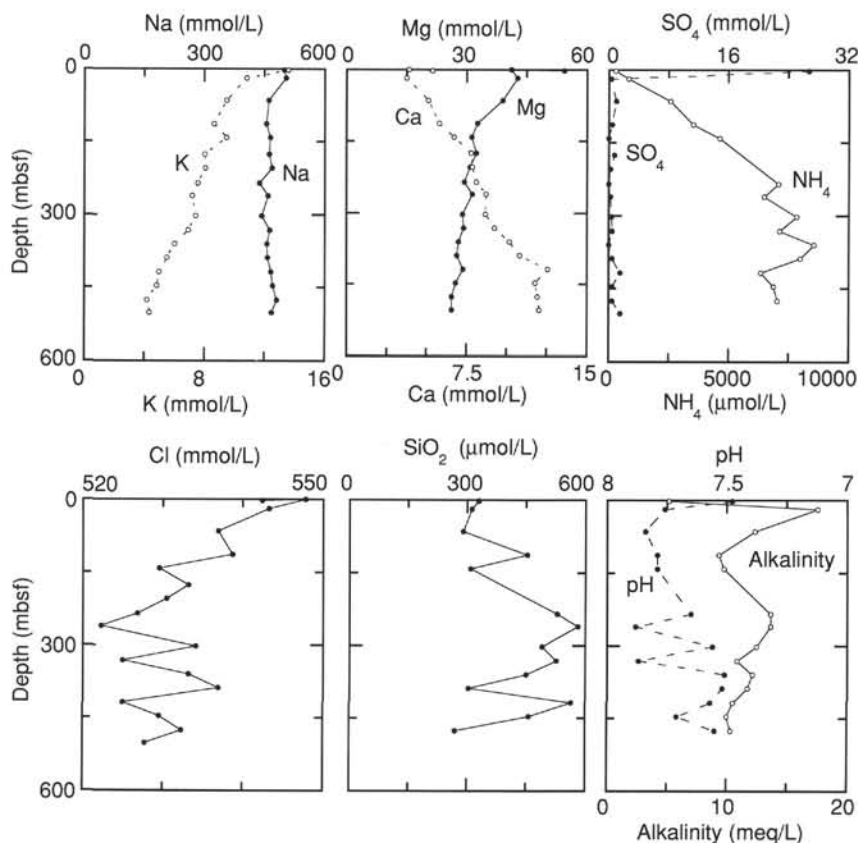


Figure 20. Interstitial water compositions at Site 910.

very active diagenesis of organic matter at this site. Chloride (Fig. 20) shows a very slight decrease as a result of dilution with water from the dehydration of clays.

Silica (Fig. 20) in the interstitial waters at Site 910 is substantially lower than at Sites 907 and 908. Silica concentrations are ~400–500 μmol/L in this section as opposed to levels above 1000 μmol/L at Sites 907 and 908. This appears to reflect equilibrium with diagenetic opal CT rather than amorphous, biogenic silica as at the other sites (Kastner, 1979). The general absence of siliceous microfossils (see

“Biostratigraphy” section, this chapter) suggests that insufficient biogenic silica is present in these cores to support higher silica levels.

Alkalinity and pH (Fig. 20) appear to parallel the abundance of sulfur in the sediments at Site 910 (Fig. 21). Sulfate reduction in the presence of carbonate minerals produces alkalinity, but, of course, sulfate reduction is not occurring at depth in these cores as sulfate goes to zero at the very top of the section (Fig. 20). Diffusion will likely erase unsupported variations in interstitial water compositions in substantially less than 1 m.y.; the persistence of this alkalinity pro-

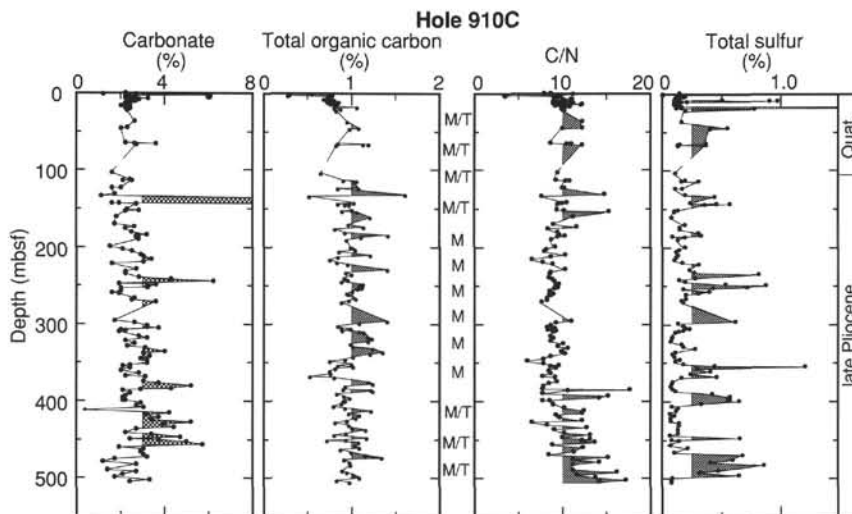


Figure 21. Carbonate contents, total organic carbon contents, organic carbon/total nitrogen (C/N) ratios, and total sulfur contents in sediments at Hole 910C. "M/T" and "M" mark intervals dominated by marine/terrestrial (mixed) organic matter and marine organic matter, respectively.

file is puzzling and must reflect some other carbonate dissolution process.

Sediment Geochemistry

Table 5 shows the results of major element analyses on sediments from Site 910. CaO and MgO (Fig. 22) show little variation in the upper parts of the section but appear more variable below 200–225 mbsf (the shipboard sedimentologists place the Unit IA/Unit IB boundary at 208.7 mbsf; see Table 2). The CaO content of these cores is relatively low and indicates a scarce calcium carbonate component. Potash and soda (Fig. 22) are similar in that they appear more constant above 200–225 mbsf than below. Potash, in particular, is less abundant in the lower parts of the section no doubt because of fixation in clay minerals.

Silica (Fig. 22) also shows increased variability below 200–225 mbsf. Silica is quite high in these sediments, well above average shale values (Wedepohl, 1969), averaging more than 60%. Silica varies inversely with alumina (Fig. 22), reflecting variations in the abundance of quartz and the feldspar/mica/clay component carrying the alumina. Alumina also shows an anomalous covariation with iron (Fig. 22). This may indicate the presence of an iron-rich clay mineral, presumably glauconite (cf. "Lithostratigraphy" section, this chapter), in these sediments.

Discussion

The sediments at Site 910 are highly siliceous and are lacking in siliceous fossils. The amount of silica necessary to raise the concentration from 500 $\mu\text{mol/L}$ to 1000 $\mu\text{mol/L}$ in one cubic centimeter of sediment (with a porosity of 50%) is about 250 nanmoles or about 23 μg . The mass of solids in one cubic centimeter of the same sediment is more than one gram. If amorphous silica in fossil skeletons were present at about 20 parts per million, it would be sufficient to raise the silica concentration to 1000 $\mu\text{mol/L}$. It is not surprising that siliceous fossils are difficult to find in these sediments. Whether siliceous fossils were ever present is unclear, although it appears from a cursory examination of these data that they were probably never present in any abundance. The low and relatively stable CaO concentration in these sediments suggests that CaCO_3 is similarly scarce (see also the data in "Organic Geochemistry" section, this chapter) and leads one to wonder at the relative scarcity of fossil material in these sediments, especially in view of the evidence for high levels of organ-

ic matter (see Fig. 20 and the discussion in "Organic Geochemistry" section, this chapter), although much of this carbon may be of terrestrial origin.

These sediments continue the very high total silica content seen in sediments from Site 908. This presumably reflects the abundance of quartz in these sediments. The silica content is quite variable below the Unit IA/IB boundary. This may reflect sorting by the bioturbation processes in the lower parts of the section, which appear to sort sand-sized particles preferentially into burrows. The inverse relationship between silica and alumina (Fig. 22) indicates that the clay fraction is less aluminous than the bulk sediment and is not responsible for the high silica content of these sediments.

Although the methane concentration at Site 910 is substantial (see Table 6 and Fig. 23 of "Organic Geochemistry" section, this chapter), there is no evidence in the chloride (or sodium) profile for the degradation of a gas hydrate phase. Gas hydrates are salt-free, ice-like structures that melt upon decompression and/or heating, returning fresh water to the formation. The absence of substantial dilution of chloride or sodium in these sediments indicates that hydrates were not present.

ORGANIC GEOCHEMISTRY

The shipboard organic geochemistry program at Site 910 consisted of analyses of volatile hydrocarbons and determinations of inorganic carbon, total nitrogen, total carbon, and total sulfur (for methods see "Explanatory Notes" chapter, this volume).

Volatile Hydrocarbons

As part of the shipboard safety and pollution monitoring program, concentrations of methane (C_1), ethane (C_2), and propane (C_3) gases were monitored every core using standard ODP headspace-sampling technique. Below 140 mbsf, vacutainer samples also were taken from gas voids (for comparison of headspace and vacutainer data).

Except for the uppermost ~20 mbsf (Hole 910A; Table 6), concentrations of headspace methane are high throughout the sedimentary section, ranging from 8000 to 80,000 ppm (Fig. 23). No distinct long-term change is obvious. Ethane and propane values occur in detectable amounts below 20 mbsf as well, but show a distinct down-hole increase. At about 500 mbsf, ethane and propane concentrations reach maximum concentrations of 80 to almost 100 ppm (Fig. 23).

Table 5. Major element composition of sediments in Holes 910A and 910C.

Core, section	Depth (mbsf)	SiO ₂ (wt%)	TiO ₂ (wt%)	Al ₂ O ₃ (wt%)	Fe ₂ O ₃ (wt%)	MnO (wt%)	MgO (wt%)	CaO (wt%)	Na ₂ O (wt%)	K ₂ O (wt%)	P ₂ O ₅ (wt%)	Total (wt%)
151-910A-												
1H-3	4.24	61.42	0.88	15.89	6.08	0.05	3.06	2.20	2.05	3.14	0.20	94.97
2H-3	9.74	61.42	0.89	15.64	6.11	0.05	3.03	2.24	1.96	3.15	0.20	94.69
3H-2	17.13	61.22	0.90	15.83	6.06	0.05	3.04	2.19	1.92	3.17	0.20	94.58
4H-2	21.74	62.55	0.89	15.55	5.90	0.05	2.99	2.15	1.95	3.17	0.20	95.41
151-910C-												
1R-1	0.75	60.32	0.88	15.61	6.35	0.05	3.05	2.09	2.10	3.11	0.25	93.80
4R-3	30.00	61.15	0.89	15.28	6.11	0.05	2.95	2.17	1.90	3.15	0.19	93.85
5R-1	35.90	61.05	0.91	15.53	6.21	0.05	2.92	2.10	1.91	3.15	0.19	94.01
8R-1	64.84	60.81	0.93	16.74	6.64	0.05	2.97	2.02	2.01	3.14	0.17	95.48
12R-1	103.47	61.57	0.92	16.02	6.50	0.05	2.90	1.99	1.87	3.11	0.18	95.11
13R-1	113.04	60.77	0.90	15.83	7.00	0.05	2.85	1.98	1.86	2.97	0.19	94.41
14R-1	123.16	61.53	0.94	16.70	6.18	0.04	2.87	1.95	1.83	3.30	0.14	95.49
15R-1	132.44	61.40	0.91	16.27	6.47	0.04	2.91	1.91	2.04	3.22	0.15	95.33
16R-1	141.82	61.32	0.89	16.12	6.33	0.04	2.93	2.03	1.94	3.10	0.18	94.89
17R-2	153.20	61.69	0.93	16.24	6.72	0.05	2.72	1.89	1.86	3.01	0.17	95.29
18R-1	160.88	61.94	0.94	16.26	6.80	0.05	2.74	1.84	1.91	3.07	0.16	95.72
19R-3	173.82	61.50	0.97	15.65	6.69	0.05	2.81	1.89	1.90	3.01	0.14	94.61
20R-3	183.44	61.32	0.97	16.80	6.72	0.04	2.74	1.85	1.78	3.17	0.16	95.55
22R-2	201.11	62.29	0.90	14.76	5.84	0.06	2.43	1.77	1.93	2.64	0.18	92.79
23R-3	212.30	60.62	0.97	16.45	6.34	0.05	2.67	1.80	1.83	2.93	0.15	93.81
24R-3	221.93	63.16	0.93	15.19	5.83	0.03	2.57	1.78	1.97	2.79	0.14	94.39
25R-3	231.61	60.14	0.95	16.59	6.50	0.05	2.99	1.99	2.10	3.10	0.15	94.56
26R-3	241.22	60.71	0.96	16.25	6.97	0.05	3.04	2.11	1.94	2.96	0.16	95.15
27R-2	249.35	60.96	0.90	15.82	6.79	0.05	3.08	2.19	1.86	3.04	0.19	94.87
28R-1	257.44	62.13	0.93	16.19	6.37	0.04	2.73	1.90	1.94	2.92	0.17	95.32
29R-3	269.14	61.59	0.95	16.14	6.73	0.05	2.91	2.03	1.97	2.87	0.18	95.41
32R-3	298.19	62.76	0.90	15.52	6.23	0.04	2.59	1.87	1.94	2.68	0.22	94.76
33R-2	307.40	59.18	0.97	17.13	7.68	0.05	2.76	1.86	1.97	2.80	0.22	94.61
34R-3	318.44	59.23	0.97	16.78	8.38	0.06	2.71	1.77	1.91	2.70	0.17	94.69
35R-3	328.03	60.14	0.97	16.25	6.88	0.05	2.75	1.98	1.95	2.87	0.18	94.03
36R-3	338.20	59.53	0.96	17.03	7.68	0.05	2.82	1.93	1.92	2.90	0.17	94.98
37R-3	347.43	59.34	1.02	16.91	8.10	0.05	2.90	1.95	1.92	2.85	0.16	95.21
38R-3	357.03	65.50	0.84	13.23	4.58	0.03	2.40	1.98	2.15	2.42	0.23	93.36
39R-3	366.53	62.60	0.91	15.30	5.60	0.04	2.61	1.98	1.96	2.76	0.18	93.95
40R-3	376.02	57.48	0.99	17.09	8.74	0.07	2.83	1.81	1.84	2.68	0.15	93.68
41R-3	385.51	59.11	1.05	17.10	7.49	0.04	2.63	1.90	1.89	2.77	0.15	94.12
42R-3	395.14	62.49	0.87	14.78	5.29	0.04	2.54	2.18	1.94	2.75	0.19	93.06
43R-3	404.84	63.14	0.90	14.98	5.29	0.04	2.50	1.93	1.88	2.73	0.17	93.54
44R-3	414.43	54.70	0.77	13.67	10.68	0.05	2.72	1.94	1.58	2.37	0.27	88.75
45R-3	424.14	60.36	0.96	16.36	7.13	0.05	2.63	1.86	1.80	2.67	0.19	94.01
46R-3	433.74	58.69	0.95	16.16	8.37	0.06	2.95	2.27	1.78	2.95	0.24	94.41
47R-3	443.46	64.26	0.94	15.84	5.13	0.03	2.56	1.88	1.93	2.85	0.14	95.55
48R-3	453.71	60.36	0.99	16.77	7.13	0.05	2.77	2.02	1.78	3.01	0.16	95.03
49R-3	462.65	55.73	1.04	19.51	8.91	0.06	2.89	1.97	1.83	2.88	0.20	95.02
50R-3	472.36	62.25	1.04	17.21	6.96	0.04	2.56	1.87	1.96	2.74	0.12	96.75
52R-3	491.61	63.01	0.93	15.90	6.00	0.04	2.70	1.94	1.97	2.91	0.23	95.64
53R-3	501.30	63.22	0.88	14.75	6.01	0.04	2.51	1.94	1.78	2.63	0.25	94.01

For safety considerations, the C_1/C_2 ratio is generally used to get quick information about the origin of the hydrocarbons (i.e., to distinguish between biogenic gas and gas migrated from a deeper source of thermogenic hydrocarbons). Very high C_1/C_2 ratios indicate a gas (C_1) formation by microbiological processes. On the other hand, the occurrence of major amounts of C_2 (to C_3) in shallow depths is associated with thermogenic hydrocarbon generation. In general, the C_1/C_2 ratios consistently decrease with burial depth due to the increasing influence of early diagenetic generation of hydrocarbons.

Starting from high values between 2000 and 8000 in the upper 100 mbsf, C_1/C_2 ratios show the "normal" general decrease with depth, reaching values of 400 at 500 mbsf (Fig. 23). The same trend also is recorded in the vacutainer data, but with an offset toward higher values. The high C_1/C_2 ratios suggest a biogenic origin of the methane. It is probably formed by in-situ microbial fermentation of the marine organic carbon that is present in major amounts in the entire sedimentary sequence. At Hole 910A, the methanogenesis has begun at depths shallower than 20 mbsf, as clearly indicated by the sharp increase in methane concentration and the contemporaneous sharp cessation of sulfate reduction (see "Inorganic Geochemistry" section, this chapter).

According to the pressure-temperature stability field of gas hydrates (cf., Kvenvolden and Barnard, 1983), a geothermal temperature gradient of about 55°C/km (see "Downhole Measurements" section, this chapter), a water depth of 566 m, and a bottom-water temperature of about 0°C, gas hydrates are stable down to about 210 mbsf at the location of Site 910. Thus, the maximum concentration of methane at about 40 mbsf and, especially, at 150 mbsf may possibly be related to the presence of hydrates. Very high gas concentrations

at about 150 mbsf, indicated by the first occurrence of major gas voids and degassing sediments ("bubbling") in the core liner, may support this. No obvious gas hydrates, however, were observed at Hole 910C. The pore-water geochemistry also does not give a clear signal for the occurrence of hydrates (see "Inorganic Geochemistry" section, this chapter).

Carbon, Nitrogen, and Sulfur Concentrations

The results of determinations of inorganic carbon, carbonate, total carbon, total nitrogen, and total sulfur are summarized in Table 7 and presented in Figures 21 and 24.

The carbonate contents of the sedimentary sequence of Hole 910C vary between 1% and 6% (Fig. 21). In Sections 151-910C-1R-1 and 151-910C-16R-1 only, higher values of 9.4% and 29.5%, respectively, were determined. Several of the carbonate maxima at Hole 910C coincide with maxima of inorganic calcite as determined by smear slides (see "Lithostratigraphy" section, this chapter), indicating a nonbiogenic source of significant proportions of the carbonate.

The total organic carbon (TOC) contents are generally high and vary between 0.5% and 1.5%, with an average value of about 1% (Fig. 21). The maximum values are reached in the upper Pliocene interval, whereas the upper 100 m (Quaternary) are characterized by lower values. This distribution, however, should not be overinterpreted, because the core recovery in the Quaternary was much less than in the underlying Pliocene interval.

The total nitrogen contents are generally low, ranging between 0.05% and 0.15% (Table 7). The total sulfur values show short-term (rhythmic?) high-amplitude variations between 0.1% and 1%

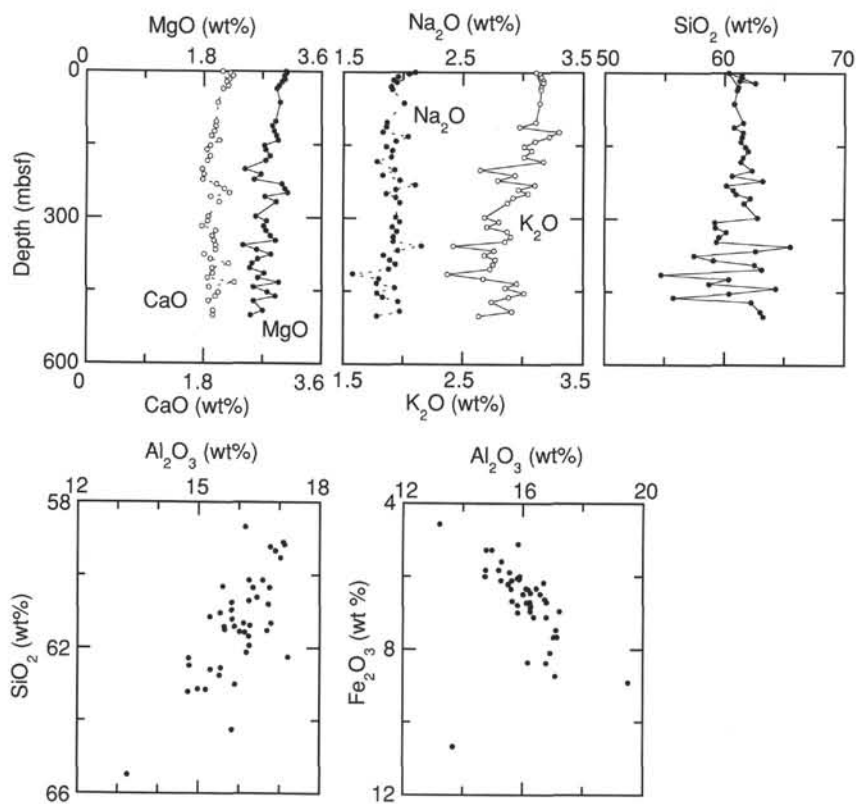


Figure 22. Sediment compositions at Site 910.

throughout the entire section (Fig. 21). Single peaks of extremely high values of 8.4% and 7.2% occur in Sections 151-910C-1R-1 and 151-910C-3R-1, probably reflecting sulfide-rich layers (see "Lithostratigraphy" section, this chapter). Two black, spherical sulfide nodules of about 0.5 cm in diameter and a sulfur content of 14.9% were found in interstitial water (IW) Sample 151-910C-28R-3, 140–150 cm.

Composition of Organic Matter

The type of the organic matter in the sediments of Hole 910C has been characterized using organic carbon/nitrogen (C/N) ratios (e.g., Stein, 1991a). The average C/N ratios of marine zoo- and phytoplankton are between 5 and 8, whereas higher land plants have ratios between 20 and 200 (Bordowski, 1965; Emerson and Hedges, 1988; see also "Organic Geochemistry" section, "Site 907" chapter, this volume).

According to the C/N ratios, the sedimentary record of Hole 910C can be divided into three intervals. The lowermost interval between 507.4 and 380 mbsf, as well as the upper 160 m, is characterized by C/N ratios between 7 and 17, indicating a mixture between marine and terrigenous organic carbon, with a dominance of the marine material (Figs. 21 and 24, Table 7). Between 160 and 380 mbsf, C/N ratios >11 are absent; most of the ratios are between 7 and 9, suggesting a marine origin of the organic matter. The distinct enrichment of marine organic carbon in the upper Pliocene sediments of Hole 910C has probably been caused by an increased preservation of organic material due to the very high sedimentation rates (cf., Müller and Suess, 1979; Stein, 1990).

Further qualitative and quantitative organic geochemical data (such as detailed records of flux rates of terrigenous and marine organic carbon as well as biomarker data) are required before a more

detailed paleoceanographic interpretation of the organic carbon data can be done.

PHYSICAL PROPERTIES

Introduction

The shipboard physical properties program at Site 910 included nondestructive measurements of bulk density, bulk magnetic susceptibility, compressional-wave velocity, and total natural gamma activity on whole sections of core using the multi-sensor track (MST), as well as discrete measurements of thermal conductivity, compressional-wave velocity, shear strength, and index properties. The downhole temperature measurements are also reported here. Methodology is discussed in the "Explanatory Notes" chapter (this volume).

Four holes were drilled at Site 910 in sediments of Quaternary and Pliocene age. Hole 910A consisted of four APC cores and one XCB core, penetrating to a depth of 34.0 mbsf. Hole 910B was only drilled to a depth of 15.6 mbsf, recovering only two APC cores before the hole was abandoned. Rotary drilling was used throughout Hole 910C to a depth of 507.4 mbsf. Hole 910C had less than 60% recovery, thus creating segments of missing data in the physical property record. Core disturbance increased substantially between the APC and XCB cores. Sample intervals for the discrete measurements were selected from the most undisturbed sections of the working half of the core. For Hole 910D, see separate section below.

Whole-core Measurements

Multi-sensor Track

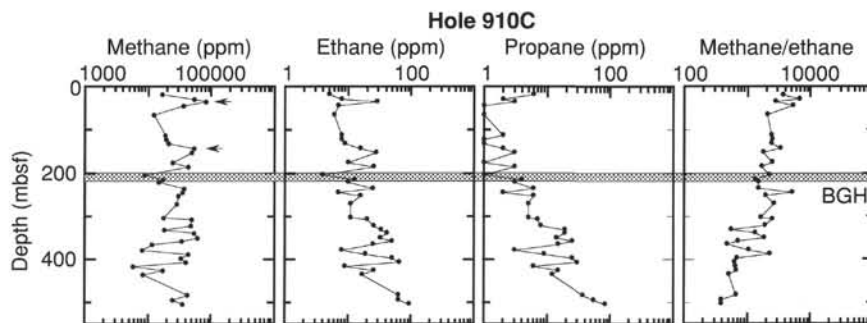
Whole-round measurements of GRAPE density, magnetic susceptibility, and natural gamma activity were performed on all of the

Table 6. Results of headspace and vacutainer gas analysis from Holes 910A and 910C.

Core, section, top interval (cm)	Depth (mbsf)	C ₁ -HS (ppm)	C ₂ -HS (ppm)	C ₃ -HS (ppm)	C ₁ /C ₂ -HS	C ₁ -VAC (ppm)	C ₂ -VAC (ppm)	C ₃ -VAC (ppm)	C ₁ /C ₂ -VAC
151-910A-									
1H-3, 0	3.0	7	0	0	0				
2H-5, 0	11.5	6	0	0	0				
3H-2, 0	16.5	14	0	0	0				
4H-3, 0	22.5	3646	1	0	3646				
151-910C-									
3R-2, 0	18.9	16756	5	6	3351				
4R-4, 0	30.9	53776	8	2	6722				
5R-2, 0	36.8	82053	29	3	2829				
6R-1, 0	44.9	36722	7	1	5246				
8R-2, 0	65.7	12306	6	1	2051				
13R-2, 0	113.9	19192	8	2	2399				
14R-2, 0	123.5	19596	8	1	2450				
15R-2, 0	133.1	21466	9	1	2385				
16R-2, 0	142.7	53582	16	2	3349	877539	159	3	5519
17R-3, 0	153.9	49499	28	3	1768	679714	117	5	5810
19R-5, 0	176.2	24726	10	1	2473				
20R-5, 0	185.8	43480	26	3	1672				
22R-5, 0	205.0	8836	4	1	2209	66399	7	0	9486
23R-5, 0	214.7	17455	13	4	1343				
24R-3, 0	221.3	15131	10	3	1513	839	0		2797
25R-6, 0	235.5	37479	25	6	1499				
26R-5, 145	245.1	35497	7	2	5071	96443	9	1	10716
27R-5, 0	253.2	30855	16	6	1928	619568	166	13	3732
29R-5, 0	272.5	29298	11	5	2663	856662	231	17	3708
32R-7, 0	304.5	17985	11	5	1635	896225	323	24	2775
33R-3, 0	308.1	49789	20	7	2489	896225	323	24	2775
34R-6, 0	322.3	48743	26	8	1875	917226	328	27	2796
35R-6, 0	331.9	18666	34	19	549				
36R-5, 0	340.1	54946	42	19	1308	893601	350	28	2553
37R-6, 0	351.3	61095	33	14	1851	1010351	404	45	2501
38R-5, 0	359.4	34744	49	25	709	1007765	384	33	2624
39R-4, 0	367.4	11899	25	15	476				
40R-6, 0	379.9	8244	8	3	1031				
41R-6, 0	389.4	43658	19	9	2298	900884	398	44	2264
42R-6, 0	399.0	33171	49	25	677	885441	393	39	2253
43R-6, 0	408.7	40650	65	30	625	92277	23	2	4012
44R-6, 0	418.3	5816	9	6	646	25745	5	0	5149
45R-6, 0	428.0	17247	26	15	663	98022	174	5	2883
46R-5, 0	436.1	8551	17	12	503				
47R-5, 0	445.7					88043	26	4	3386
51R-4, 0	482.9	42257	63	37	671				
52R-6, 0	495.5	25097	64	55	392				
53R-5, 0	503.7	35361	92	82	384				

Notes: HS = headspace; VAC = vacutainer.

Figure 23. Records of headspace methane (C₁), ethane (C₂), and propane (C₃) concentrations and C₁/C₂ ratios in sediments from Hole 910C. "BGH" marks the calculated depth of the base of gas hydrates possibly present at Hole 910C (see text for further explanation). Arrows indicate maximum concentrations of methane above the BGH.



cores retrieved from the A–C holes drilled at Site 910. Whole-round measurements of compressional-wave velocity were performed only on the sediments from Holes 910A and 910B. Velocity measurements were not performed on Hole 910C because it was rotary drilled, and thus disturbed. Figures 25 through 27 show the MST results for Holes 910A, 910B, and 910C, respectively. The plots for Holes 910A and 910B (0–25 mbsf and 0–15 mbsf, respectively) show that relatively fine scale (<1 m) variations occur in all four parameters. Despite the very poor core recovery for the upper 280 mbsf in Hole 910C, the plots for this hole show significant large-scale changes in GRAPE density, magnetic susceptibility, and natural gamma ac-

tivity. GRAPE density and natural gamma activity increase downhole as a general trend, although significant variability is noted; magnetic susceptibility increases to about 350 mbsf with large fluctuations overlain on a decreasing trend in the lower 150 m of the hole.

These changes correlate somewhat with the lithologic units defined by the sedimentologists (see "Lithostratigraphy" section, this chapter). The increase in magnetic susceptibility at 200 mbsf coincides with the boundary between lithologic Subunits IA and IB, which is defined by the increased occurrence of dropstones in Subunit IA. Lithologic variations at this site are otherwise minor, with the sediments primarily consisting of dark gray, homogeneous silty clays

Table 7. Summary of geochemical analyses of sediments in Hole 910C.

Core, section, interval top (cm)	Depth (mbsf)	TC (%)	IC (%)	TOC (%)	CaCO ₃ (%)	TN (%)	TS (%)	C/N	C/S
151-910A-									
1H-1, 5	0.05	1.04	0.27	0.77	2.2	0.09	0.00	8.5	
1H-1, 28	0.28	1.68	1.13	0.55	9.4	0.07	0.00	7.8	
1H-1, 68	0.68	0.44	0.14	0.30	1.2	0.00	8.36		0.0
1H-1, 112	1.12	1.09	0.33	0.76	2.7	0.07	0.11	11.0	6.9
1H-2, 58	2.08	1.08	0.33	0.75	2.7	0.08	0.11	9.4	6.8
1H-2, 116	2.66	1.01	0.73	0.28	6.1	0.08	0.14	3.5	2.0
1H-3, 9	3.09	1.01	0.28	0.73	2.3	0.08	0.18	9.1	4.0
1H-3, 112	4.12	1.04	0.31	0.73	2.6	0.08	0.17	9.1	4.3
1H-4, 51	5.01	1.04	0.27	0.77	2.2	0.08	0.14	9.6	5.5
2H-1, 28	5.78	0.99	0.28	0.71	2.3	0.08	0.10	8.9	7.1
2H-1, 108	6.58	1.07	0.39	0.68	3.2	0.09	0.10		
2H-2, 29	7.29	1.03	0.27	0.76	2.2	0.07	0.11	11.0	6.9
2H-2, 108	8.08	1.03	0.30	0.73	2.5	0.07	0.11	10.0	6.6
2H-3, 29	8.79	1.13	0.34	0.79	2.8	0.08	0.50	9.9	1.6
2H-3, 64	9.14	1.06	0.28	0.78	2.3	0.07	0.90	11.0	0.9
2H-3, 108	9.58	1.13	0.32	0.81	2.7	0.08	0.97	10.0	0.8
2H-4, 29	10.29	1.00	0.28	0.72	2.3	0.08	0.20	9.0	3.6
2H-4, 108	11.08	1.17	0.31	0.86	2.6	0.08	0.15	11.0	5.7
2H-5, 29	11.79	1.05	0.29	0.76	2.4	0.08	0.14	9.5	5.4
2H-5, 108	12.58	1.03	0.27	0.76	2.2	0.07	0.10	11.0	7.6
2H-6, 29	13.29	1.05	0.28	0.77	2.3	0.07	0.11	11.0	7.0
2H-6, 108	14.08	1.10	0.28	0.82	2.3	0.07	0.10	12.0	8.2
2H-CC, 29	14.38	1.11	0.28	0.83	2.3	0.07	0.13	12.0	6.4
3H-1, 28	15.28	1.10	0.27	0.83	2.2	0.08	0.14	10.0	5.9
3H-2, 28	16.78	1.05	0.24	0.81	2.0	0.09	0.16	9.0	5.0
3H-2, 63	18.03	1.33	0.27	1.06	2.2	0.10	7.16	10.6	0.2
3H-3, 54	18.54	1.09	0.28	0.81	2.3	0.08	0.11	10.0	7.3
3H-4, 60	19.50	1.17	0.29	0.88	2.4	0.09	0.77	9.8	1.1
4H-3, 22	22.72	1.11	0.28	0.83	2.3	0.08	0.18	10.0	4.6
151-910C-									
5R-2, 0	36.80	1.26	0.31	0.95	2.6	0.08	0.15	12.0	6.3
6R-1, 5	44.95	1.36	0.28	1.08	2.3	0.09	0.54	12.0	2.0
6R-1, 43	45.33	1.22	0.24	0.98	2.0	0.10	0.40	9.8	2.4
8R-1, 41	64.61	1.12	0.27	0.85	2.2	0.10	0.36	8.5	2.3
8R-1, 134	65.54	1.62	0.43	1.19	3.6	0.11	0.13	10.8	9.1
8R-2, 13	65.83	1.44	0.31	1.13	2.6	0.11	0.14	10.3	8.1
8R-2, 73	66.43	1.16	0.33	0.83	2.7	0.07	0.36	12.0	2.3
12R-1, 55	103.35	0.84	0.19	0.65	1.6	0.07	0.10	9.3	6.5
13R-1, 33	112.73	1.20	0.29	0.91	2.4	0.10	0.18	9.1	5.0
13R-1, 103	113.43	1.31	0.25	1.06	2.1	0.10	0.15	10.6	7.1
13R-2, 22	114.12	1.32	0.30	1.02	2.5	0.10	0.30	10.2	3.4
14R-1, 101	123.01	1.32	0.24	1.08	2.0	0.11	0.16	9.8	6.8
14R-2, 19	123.69	1.04	0.19	0.85	1.6	0.08	0.10	10.0	8.5
15R-1, 26	131.86	1.81	0.20	1.61	1.7	0.11	0.18	14.6	8.9
15R-2, 17	133.27	0.65	0.13	0.52	1.1	0.07	0.44	7.4	1.2
16R-1, 17	141.37	4.57	3.54	1.03	29.5	0.10	0.23	10.3	4.5
16R-1, 140	142.60	1.08	0.23	0.85	1.9	0.09	0.45	9.4	1.9
16R-2, 35	143.05	1.17	0.19	0.98	1.6	0.10	0.57	9.8	1.7
16R-3, 12	144.32	1.26	0.33	0.93	2.7	0.10	0.35	9.3	2.6
17R-1, 26	151.16	1.29	0.28	1.01	2.3	0.11	0.12	9.2	8.4
17R-2, 23	152.63	1.24	0.34	0.90	2.8	0.09	0.09	10.0	10.0
17R-3, 23	154.13	1.33	0.27	1.06	2.2	0.07	0.09	15.1	11.8
18R-1, 19	160.69	1.43	0.22	1.21	1.8	0.11	0.07	11.0	17.3
19R-1, 23	170.43	1.17	0.20	0.97	1.7	0.11	0.18	8.8	5.4
19R-3, 19	173.39	1.45	0.31	1.14	2.6	0.10	0.14	11.4	8.1
19R-5, 21	176.41	1.08	0.26	0.82	2.2	0.10	0.14	8.2	5.8
20R-1, 74	180.54	1.23	0.30	0.93	2.5	0.10	0.30	9.3	3.1
20R-3, 74	183.54	1.80	0.38	1.42	3.2	0.15	0.32	9.5	4.4
20R-5, 0	185.80	1.44	0.33	1.11	2.7	0.11	0.08	10.1	13.9
20R-5, 73	186.53	1.44	0.33	1.11	2.7	0.12	0.18	9.2	6.2
21R-1, 24	189.64	1.29	0.34	0.95	2.8	0.11	0.12	8.6	7.9
22R-1, 40	199.40	1.17	0.18	0.99	1.5	0.11	0.18	9.0	5.5
22R-3, 37	202.37	1.29	0.25	1.04	2.1	0.13	0.13	8.0	8.0
22R-5, 22	205.22	1.16	0.30	0.86	2.5	0.11	0.11	7.8	7.8
23R-1, 68	209.38	1.56	0.35	1.21	2.9	0.12	0.12	10.1	10.1
23R-3, 73	212.43	1.21	0.36	0.85	3.0	0.10	0.11	8.5	7.7
23R-5, 68	215.38	1.17	0.41	0.76	3.4	0.12	0.09	6.3	8.4
24R-1, 71	219.01	1.20	0.36	0.84	3.0	0.11	0.16	7.6	5.2
24R-3, 70	222.00	1.14	0.19	0.96	1.6	0.11	0.30	8.7	3.2
25R-1, 72	228.72	1.73	0.32	1.41	2.7	0.14	0.22	10.1	6.4
25R-3, 73	231.73	1.21	0.27	0.94	2.2	0.11	0.26	8.5	3.6
25R-5, 74	234.74	1.27	0.27	1.00	2.2	0.12	0.81	8.3	1.2
26R-1, 110	238.70	1.26	0.34	0.92	2.8	0.11	0.27	8.3	3.4
26R-3, 110	241.70	1.48	0.52	0.96	4.3	0.11	0.13	8.7	7.4
26R-5, 22	243.82	1.64	0.75	0.89	6.2	0.10	0.18	8.9	4.9
27R-1, 28	247.48	1.36	0.23	1.13	1.9	0.12	0.53	9.4	2.1
27R-2, 28	248.98	1.52	0.43	1.09	3.6	0.12	0.87	9.1	1.2
27R-3, 27	250.47	1.51	0.39	1.12	3.2	0.12	0.71	9.3	1.6
27R-4, 27	251.97	1.50	0.39	1.11	3.2	0.12	0.42	9.2	2.6
27R-5, 27	253.47	1.31	0.24	1.07	2.0	0.12	0.17	8.9	6.3
28R-1, 27	257.17	1.25	0.24	1.01	2.0	0.12	0.39	8.4	2.6
28R-2, 27	258.67	1.14	0.19	0.95	1.6	0.11	0.30	8.6	3.1
28R-3, 28	260.18	1.20	0.23	0.97	1.9	0.11	0.19	8.8	5.1
29R-1, 23	266.73	1.36	0.31	1.05	2.6	0.13	0.19	8.1	5.5
29R-3, 25	268.77	1.27	0.30	0.97	2.5	0.12	0.15	8.1	6.4
29R-4, 96	270.98	1.32	0.43	0.89	3.6	0.12	0.17	7.4	5.2

Table 7 (continued).

Core, section, interval top (cm)	Depth (mbsf)	TC (%)	IC (%)	TOC (%)	CaCO ₃ (%)	TN (%)	TS (%)	C/N	C/S
32R-1, 26	295.76	1.62	0.21	1.41	1.7	0.13	0.61	10.8	2.3
32R-3, 30	297.80	1.40	0.31	1.09	2.6	0.12	0.12	9.1	9.1
32R-5, 30	300.80	1.23	0.38	0.85	3.2	0.10	0.17	8.5	5.0
32R-7, 33	303.79	1.27	0.38	0.89	3.2	0.11	0.18	8.1	4.9
33R-1, 38	305.48	1.43	0.44	0.99	3.7	0.11	0.22	9.0	4.5
33R-2, 28	306.88	1.14	0.24	0.90	2.0	0.11	0.17	8.2	5.3
33R-3, 28	308.38	1.36	0.27	1.09	2.2	0.12	0.13	9.1	8.4
33R-4, 28	309.88	1.37	0.23	1.14	1.9	0.13	0.10	8.8	11.4
34R-1, 20	315.00	1.52	0.34	1.18	2.8	0.14	0.08	8.4	14.7
34R-3, 58	318.38	1.61	0.38	1.23	3.2	0.14	0.07	8.8	17.6
34R-5, 60	321.40	1.45	0.26	1.19	2.2	0.14	0.06	8.5	19.8
35R-1, 61	325.01	1.30	0.31	0.99	2.6	0.10	0.15	9.9	6.6
35R-3, 61	328.01	1.30	0.28	1.02	2.3	0.11	0.17	9.3	6.0
35R-5, 61	331.01	1.62	0.37	1.25	3.1	0.12	0.27	10.4	4.6
36R-1, 117	335.27	1.84	0.48	1.36	4.0	0.14	0.10	9.7	13.6
36R-3, 117	338.27	1.57	0.36	1.21	3.0	0.12	0.08	10.1	15.1
36R-5, 63	340.73	1.42	0.40	1.02	3.3	0.12	0.09	8.5	11.3
37R-1, 68	344.48	1.28	0.35	0.93	2.9	0.12	0.14	7.7	6.6
37R-3, 66	347.46	1.14	0.38	0.76	3.2	0.13	0.10	5.8	7.6
37R-5, 66	350.46	1.38	0.38	1.00	3.2	0.13	0.17	7.7	5.9
37R-7, 41	353.21	1.14	0.29	0.85	2.4	0.09	0.44	9.4	1.9
38R-1, 68	354.08	1.27	0.25	1.02	2.1	0.12	1.21	8.5	0.8
38R-3, 68	357.08	1.11	0.29	0.82	2.4	0.09	0.28	9.1	2.9
38R-5, 68	360.08	0.99	0.24	0.75	2.0	0.09	0.40	8.3	1.9
39R-1, 118	364.08	1.11	0.34	0.77	2.8	0.09	0.23	8.5	3.3
39R-3, 118	367.08	0.79	0.26	0.53	2.2	0.07	0.45	7.6	1.2
39R-4, 120	368.60	1.18	0.37	0.81	3.1	0.09	0.15	9.0	5.4
40R-1, 115	373.55	1.55	0.36	1.19	3.0	0.13	0.08	9.1	14.9
40R-3, 116	376.56	1.68	0.44	1.24	3.7	0.15	0.07	8.3	17.7
40R-5, 116	379.56	1.56	0.63	0.93	5.2	0.12	0.06	7.7	15.0
41R-1, 121	383.11	1.43	0.52	0.91	4.3	0.12	0.08	7.6	11.0
41R-2, 110	384.50	1.57	0.35	1.22	2.9	0.07	0.00	17.4	
41R-3, 121	386.11	1.50	0.25	1.25	2.1	0.12	0.10	10.4	12.5
41R-5, 122	389.12	1.13	0.29	0.84	2.4	0.11	0.41	7.6	2.0
42R-1, 101	392.51	1.18	0.26	0.92	2.2	0.06	0.57	15.0	1.6
42R-3, 101	395.51	1.23	0.25	0.98	2.1	0.07	0.57	14.0	1.7
42R-5, 101	398.51	1.16	0.25	0.91	2.1	0.12	0.56	7.6	1.6
42R-6, 0	399.00	1.20	0.27	0.93	2.2	0.11	0.64	8.4	1.4
43R-1, 100	402.20	1.24	0.35	0.89	2.9	0.10	0.32	8.9	2.8
43R-3, 101	405.21	1.12	0.32	0.80	2.7	0.00	0.07		11.0
43R-5, 113	408.33	1.29	0.36	0.93	3.0	0.09	0.12	10.0	7.7
44R-1, 101	411.81	1.27	0.05	1.22	0.4	0.10	0.11	12.2	11.1
44R-3, 84	414.64	1.47	0.50	0.97	4.2	0.08	0.05	12.0	19.0
44R-5, 101	417.81	1.46	0.37	1.09	3.1	0.12	0.09	9.1	12.1
45R-1, 84	421.34	1.49	0.44	1.05	3.7	0.11	0.06	9.5	17.5
45R-3, 84	424.34	1.36	0.41	0.95	3.4	0.08	0.06	12.0	16.0
45R-5, 84	427.34	1.44	0.62	0.82	5.2	0.13	0.13	6.3	6.3
46R-1, 82	430.92	1.44	0.47	0.97	3.9	0.12	0.13	8.1	7.4
46R-3, 82	433.92	1.54	0.53	1.01	4.4	0.08	0.00	12.6	
46R-5, 69	436.79	1.48	0.32	1.16	2.7	0.13	0.12	8.9	9.7
47R-1, 73	440.43	1.21	0.27	0.94	2.2	0.09	0.12	10.0	7.8
47R-3, 53	443.23	1.22	0.41	0.81	3.4	0.06	0.05	13.0	16.0
47R-5, 69	446.39	1.73	0.56	1.17	4.7	0.12	0.65	9.8	1.8
47R-7, 24	448.94	1.23	0.29	0.94	2.4	0.07	0.07	13.0	13.0
48R-1, 60	450.00	1.16	0.44	0.72	3.7	0.06	0.13	12.0	5.5
48R-3, 60	453.00	1.68	0.60	1.08	5.0	0.08	0.00	13.5	
48R-5, 60	456.00	1.72	0.68	1.04	5.7	0.12	0.06	8.7	17.3
49R-1, 59	459.59	1.32	0.23	1.09	1.9	0.09	0.21	12.1	5.2
49R-3, 59	462.59	1.24	0.36	0.88	3.0	0.00	0.00		
49R-5, 60	465.60	1.35	0.35	1.00	2.9	0.09	0.09	11.1	11.1
50R-1, 64	469.34	1.52	0.36	1.16	3.0	0.14	0.67	8.3	1.7
50R-3, 64	472.34	1.73	0.38	1.35	3.2	0.09	0.00	15.0	
50R-5, 64	475.34	1.12	0.20	0.92	1.7	0.08	0.59	11.0	1.5
51R-1, 62	479.02	1.13	0.15	0.98	1.2	0.07	0.40	14.0	2.4
51R-3, 62	482.02	1.32	0.33	0.99	2.7	0.09	0.86	11.0	1.1
52R-1, 63	488.63	1.07	0.17	0.90	1.4	0.08	0.47	11.0	1.9
52R-3, 63	491.63	1.27	0.32	0.95	2.7	0.06	0.31	16.0	3.0
52R-5, 63	494.63	1.28	0.25	1.03	2.1	0.09	0.64	11.4	1.6
53R-1, 66	498.36	1.30	0.21	1.09	1.7	0.08	0.08	13.6	13.6
53R-3, 66	501.36	1.24	0.40	0.84	3.3	0.05	0.07	17.0	12.0
53R-5, 115	504.38	1.27	0.29	0.98	2.4	0.07	0.07	14.0	14.0

Notes: IC = inorganic carbon; CaCO₃ = carbonate; TC = total carbon; TOC = total organic carbon; TN = total nitrogen, TS = total sulfur; C/N = total organic carbon/total nitrogen ratios; C/S = total organic carbon/total sulfur ratios.

and clayey silts. The increase in natural gamma activity below 400 mbsf coincides with an increased siliciclastic mineral abundance, which is used to designate lithologic Subunit IC.

Thermal Conductivity

Thermal conductivity measurements were performed only in Hole 910A and 910B. Although Hole 910C was the deepest hole, it was ro-

tary drilled and thus too disturbed to provide reliable thermal conductivity measurements. Measurements generally were performed in four whole-round sections from each core at 75 cm using a red rubber standard (conductivity = $0.96 + 0.05 \text{ W/m-K}$) each time to evaluate the degree of error in the measurements. Thermal conductivities ranged between 1.258 and $1.976 \text{ W/m-K} \pm 0.184$ (see Table 8). Although the data are widely scattered, a linear fit shows a general increase with depth. Figure 28 presents a plot of thermal conductivity

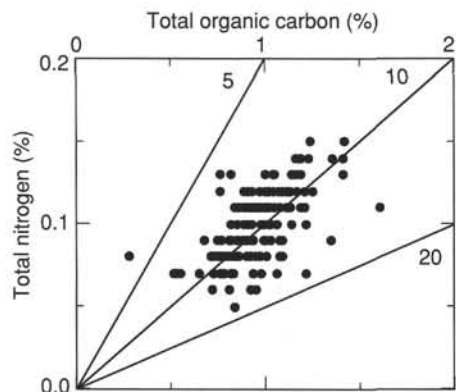


Figure 24. Diagram of total organic carbon vs. total nitrogen. Lines of C/N ratios of 5, 10, and 20 are indicated. Data points with nitrogen values of zero (determined on organic-carbon-lean samples) were not included in the diagram.

values alongside plots of wet-bulk density, wet water content, and porosity for 0–25 mbsf in Holes 910A and 910B. Some of the scatter in thermal conductivity may be the result of variations in the water content and porosity, as lower thermal conductivity correlates with higher water contents and porosities and vice versa. The average thermal conductivity for Holes 910A and 910B is 1.55 W/m-K, although the “average” is really reflecting the near surface (0–25 mbsf) of these sediments.

Heat Flow

The Adara Temperature Tool was used to measure downhole temperatures at the mud line, 3.30°C, and at two other depths in Hole 910C: 5.69°C at 64.20 mbsf and 6.74°C at 93.10 mbsf. From these discrete measurements the thermal gradient was determined as 37.0°C/km by a least squares fit of the data (Fig. 29). The downhole thermal gradient and the average thermal conductivity (1.55 W/m-K) were used to calculate an average heat flow of 57.4 mW/m² for (the upper 25 mbsf of) Site 910.

Split-core Measurements

Compressional Velocity

The velocities generally range between 1458 and 1699 m/s (see Table 9). Some notable exceptions of marked increase in velocity, 1789 and 1801 m/s, occur at depths of 18.55 and 17.99 mbsf, respectively. The general trend of velocity increase with depth is quite high (1450 to 1800 m/s) for this short interval (0 to 18.55 mbsf). High signal attenuation occurred in most of the Site 910 sediments, presumably because of excess fracturing caused by gas expansion (see “Organic Geochemistry” section, this chapter, for a discussion on the high gas content at Site 910); thus, reliable velocities could not be obtained below 45 mbsf. Three velocities were obtained at depths of approximately 230 mbsf and again at 339–341 mbsf. These depths correspond to intervals of lower gas content.

Travel times are typically picked automatically using a threshold of approximately 1.04 μ s. However, at Site 910, the transmitted signals had such low amplitudes that all the first break arrival times had to be hand picked. This subjective and variable picking leads to a lower degree of precision in the velocity spectrum. The sonic transducers of the digital sound velocimeter (DSV) were inserted along the core axis in Cores 151-910A-1H through -4H (0 to 20.06 mbsf), Cores 151-910B-1H through -2H (0 to 14.11 mbsf), and Cores 151-910C-1R through -3R (0 to 18.55 mbsf). Highly consolidated sediment was encountered at 151C-910-3R (19.43 mbsf), which precluded further use of the DSV. All Hamilton Frame measurements at Sites 910A and 910B were performed along the core axis using pieces of core removed from the liner. A single Hamilton Frame measurement was performed on Core 151-910A-4H (20.94 mbsf) and gave a velocity within 2 m/s of a DSV measurement of 151-910A-4H made only 0.88 m away. Velocity measurements are shown in Figure 30 alongside wet-bulk density, porosity, and strength. The downhole velocities from the sonic log tend to be higher than those measured in the laboratory because of lower in-situ temperature and higher pressure in the borehole.

Shear Strength

Both the mechanical vane shear and the hand-held penetrometer were used to measure strength where possible to provide a means of

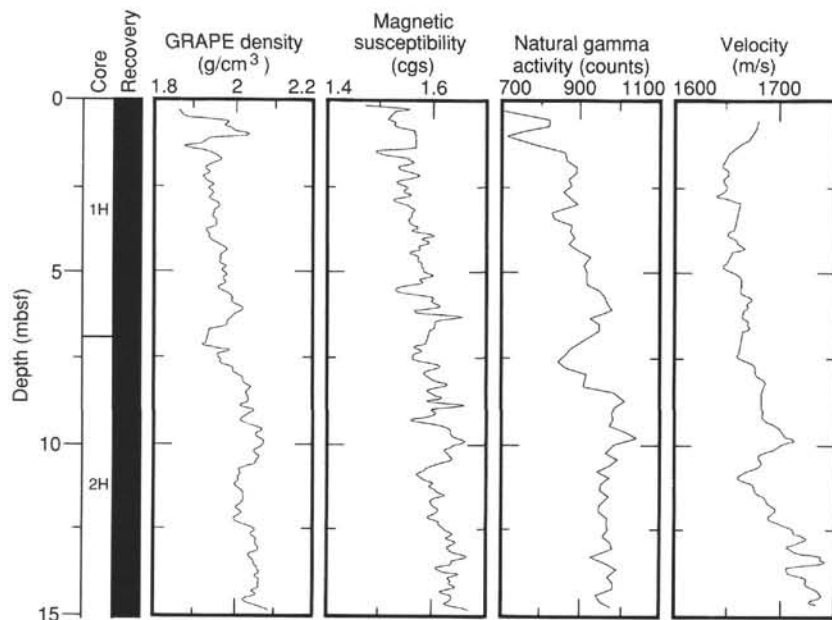


Figure 25. Multi-sensor track results for Hole 910A.

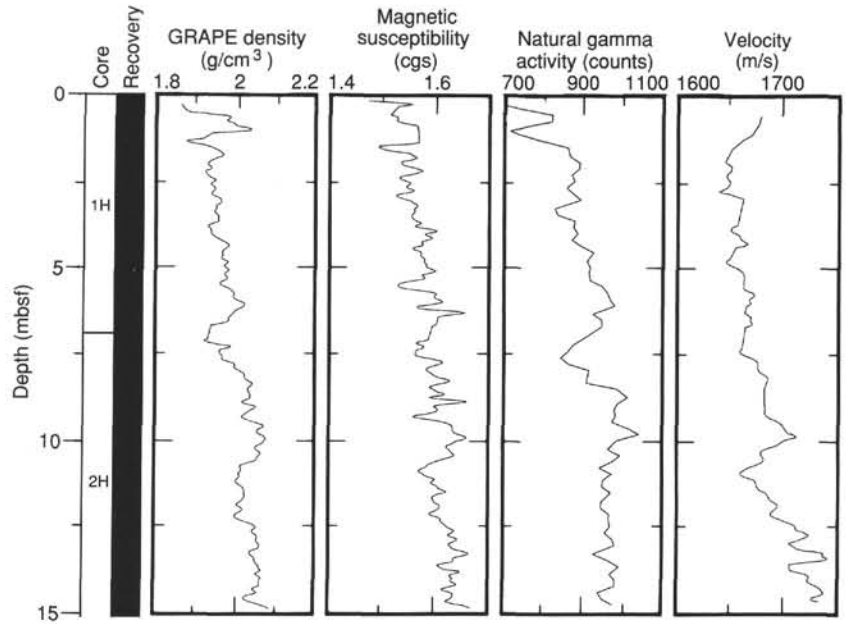


Figure 26. Multi-sensor track results for Hole 910B.

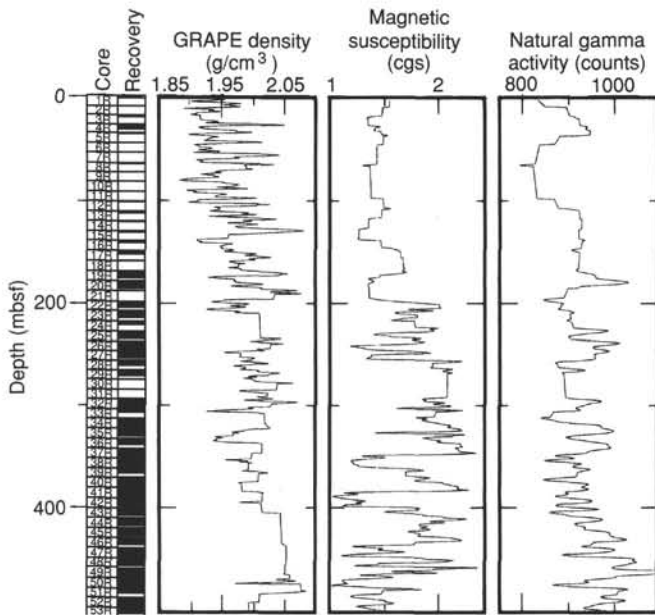


Figure 27. Multi-sensor track results for Hole 910C.

Table 8. Thermal conductivity measurements from Holes 910A and 910B.

Core, section, interval top (cm)	Depth (mbsf)	M	P #	TC _{corr} (W/m-K)	Std dev (W/m-K)	Drift (°C/min)
151-910A-						
1H-1, 75	0.75	F	332	1.310	0.00410	0.007
1H-2, 75	2.25	F	325	1.258	0.00467	-0.003
1H-3, 75	3.75	F	338	1.439	0.00279	0.005
1H-4, 75	4.90	F	339	1.711	0.00670	0.032
2H-2, 75	7.75	F	332	1.607	0.00154	0.018
2H-3, 75	9.25	F	325	1.383	0.00693	0.029
2H-5, 75	12.25	F	338	1.426	0.00198	-0.005
2H-6, 75	13.75	F	339	1.846	0.00330	0.025
3H-1, 75	15.75	F	332	1.566	0.00271	0.017
3H-2, 75	17.25	F	325	1.317	0.00424	0.010
3H-3, 75	18.75	F	338	1.830	0.00259	0.014
4H-1, 50	20.00	F	339	1.655	0.00157	0.015
4H-1, 100	20.50	F	332	1.445	0.00194	-0.004
4H-2, 75	21.75	F	325	1.536	0.00543	0.001
4H-3, 75	23.25	F	338	1.976	0.00159	0.028
151-910B-						
1H-1, 75	0.75	F	339	1.498	0.00302	0.009
1H-2, 75	2.25	F	332	1.464	0.00372	0.027
1H-3, 75	3.75	F	325	1.513	0.00231	0.010
1H-4, 75	5.25	F	338	1.724	0.00373	0.036
2H-2, 75	9.15	F	332	1.442	0.00198	0.004
2H-3, 75	10.65	F	325	1.702	0.00223	0.028
2H-4, 75	12.15	F	338	1.418	0.00200	-0.007
2H-6, 75	14.22	F	339	1.555	0.00208	-0.002

Notes: M = method used, either F = full-space or H = half-space; P # = probe number used for test; TC_{corr} = thermal conductivity corrected for drift; Std dev = standard deviation of the measurement.

comparison between the two instruments. Vane shear measurements were performed as deep as Section 151-910A-4H-1 (20.67 mbsf) of Hole 910A, throughout 151-910B-1H (to 15.6 mbsf) in Hole 910B, and only in Sections 151-910C-1R-1 (0.97 mbsf) and 151-910C-2R-1 (9.15 mbsf) of Hole 910C. Beyond these depths, only penetrometer measurements were performed. The penetrometer was used before the limit of the vane shear was reached, beginning in Section 151-910A-1H-3 and in Section 151-910C-1R-3. The data are presented in Table 10 and plotted in Figure 30. Notice that the vane shear and penetrometer values correlate well throughout the entire interval in which both measurements were performed.

A sharp increase with depth of 2.76 kPa/m is observed at Site 910 from 0 to 18 mbsf. At 18 mbsf, strength suddenly increases threefold. Between 45 and 103 mbsf, recovery was so poor that from strength data alone we are unable to determine just how deep this trend would have continued. Nevertheless, when good core recovery resumed

(103 mbsf), strength values dropped significantly and then followed a more gentle gradient (approximately 1 kPa/m), increasing with depth from values of approximately 74 to 221 kPa at 243 mbsf. Strength below 150 mbsf is, in general, high in the rotary drilled sequences but has significant variability as a result of biscuiting and disturbance.

The increases in shear strength and velocities at ~18 mbsf may indicate a higher degree of consolidation of the sediment at this level as reflected in an increase in bulk density and decrease in porosity (see Fig. 30). No marked change in composition is indicated at this depth (see "Lithostratigraphy" section, this chapter). Therefore, the idea that there is increased consolidation in the upper portion at Site 910

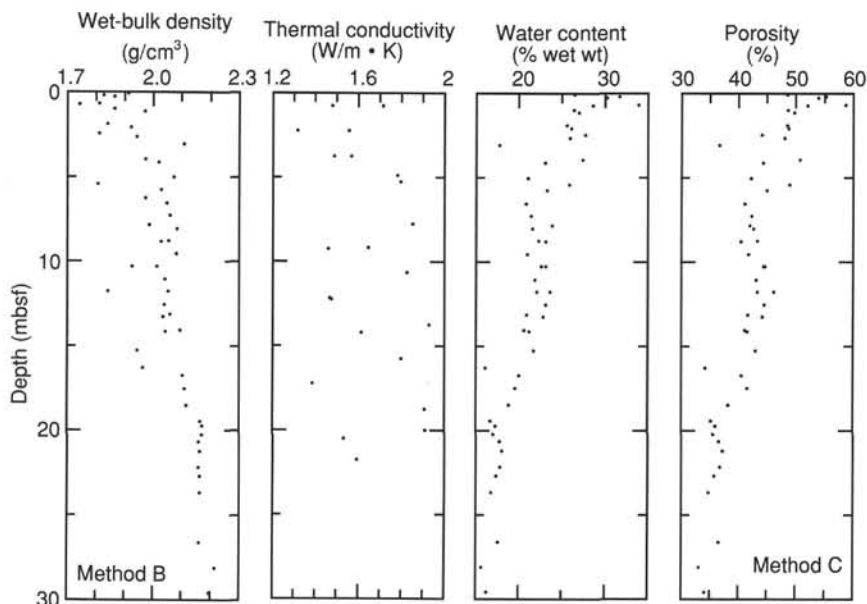


Figure 28. Wet-bulk density, thermal conductivity, wet water content, and porosity from the shallow region of Holes 910A and 910B.

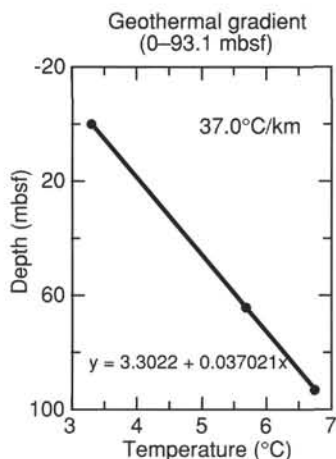


Figure 29. Thermal gradient measured downhole from Hole 910C.

Table 12 summarizes the mean values and range of index properties determined for each downhole interval at this site, as defined by the lithologic subunits (see “Lithostratigraphy” section, this chapter) and geotechnical units.

In geotechnical Unit G-I (0–19 mbsf), laboratory values of bulk density show a large increase from the seafloor (1.8 g/cm^3) to ~19 mbsf ($>2.1 \text{ g/cm}^3$); porosity values decrease from ~53% to <37% across this same interval, and shear strength increases sharply near the base of the unit (Table 12; Fig. 33). That such large changes in properties are observed at such shallow burial depths is quite anomalous and merits further investigation.

The boundary between geotechnical Units G-I and G-II is placed at 19 mbsf, where large increases in shear strength and bulk density, and decreases in porosity and water content are observed. Just below the transition to geotechnical Unit G-II in each of the holes drilled at Site 910, the core recovery decreased substantially, and the laboratory values of bulk density were the highest measured. The downhole property trends reversed slope below this level, as porosity increased and bulk density decreased to the base of geotechnical Unit G-II at ~190 mbsf.

Geotechnical Unit G-III is divided into two subunits at 317 mbsf. Although the overall trends observed in this unit are similar, the upper subunit (G-IIIA) exhibits slightly higher porosity and lower bulk density values than does the lower subunit (G-IIIB). The average properties of geotechnical Subunit G-IIIB are similar to those of geotechnical Unit G-II, but Subunit G-IIIB has more typical gradients in physical properties than the reversed gradients that are observed in Unit G-II.

Downhole boundaries for the geotechnical units are shown in Figure 33. This figure also illustrates the relationship between laboratory values of bulk density measured at Site 910 (uncorrected for rebound effects) and the in-situ bulk density curve for this sediment type, using a regression equation derived from rotary-drilled sediments that were recovered by the Deep Sea Drilling Project (Hamilton, 1976).

The in-situ bulk density curve for a terrigenous silty clay, determined by Hamilton (1976) using a surficial density value of 1.53 g/cm^3 , is defined by the equation:

$$\text{Bulk density (g/cm}^3\text{)} = 1.530 + 1.395(D) - 0.617(D^2), \quad (1)$$

needs to be confirmed by shore-based geotechnical studies. Hole 910D was drilled for this specific purpose.

Index Properties

Index properties were determined by gravimetric methods using discrete samples taken at a rate of two samples/core section in each hole at Site 910. Values of index properties from both methods are presented in Table 11. Figure 31 presents the wet-bulk density, grain density, wet water content, and porosity. Figure 32 shows dry-bulk density, strength, void ratio, and dry water content. All these data show steeper property gradients in the upper 30 mbsf and more gradual trends deeper in Hole 910C.

Geotechnical Units

The sedimentary sequence that was cored at Site 910 was divided into three geotechnical units based on an evaluation of the downhole trends in laboratory index property and shear strength measurements.

Table 9. Compressional-wave velocity measurements from Holes 910A, 910B, and 910C.

Core, section, interval (cm)	Tool	Depth (mbsf)	Velocity (m/s)		Core, section, interval (cm)	Tool	Depth (mbsf)	Velocity (m/s)	
			Perp	Par				Perp	Par
151-910A-				151-910B-					
1H-1, 20-27	dsv	0.20	1000		1H-1, 125-132	dsv	1.25	1556	
1H-1, 33-40	dsv	0.33	1588		1H-2, 43-50	dsv	1.93	1572	
1H-1, 70-77	dsv	0.70	1588		1H-3, 35-42	dsv	3.35	1574	
1H-1, 108-115	dsv	1.08	1579		1H-4, 35-42	dsv	4.85	1551	
1H-2, 25-32	dsv	1.75	1516		1H-5, 30-37	dsv	6.30	1572	
1H-2, 118-125	dsv	2.68	1538		2H-1, 35-42	dsv	7.25	1544	
1H-3, 25-32	dsv	3.25	1458		2H-3, 35-42	dsv	10.25	1641	
1H-3, 114-121	dsv	4.14	1493		2H-4, 35-42	dsv	11.75	1618	
1H-4, 48-55	dsv	4.98	1554		2H-5, 20-27	dsv	13.10	1657	
1H-4, 48-55	dsv	4.98	1556		2H-6, 64-71	dsv	14.11	1671	
2H-1, 50-57	dsv	6.00	1594		151-910C-				
2H-2, 50-57	dsv	7.50	1620		1R-1, 94-101	dsv	0.94	1590	
2H-2, 100-107	dsv	8.00	1585		2R-1, 59-66	dsv	9.09	1586	
2H-3, 50-57	dsv	9.00	1639		3R-1, 59-66	dsv	17.99	1801	
2H-3, 110-117	dsv	9.60	1641		3R-1, 115-122	dsv	18.55	1789	
2H-4, 110-117	dsv	11.10	1628		3R-2, 53-55	ham	19.43	1704	
2H-5, 43-50	dsv	11.93	1585		4R-1, 24-26	ham	26.64	1689	
2H-5, 43-50	dsv	11.93	1558		4R-2, 24-26	ham	28.14	1643	
2H-6, 50-57	dsv	13.50	1592		6R-1, 36-38	ham	45.26	1601	
3H-1, 92-99	dsv	15.92	1649		25R-2, 132-134	ham	230.82	1699	
3H-1, 134-141	dsv	16.34	1663		36R-4, 63-65	ham	339.23	1620	
3H-2, 23-30	dsv	16.73	1651		36R-5, 63-65	ham	340.73	1557	
3H-2, 100-107	dsv	17.50	1684						
3H-3, 37-44	dsv	18.37	1653						
4H-1, 36-43	dsv	19.86	1641						
4H-1, 56-63	dsv	20.06	1669						
4H-1, 144-146	ham	20.94	1667						

Note: Tool = device used for measurement, either dsv = digital sound velocimeter or ham = Hamilton Frame. Perp = perpendicular, Par = parallel.

where D = sediment depth in kilometers. The laboratory bulk densities measured at Site 910 all plot well above the Hamilton in-situ curve shown in Figure 33. This result is quite intriguing because, if the data are corrected (rebound corrections) to account for the porosity expansion during recovery, and thus adjusted to in-situ conditions, then the lab values would effectively move further away from the predicted curve (move toward higher values of density), rather than toward it.

An additional in-situ density curve was constructed using the same regression equation, but substituting the average bulk density measured in the upper 1 m of sediment at Site 910 (1.84 g/cm³; see Table 12) rather than the original value used by Hamilton (1976). A comparison between the laboratory bulk density measurements and

the revised in-situ curve (Fig. 33) shows that rebound corrections applied to the laboratory values from the deeper parts of the sedimentary column would result in higher density values, and thus move the data closer to this predicted curve. However, the upper (shallower) laboratory values would still remain too high by a significant margin, given the homogenous nature of the sediments.

The most likely explanation for the anomalies in physical properties at Site 910 is that the sediments have been subjected to increased overburden pressures in the past (increased levels of vertical effective stress; i.e., vertical loading), and that this excess overburden caused an apparent overconsolidation of the sedimentary column, which decreases with depth and may be dissipated by fluid escape through deeper, more permeable sedimentary layers. Two possible mecha-

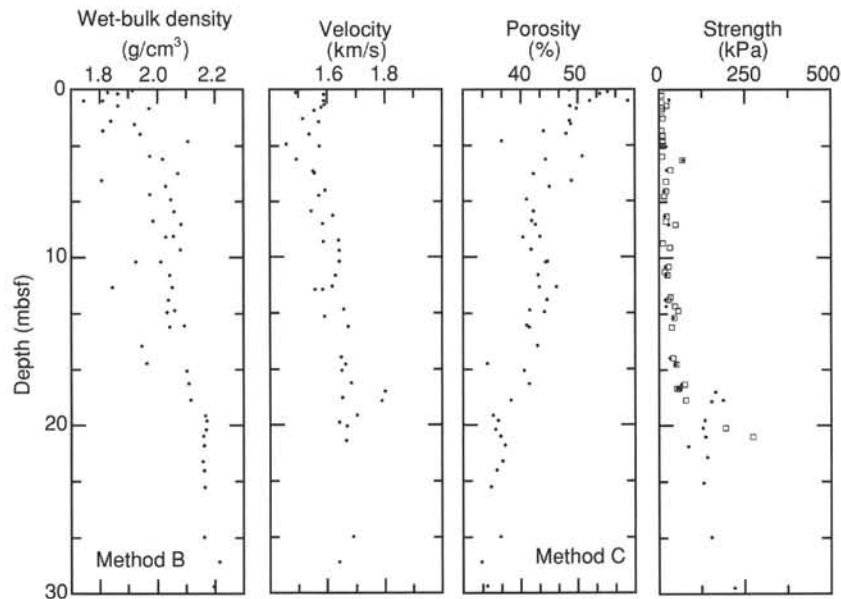


Figure 30. Velocity, wet-bulk density, porosity, and strength (closed circles = vane shear; open squares = penetrometer) from the shallow regions of Holes 910A, 910B, and 910C.

Table 10. Strength measurements from Holes 910A, 910B, and 910C.

Core, section, interval (cm)	Depth (mbsf)	SN	Vane (kPa)	Res (kPa)	Pen (kPa)	Core, section, interval (cm)	Depth (mbsf)	SN	Vane (kPa)	Res (kPa)	Pen (kPa)
151-910A-						13R-2, 25-26	114.15				159
1H-1, 35-36	0.35	3	8	4		14R-1, 115-116	123.15				155
1H-1, 77-78	0.77	3	9	5		14R-2, 25-26	123.75				127
1H-1, 112-113	1.12	3	9	8		15R-1, 25-26	131.85				74
1H-2, 23-24	1.73	3	11	6		15R-1, 60-61	132.20				83
1H-2, 121-122	2.71	3	12	5		15R-1, 110-111	132.70				96
1H-3, 30-31	3.07	3	12	8		15R-2, 13-14	133.23				78
1H-3, 119-120	3.30	3	14	8		16R-1, 45-46	141.65				74
1H-3, 7-8	4.19	3	69	30	71	16R-1, 80-81	142.00				74
1H-4, 30-31	4.80	3	34	17	33	16R-1, 110-111	142.30				74
2H-1, 55-56	6.05	3	20	9	22	16R-2, 25-26	142.95				108
2H-2, 55-56	7.55	3	23	13	25	16R-2, 45-46	143.15				113
2H-2, 104-105	8.04	3	48	11	42	16R-2, 70-71	143.40				132
2H-4, 104-105	10.53	3	28	14	19	17R-1, 21-22	151.11				135
2H-4, 53-54	11.04	3	24	13	21	17R-1, 74-75	151.64				119
2H-5, 102-103	12.52	3	27	14	18	17R-2, 75-76	153.15				170
2H-5, 140-141	12.90	3	47	22	32	17R-3, 65-66	154.55				210
2H-6, 55-56	13.55	3	44	25	40	18R-1, 31-32	160.81				164
3H-1, 94-95	15.94	3	41	21	333	19R-1, 18-19	170.38				129
3H-1, 131-132	16.31	3	50	25	49	19R-2, 19-20	171.89				163
3H-2, 104-105	17.54	3	75	45	65	19R-3, 17-18	173.37				186
3H-2, 126-127	17.76	3	53	25	54	19R-4, 19-20	174.89				179
3H-2, 130-131	17.80	3	57	26	62	19R-5, 19-20	176.39				199
3H-3, 50-51	18.50	3	79	36	188	20R-1, 75-76	180.55				110
4H-1, 65-66	19.70					20R-2, 75-76	182.05				178
4H-1, 117-118	20.15	3	195	170	127	20R-3, 75-76	183.55				166
4H-1, 20-21	20.67	4	274		136	20R-4, 73-74	185.03				168
4H-2, 25-26	21.25				128	20R-5, 73-74	186.53				197
4H-2, 90-91	21.90				141	21R-1, 22-23	189.62				91
4H-3, 90-91	23.40				129	22R-1, 75-76	199.75				109
151-910B-						22R-2, 75-76	201.25				190
1H-1, 128-129	1.28	1	7	3		22R-3, 75-76	202.75				185
1H-2, 95-96	2.45	1	8	5		22R-4, 78-79	204.28				167
1H-3, 95-96	3.95	1	10	5		22R-5, 72-73	205.72				167
1H-4, 95-96	5.45	3	20	12		23R-1, 70-71	209.40				185
1H-5, 33-34	6.33	1	15	11		23R-2, 70-71	210.90				202
2H-1, 94-95	7.84	1	21	10		23R-3, 70-71	212.40				197
2H-2, 100-101	9.40	1	33	21		23R-4, 70-71	213.90				214
2H-3, 94-95	10.84	1	18	9		23R-5, 70-71	215.40				216
2H-4, 94-95	12.34	1	33	18		24R-1, 70-71	219.00				134
2H-5, 24-25	13.14	1	56			24R-2, 72-73	220.52				169
2H-6, 67-68	14.14	1	36	20		24R-3, 30-31	221.60				172
151-910C-						25R-1, 50-51	228.50				151
1R-1, 61-62	0.97	1	23	12		25R-2, 51-52	230.01				163
2R-1, 65-66	0.61				29	25R-3, 69-70	231.69				180
2R-1, 97-98	9.15	1	12	6		25R-4, 70-71	233.20				195
3R-1, 60-61	18.00				164	26R-1, 125-126	238.85				216
3R-1, 118-119	18.58				154	26R-2, 125-126	240.35				174
4R-1, 25-26	26.65				153	26R-3, 125-126	241.85				207
4R-3, 25-26	29.65				221	26R-4, 125-126	243.35				203
5R-1, 24-25	35.54				190						
5R-2, 17-18	36.97				178						
6R-1, 36-37	45.26				221						
12R-1, 60-61	103.40				162						
13R-1, 40-41	112.80				162						
13R-1, 100-101	113.40				169						

Notes: SN = numbered spring used to make the measurement. Vane = undrained shear strength; Res = residual shear strength; Pen = unconfined shear strength as measured by the penetrometer.

nisms for loading the sediments at this site are (1) a mass of additional sediments that has since been removed, or (2) an equivalent mass of ice resting on this site in the geologic past.

At Site 910, the interval of high strength near 19 mbsf (Unit G-I/G-II boundary) exhibits the highest densities measured downhole and also the largest excess density values above the predicted curves. An estimate of the amount of excess bulk density can be determined by subtracting the predicted values from the laboratory measurements. In Figure 34, the excess density at 19 mbsf is about 0.3 g/cm³ (before rebound corrections) and this excess increases to almost 0.4 g/cm³ near 40 mbsf, even allowing for the more disturbed nature of the sediment recovered by rotary drilling at this level. The amount of excess density observed at these shallow burial depths suggests that about 150–300 m of silty clay, or an equivalent mass of other material (such as ice), was originally present at this site, but has since been removed. Corrections to the laboratory values to in-situ conditions (correction for porosity increase due to rebound of sediment upon core recovery) would increase this excess density to the equivalent of ~350–500 m of silty clay overburden, or an equivalent mass of ice. If the grain size of these sediments is actually coarser than the silty clay

described by the shipboard sedimentologists, then these estimates of excess density would, of course, be reduced accordingly. Only shore-based testing can resolve these uncertainties about the degree of over-consolidation of these sediments.

Hole 910D: A Dedicated Geotechnical Drillhole

Hole 910D was proposed as a dedicated geotechnical borehole to acquire a relatively undisturbed sedimentary section from this site on the Yermak Plateau. The cores from this hole will be used to perform post-cruise geotechnical testing and geoaoustic measurements under in-situ pressures and controlled environmental conditions in shore-based laboratories. These cores are also intended for use in the potential intercalibration of shore-based systems and the multi-sensor track on board the drill ship.

Hole 910D was drilled at 80°15.881'N, 06°35.424'E, in 567.7 m of water on the Yermak Plateau. Hole 910D comprised three APC cores and 15 XCB cores. The total depth of the cored section was 160.6 mbsf. The recovery was 99.7% in the APC section to 18.6 mbsf, dropping off throughout the XCB cored interval from 18.6 to

Table 11. Index properties of samples from Holes 910A, 910B, and 910C.

Core, section, interval (cm)	Depth (mbsf)	WC-d (%)	WC-w (%)	WBD ^a (g/cm ³)	WBD ^b (g/cm ³)	GD ^a (g/cm ³)	GD ^b (g/cm ³)	DBD ^a (g/cm ³)	DBD ^b (g/cm ³)	Por ^a (%)	Por ^b (%)	VR ^a	VR ^b
151-910A-													
IH-1, 6-8	0.06	35.94	26.44	1.91	1.88	2.78	2.69	1.41	1.38	49.35	48.53	0.97	0.94
IH-1, 28-30	0.28	43.31	30.22	1.86	1.83	2.89	2.77	1.30	1.28	54.95	53.90	1.22	1.17
IH-1, 114-116	1.14	36.93	26.97	1.97	1.89	2.99	2.75	1.44	1.38	51.87	49.76	1.08	0.99
IH-2, 58-60	2.08	35.34	26.11	1.92	1.91	2.78	2.76	1.42	1.41	48.94	48.78	0.96	0.95
IH-2, 114-116	2.64	35.02	25.94	1.94	1.90	2.83	2.71	1.44	1.41	49.14	48.08	0.97	0.93
IH-3, 6-8	3.06	21.56	17.74	2.11	2.12	2.73	2.76	1.73	1.74	36.46	36.70	0.57	0.58
IH-3, 114-116	4.14	30.01	23.08	2.02	1.97	2.85	2.72	1.55	1.51	45.46	44.35	0.83	0.80
IH-4, 52-54	5.02	26.68	21.06	2.07	2.05	2.85	2.81	1.64	1.62	42.57	42.22	0.74	0.73
2H-1, 27-29	5.77	30.34	23.28	2.03	1.98	2.89	2.76	1.56	1.52	46.09	44.99	0.85	0.82
2H-1, 105-107	6.55	26.34	20.85	2.05	2.02	2.78	2.71	1.62	1.60	41.65	41.06	0.71	0.70
2H-2, 27-29	7.27	27.35	21.48	2.06	2.02	2.84	2.74	1.62	1.58	43.13	42.27	0.76	0.73
2H-2, 105-107	8.05	27.60	21.63	2.08	2.02	2.91	2.76	1.63	1.58	43.96	42.60	0.78	0.74
2H-3, 27-29	8.77	28.75	22.33	2.06	1.99	2.89	2.73	1.60	1.55	44.78	43.36	0.81	0.77
2H-3, 105-107	9.55	26.65	21.04	2.08	2.03	2.87	2.76	1.64	1.61	42.71	41.78	0.75	0.72
2H-4, 27-29	10.27	30.10	23.14	1.93	1.98	2.62	2.75	1.48	1.52	43.47	44.70	0.77	0.81
2H-4, 105-107	11.05	27.99	21.87	2.04	2.02	2.83	2.77	1.60	1.58	43.58	43.08	0.77	0.76
2H-5, 27-29	11.77	28.41	22.12	2.05	2.01	2.87	2.76	1.60	1.56	44.28	43.30	0.79	0.76
2H-5, 105-107	12.55	30.12	23.15	2.04	1.97	2.90	2.73	1.57	1.52	46.04	44.54	0.85	0.80
2H-6, 27-29	13.27	29.59	22.84	2.04	1.98	2.87	2.74	1.57	1.53	45.34	44.17	0.83	0.79
2H-6, 105-107	14.05	26.02	20.65	2.10	2.04	2.88	2.75	1.66	1.62	42.21	41.11	0.73	0.70
3H-1, 25-27	15.25	27.78	21.74	1.94	2.02	2.59	2.78	1.52	1.58	41.25	42.93	0.70	0.75
3H-1, 130-132	16.30	19.21	16.11	1.96	2.18	2.38	2.78	1.65	1.83	30.86	34.22	0.45	0.52
3H-2, 25-27	16.75	25.06	20.04	2.10	2.07	2.86	2.79	1.68	1.66	41.11	40.55	0.70	0.68
3H-2, 102-104	17.52	24.34	19.58	2.11	2.17	2.84	2.99	1.70	1.75	40.28	41.52	0.67	0.71
3H-3, 50-52	18.50	23.20	18.83	2.12	2.08	2.81	2.73	1.72	1.69	38.89	38.21	0.64	0.62
4H-1, 23-25	19.73	20.97	17.33	2.17	2.13	2.84	2.75	1.80	1.76	36.74	36.01	0.58	0.56
4H-1, 75-77	20.25	20.50	17.01	2.17	2.14	2.81	2.76	1.80	1.78	36.02	35.59	0.56	0.55
4H-1, 117-119	20.67	21.56	17.73	2.16	2.11	2.84	2.74	1.78	1.74	37.37	36.53	0.60	0.58
4H-2, 21-23	21.21	22.03	18.05	2.16	2.12	2.86	2.76	1.77	1.73	38.09	37.26	0.62	0.59
4H-2, 117-119	22.17	21.65	17.80	2.16	2.12	2.84	2.76	1.77	1.74	37.47	36.79	0.60	0.58
4H-3, 21-23	22.71	21.00	17.36	2.16	2.11	2.82	2.72	1.79	1.75	36.64	35.77	0.58	0.56
4H-3, 117-119	23.67	20.20	16.80	2.16	2.12	2.79	2.71	1.80	1.77	35.47	34.78	0.55	0.53
151-910B-													
IH-1, 19-21	0.19	46.40	31.69	1.83	1.79	2.87	2.73	1.25	1.22	56.51	55.26	1.30	1.24
IH-1, 68-70	0.68	51.30	33.91	1.81	1.78	2.99	2.84	1.20	1.17	59.92	58.72	1.50	1.42
IH-2, 38-40	1.88	34.34	25.56	1.84	1.95	2.53	2.82	1.37	1.45	45.87	48.55	0.85	0.94
IH-2, 96-98	2.46	38.38	27.73	1.81	1.63	2.57	2.10	1.31	1.18	49.01	44.07	0.96	0.79
IH-3, 95-97	3.95	37.79	27.42	1.97	1.90	3.03	2.79	1.43	1.38	52.80	50.75	1.12	1.03
IH-4, 93-95	5.43	34.94	25.90	1.81	1.94	2.46	2.81	1.34	1.43	45.64	48.92	0.84	0.96
IH-5, 25-27	6.25	32.72	24.65	1.97	3.02	2.83	8.27	1.49	2.27	47.47	72.53	0.90	2.64
2H-1, 94-96	7.84	31.37	23.88	1.99	1.80	2.81	2.37	1.51	1.37	46.26	41.99	0.86	0.72
2H-2, 40-42	8.80	30.13	23.15	2.03	1.79	2.88	2.31	1.56	1.38	45.84	40.44	0.85	0.68
2H-3, 38-40	10.28	29.17	22.58	2.01	2.02	2.80	2.81	1.56	1.56	44.35	44.43	0.80	0.80
2H-4, 38-40	11.78	30.96	23.64	1.84	2.00	2.45	2.85	1.41	1.53	42.53	46.24	0.74	0.86
2H-5, 23-25	13.13	26.47	20.93	2.06	2.04	2.81	2.76	1.63	1.61	42.08	41.65	0.73	0.71
2H-6, 68-70	14.15	26.90	21.20	2.04	2.01	2.79	2.71	1.61	1.58	42.27	41.52	0.73	0.71
151-910C-													
1R-1, 70-72	0.70	40.10	28.62	1.74	1.87	2.43	2.78	1.24	1.33	48.69	52.12	0.95	1.09
1R-1, 99-101	0.99	35.88	26.40	1.86	1.89	2.64	2.71	1.37	1.39	48.04	48.66	0.92	0.95
3R-2, 54-56	19.44	20.08	16.72	2.17	2.16	2.79	2.77	1.80	1.80	35.34	35.20	0.55	0.54
4R-1, 23-25	26.63	21.40	17.63	2.16	2.13	2.83	2.76	1.78	1.75	37.18	36.55	0.59	0.58
4R-2, 23-25	28.13	18.62	15.69	2.22	2.17	2.83	2.74	1.87	1.83	33.92	33.19	0.51	0.50
4R-3, 19-21	29.59	19.49	16.31	2.20	2.15	2.83	2.73	1.84	1.80	34.96	34.16	0.54	0.52
4R-4, 22-24	31.12	19.51	16.33	2.21	2.16	2.85	2.75	1.85	1.80	35.19	34.34	0.54	0.52
4R-5, 15-17	32.55	18.90	15.89	2.25	2.15	2.90	2.72	1.89	1.81	34.83	33.40	0.53	0.50
5R-1, 23-25	35.53	20.45	16.98	2.20	2.13	2.88	2.73	1.83	1.77	36.48	35.24	0.57	0.54
5R-2, 17-19	36.97	19.39	16.24	2.22	2.15	2.88	2.74	1.86	1.80	35.24	34.14	0.54	0.52
6R-1, 3-5	44.93	20.18	16.80	2.23	2.16	2.93	2.78	1.86	1.80	36.55	35.41	0.58	0.55
6R-1, 40-42	45.30	21.46	17.67	2.15	2.11	2.82	2.73	1.77	1.74	37.12	36.38	0.59	0.57
11R-1, 10-12	93.20	29.84	22.98	2.05	1.99	2.91	2.76	1.58	1.53	45.87	44.58	0.85	0.80
12R-1, 51-53	103.31	21.84	17.93	2.13	2.09	2.79	2.70	1.75	1.71	37.28	36.54	0.59	0.58
13R-1, 30-32	112.70	24.51	19.68	2.07	2.03	2.77	2.67	1.67	1.63	39.84	38.99	0.66	0.64
13R-1, 99-101	113.39	23.73	19.18	2.09	2.05	2.78	2.69	1.69	1.66	39.16	38.37	0.64	0.62
13R-2, 20-22	114.10	23.72	19.17	2.09	2.06	2.78	2.71	1.69	1.66	39.11	38.53	0.64	0.63
14R-1, 99-101	122.99	29.49	22.77	1.98	1.95	2.73	2.67	1.53	1.51	44.01	43.41	0.79	0.77
14R-2, 19-21	123.69	22.24	18.19	2.11	2.07	2.75	2.68	1.72	1.69	37.37	36.76	0.60	0.58
15R-1, 22-24	131.82	26.00	20.64	2.01	1.99	2.68	2.63	1.59	1.58	40.45	40.06	0.68	0.67
15R-1, 110-112	132.70	23.44	18.99	2.09	2.05	2.76	2.68	1.69	1.66	38.69	38.05	0.63	0.61
16R-1, 30-32	141.50	27.30	21.45	2.01	1.98	2.72	2.67	1.58	1.56	42.05	41.52	0.73	0.71
16R-1, 106-108	142.26	27.96	21.85	2.04	2.00	2.83	2.74	1.60	1.57	43.57	42.74	0.77	0.75
16R-2, 31-33	143.01	29.97	23.06	1.99	1.94	2.76	2.66	1.53	1.49	44.68	43.71	0.81	0.78
16R-2, 106-108	143.76	24.67	19.79	2.08	2.04	2.78	2.69	1.67	1.63	40.12	39.29	0.67	0.65
16R-3, 10-12	144.30	25.39	20.25	2.09	2.04	2.84	2.72	1.67	1.62	41.27	40.23	0.70	0.67
17R-1, 27-29	151.17	27.90	21.82	2.03	1.98	2.80	2.68	1.59	1.55	43.28	42.20	0.76	0.73
17R-2, 24-26	152.64	27.88	21.80	2.08	2.00	2.93	2.72	1.63	1.56	44.32	42.49	0.80	0.74
17R-3, 24-26	154.14	26.80	21.13	2.04	2.01	2.77	2.72	1.61	1.59	42.00	41.53	0.72	0.71
18R-1, 21-23	160.71	27.65	21.66	2.04	2.00	2.81	2.71	1.60	1.56	43.15	42.20	0.76	0.73
19R-1, 21-23	170.41	28.31	22.06	2.05	1.99	2.85	2.71	1.60	1.55	44.05	42.83	0.79	0.75
19R-2, 21-23	171.91	24.98	19.99	2.09	2.04	2.82	2.72	1.67	1.63	40.72	39.83	0.69	0.66
19R-3, 17-19	173.37	24.43	19.64	2.08	2.02	2.77	2.64	1.67	1.62	39.76	38.64	0.66	0.63
19R-4, 19-21	174.89	25.55	20.35	2.07	1.76	2.81	2.16	1.65	1.40	41.17	35.01	0.70	0.54
20R-1, 73-75	180.53	24.43	19.64	2.11	2.07	2.84	2.75	1.69	1.66	40.39	39.62	0.68	0.66
20R-2, 74-76	182.04	29.08	22.53	2.04	1.99	2.87	2.74	1.58	1.54	44.88	43.73	0.81	0.78
20R-3, 77-79	183.57	30.64	23.46	1.99	1.93	2.79	2.65	1.52	1.48	45.48	44.24	0.83	0.79
20R-4, 73-75	185.03	31.19	23.78	1.99	1.94	2.81	2.69	1.52	1.48	46.11	45.01	0.86	0.82

Table 11 (continued).

Core, section, interval (cm)	Depth (mbsf)	WC-d (%)	WC-w (%)	WBD ^a (g/cm ³)	WBD ^b (g/cm ³)	GD ^a (g/cm ³)	GD ^b (g/cm ³)	DBD ^a (g/cm ³)	DBD ^b (g/cm ³)	Por ^a (%)	Por ^b (%)	VR ^a	VR ^b
21R-1, 19-21	189.59	27.89	21.81	2.04	2.00	2.83	2.72	1.60	1.56	43.50	42.49	0.77	0.74
22R-1, 37-39	199.37	19.25	16.15	2.21	2.16	2.85	2.75	1.86	1.81	34.88	34.06	0.54	0.52
22R-2, 48-50	200.98	19.18	16.10	2.16	2.11	2.75	2.64	1.81	1.77	33.94	33.06	0.51	0.49
22R-3, 36-38	202.36	27.30	21.44	2.03	2.01	2.77	2.72	1.60	1.58	42.48	42.01	0.74	0.72
22R-4, 74-76	204.24	23.65	19.12	2.12	2.07	2.83	2.72	1.71	1.67	39.49	38.58	0.65	0.63
22R-5, 25-27	205.25	30.32	23.26	1.99	1.95	2.78	2.69	1.52	1.50	45.11	44.28	0.82	0.79
23R-1, 73-75	209.43	28.98	22.47	2.05	1.99	2.89	2.73	1.59	1.54	44.96	43.56	0.82	0.77
23R-2, 73-75	210.93	30.01	23.08	2.04	1.97	2.90	2.72	1.57	1.52	45.92	44.37	0.85	0.80
23R-3, 76-78	212.46	28.49	22.17	2.02	1.70	2.78	2.09	1.57	1.32	43.62	36.74	0.77	0.58
23R-4, 72-74	213.92	29.34	22.68	2.01	1.96	2.81	2.68	1.56	1.52	44.54	43.45	0.80	0.77
23R-5, 72-74	215.42	28.64	22.26	2.05	1.99	2.86	2.73	1.59	1.55	44.44	43.31	0.80	0.76
24R-1, 71-73	219.01	28.91	22.43	2.02	1.97	2.81	2.69	1.57	1.53	44.17	43.17	0.79	0.76
24R-2, 71-73	220.51	25.36	20.23	2.09	2.05	2.83	2.74	1.67	1.63	41.22	40.40	0.70	0.68
24R-3, 30-32	221.60	27.32	21.46	2.04	1.97	2.79	2.63	1.60	1.55	42.65	41.24	0.74	0.70
25R-1, 70-72	228.70	26.81	21.14	2.07	2.02	2.86	2.73	1.64	1.59	42.77	41.68	0.75	0.71
25R-2, 71-73	230.21	25.77	20.49	2.12	2.05	2.91	2.76	1.68	1.63	42.28	41.01	0.73	0.70
25R-3, 71-73	231.71	28.60	22.24	2.05	2.01	2.88	2.77	1.60	1.56	44.56	43.62	0.80	0.77
25R-4, 71-73	233.21	27.63	21.65	2.04	2.00	2.81	2.71	1.60	1.57	43.14	42.21	0.76	0.73
25R-5, 72-74	234.72	28.21	22.01	2.05	1.93	2.86	2.56	1.60	1.50	44.07	41.37	0.79	0.71
25R-6, 68-70	236.18	28.71	22.31	2.04	1.96	2.86	2.66	1.59	1.52	44.51	42.66	0.80	0.74
26R-1, 20-22	237.80	29.01	22.49	2.06	2.00	2.92	2.77	1.60	1.55	45.24	43.91	0.83	0.78
26R-1, 108-110	238.68	28.92	22.43	2.01	1.98	2.79	2.72	1.56	1.54	44.02	43.42	0.79	0.77
26R-2, 20-22	239.30	26.76	21.11	2.05	2.04	2.80	2.78	1.62	1.61	42.25	42.08	0.73	0.73
26R-2, 108-110	240.18	28.41	22.13	2.07	1.98	2.90	2.70	1.61	1.55	44.61	42.85	0.81	0.75
26R-3, 20-22	240.80	29.75	22.93	2.03	1.98	2.88	2.73	1.57	1.52	45.51	44.21	0.84	0.79
26R-3, 108-110	241.68	78.00	43.82	2.03	1.41	8.55	2.00	1.14	0.79	86.68	60.40	6.51	1.53
26R-4, 20-22	242.30	27.20	21.38	2.05	2.02	2.81	2.75	1.61	1.59	42.67	42.22	0.74	0.73
26R-4, 108-110	243.18	28.19	21.99	2.04	2.00	2.82	2.73	1.59	1.56	43.66	42.85	0.77	0.75
26R-5, 20-22	243.80	26.02	20.65	2.06	2.05	2.79	2.77	1.63	1.63	41.49	41.26	0.71	0.70
26R-5, 108-110	244.68	25.14	20.09	2.05	2.04	2.74	2.71	1.64	1.63	40.19	39.89	0.67	0.66
26R-6, 24-26	245.34	13.38	11.80	2.11	2.31	2.46	2.77	1.86	2.03	24.33	26.54	0.32	0.36
26R-6, 108-110	246.18	25.77	20.49	2.14	2.04	2.97	2.74	1.70	1.62	42.74	40.83	0.75	0.69
27R-1, 24-26	247.44	25.51	20.32	2.08	2.06	2.83	2.77	1.66	1.64	41.29	40.79	0.70	0.69
27R-1, 98-100	248.18	27.94	21.84	2.02	2.01	2.77	2.74	1.58	1.57	43.07	42.76	0.76	0.75
27R-2, 24-26	248.94	28.58	22.23	2.05	2.01	2.88	2.77	1.60	1.56	44.56	43.55	0.80	0.77
27R-2, 55-57	249.25	33.26	24.96	2.00	1.96	2.94	2.81	1.50	1.47	48.81	47.68	0.95	0.91
27R-2, 98-100	249.68	26.94	21.22	2.09	2.04	2.90	2.79	1.65	1.61	43.27	42.27	0.76	0.73
27R-3, 24-26	250.44	28.96	22.46	2.85	1.99	5.87	2.74	2.21	1.55	62.39	43.66	1.66	0.77
27R-3, 98-100	251.18	27.58	21.62	2.03	2.01	2.78	2.73	1.59	1.57	42.77	42.37	0.75	0.74
27R-4, 24-26	251.94	28.97	22.46	2.05	1.97	2.89	2.69	1.59	1.53	44.94	43.17	0.82	0.76
27R-4, 98-100	252.68	27.37	21.49	2.07	2.02	2.86	2.75	1.62	1.58	43.33	42.31	0.76	0.73
27R-5, 24-26	253.44	25.92	20.59	2.06	2.01	2.80	2.67	1.64	1.60	41.45	40.34	0.71	0.68
27R-5, 100-102	254.20	23.31	18.90	2.09	2.05	2.77	2.68	1.70	1.66	38.62	37.84	0.63	0.61
28R-1, 24-26	257.14	27.16	21.36	2.06	2.01	2.83	2.73	1.62	1.58	42.88	41.94	0.75	0.72
28R-1, 98-100	257.88	21.51	17.70	2.10	2.12	2.70	2.76	1.72	1.75	36.18	36.65	0.57	0.58
28R-2, 24-26	258.64	23.11	18.77	2.14	2.06	2.86	2.69	1.74	1.67	39.18	37.73	0.64	0.61
28R-2, 98-100	259.38	23.94	19.32	2.08	2.04	2.76	2.68	1.68	1.65	39.16	38.46	0.64	0.62
28R-3, 24-26	260.14	27.23	21.40	2.03	1.99	2.77	2.67	1.60	1.56	42.40	41.50	0.74	0.71
28R-3, 98-100	260.88	30.53	23.39	2.00	1.96	2.82	2.71	1.53	1.50	45.65	44.67	0.84	0.81
28R-4, 27-29	261.67	28.97	22.46	2.02	1.97	2.81	2.68	1.57	1.53	44.29	43.13	0.80	0.76
28R-4, 98-100	262.38	27.93	21.83	2.07	1.96	2.88	2.62	1.62	1.53	44.02	41.69	0.79	0.71
29R-1, 23-25	266.73	33.43	25.05	1.94	1.90	2.76	2.67	1.45	1.43	47.34	46.50	0.90	0.87
29R-2, 23-25	267.25	29.45	22.75	2.04	1.97	2.87	2.70	1.57	1.52	45.17	43.68	0.82	0.78
29R-2, 98-100	268.00	28.56	22.22	2.01	1.97	2.78	2.68	1.57	1.53	43.65	42.72	0.77	0.75
29R-3, 23-25	268.75	37.17	27.10	2.18	1.88	3.75	2.71	1.59	1.37	57.61	49.58	1.36	0.98
29R-4, 23-25	270.25	51.71	34.08	2.35	1.73	7.09	2.69	1.55	1.14	78.14	57.61	3.58	1.36
29R-4, 98-100	271.00	30.85	23.58	2.02	1.97	2.89	2.74	1.55	1.50	46.53	45.24	0.87	0.83
32R-1, 25-27	295.75	23.97	19.33	2.07	2.06	2.74	2.72	1.66	1.66	39.04	38.91	0.64	0.64
32R-2, 25-27	296.25	25.33	20.21	2.09	2.02	2.83	2.69	1.67	1.62	41.19	39.92	0.70	0.66
32R-2, 99-101	296.99	25.38	20.25	2.09	2.05	2.84	2.75	1.67	1.63	41.30	40.49	0.70	0.68
32R-3, 27-29	297.77	25.92	20.59	2.10	2.04	2.88	2.74	1.66	1.62	42.10	40.96	0.73	0.69
32R-3, 99-101	298.49	24.78	19.86	2.11	2.05	2.87	2.72	1.69	1.64	40.93	39.64	0.69	0.66
32R-4, 27-29	299.27	23.45	19.00	2.10	2.06	2.79	2.70	1.70	1.67	38.94	38.20	0.64	0.62
32R-4, 97-99	299.97	23.06	18.74	2.14	2.04	2.86	2.64	1.74	1.66	39.13	37.29	0.64	0.59
32R-5, 28-30	300.78	84.90	45.92	2.11	1.36	20.54	1.88	1.14	0.74	94.45	60.89	17.01	1.56
32R-5, 93-95	301.43	24.48	19.66	2.13	2.08	2.89	2.77	1.71	1.67	40.87	39.82	0.69	0.66
32R-6, 27-29	302.23	25.60	20.38	2.11	2.05	2.90	2.76	1.68	1.63	42.03	40.76	0.72	0.69
32R-6, 98-100	302.94	22.48	18.36	2.11	2.09	2.76	2.72	1.72	1.70	37.72	37.34	0.61	0.60
32R-7, 30-32	303.76	23.58	19.08	2.10	2.04	2.79	2.66	1.70	1.65	39.11	38.00	0.64	0.61
32R-7, 96-98	304.42	23.76	19.20	2.10	2.06	2.79	2.72	1.70	1.67	39.32	38.65	0.65	0.63
33R-1, 40-42	305.50	26.41	20.89	2.09	2.02	2.88	2.72	1.65	1.60	42.60	41.18	0.74	0.70
33R-1, 110-112	306.20	23.76	19.20	2.14	2.08	2.88	2.75	1.73	1.68	40.01	38.93	0.67	0.64
33R-2, 25-27	306.85	21.16	17.46	2.16	2.12	2.82	2.74	1.78	1.75	36.77	36.14	0.58	0.57
33R-2, 110-112	307.70	23.48	19.01	2.11	2.03	2.80	2.64	1.71	1.65	39.08	37.70	0.64	0.61
33R-3, 25-27	308.35	32.03	24.26	2.20	1.95	3.47	2.74	1.66	1.48	52.02	46.12	1.08	0.86
33R-3, 110-112	309.20	26.49	20.94	2.06	2.02	2.80	2.71	1.63	1.59	42.00	41.17	0.72	0.70
33R-4, 25-27	309.85	26.88	21.19	2.07	2.02	2.85	2.73	1.63	1.59	42.78	41.73	0.75	0.72
34R-1, 22-24	315.02	40.45	28.80	1.94	1.81	3.05	2.61	1.38	1.29	54.61	50.72	1.20	1.03
34R-2, 22-24	316.52	43.06	30.10	2.03	1.76	3.52	2.54	1.42	1.23	59.68	51.59	1.48	1.07
34R-3, 58-60	318.38	30.59	23.42	2.01	1.94	2.84	2.67	1.54	1.49	45.89	44.34	0.85	0.80
34R-4, 59-61	319.89	18.08	15.31	2.09	2.31	2.57	2.99	1.77	1.96	31.18	34.53	0.45	0.53
34R-5, 60-62	321.40	25.41	20.26	2.07	2.07	2.80	2.79	1.65	1.65	40.94	40.87	0.69	0.69
34R-6, 60-62	322.90	24.55	19.71	2.12	2.07	2.87	2.77	1.70	1.66</				

Table 11 (continued).

Core, section, interval (cm)	Depth (mbsf)	WC-d (%)	WC-w (%)	WBD ^a (g/cm ³)	WBD ^b (g/cm ³)	GD ^a (g/cm ³)	GD ^b (g/cm ³)	DBD ^a (g/cm ³)	DBD ^b (g/cm ³)	Por ^a (%)	Por ^b (%)	VR ^a	VR ^b
36R-3, 115-117	338.25	28.49	22.17	2.04	1.99	2.85	2.71	1.59	1.54	44.16	42.94	0.79	0.75
36R-4, 116-118	339.76	26.83	21.15	2.10	2.04	2.92	2.78	1.66	1.61	43.33	42.10	0.76	0.73
36R-5, 63-65	340.73	13.19	11.65	2.09	2.52	2.42	3.12	1.85	2.22	23.77	28.62	0.31	0.40
37R-1, 70-72	344.50	27.22	21.39	2.06	2.02	2.84	2.74	1.62	1.59	42.96	42.12	0.75	0.73
37R-2, 66-68	345.96	26.71	21.08	2.09	1.99	2.88	2.67	1.65	1.57	42.92	41.01	0.75	0.70
37R-3, 66-68	347.46	27.20	21.38	2.06	2.01	2.85	2.72	1.62	1.58	43.08	41.93	0.76	0.72
37R-4, 66-68	348.96	27.47	21.55	2.09	2.02	2.92	2.76	1.64	1.59	43.90	42.55	0.78	0.74
37R-5, 65-67	350.45	28.01	21.88	2.08	2.02	2.93	2.78	1.63	1.58	44.46	43.18	0.80	0.76
37R-6, 64-66	351.94	23.32	18.91	2.11	2.08	2.81	2.74	1.71	1.69	38.99	38.36	0.64	0.62
37R-7, 40-42	353.20	24.49	19.67	2.10	2.04	2.82	2.69	1.69	1.64	40.27	39.10	0.67	0.64
38R-1, 66-68	354.06	27.43	21.53	2.06	2.02	2.86	2.75	1.62	1.58	43.33	42.41	0.76	0.74
38R-2, 67-69	355.57	25.21	20.14	2.13	2.05	2.93	2.73	1.70	1.63	41.90	40.18	0.72	0.67
38R-3, 68-70	357.08	21.36	17.60	2.19	2.12	2.89	2.76	1.80	1.75	37.56	36.47	0.60	0.57
38R-4, 68-70	358.58	22.61	18.44	2.16	2.08	2.88	2.71	1.76	1.70	38.88	37.41	0.64	0.60
38R-5, 68-70	360.08	22.70	18.50	2.15	2.10	2.86	2.76	1.75	1.71	38.78	37.96	0.63	0.61
38R-6, 68-70	361.58	22.97	18.68	2.15	2.10	2.86	2.76	1.74	1.71	39.09	38.22	0.64	0.62
39R-1, 115-117	364.05	22.47	18.35	2.16	2.10	2.87	2.76	1.76	1.72	38.60	37.66	0.63	0.60
39R-2, 115-117	365.55	22.39	18.30	2.16	2.11	2.88	2.76	1.77	1.72	38.60	37.65	0.63	0.60
39R-3, 116-118	367.06	21.83	17.92	2.13	2.07	2.78	2.66	1.74	1.70	37.16	36.15	0.59	0.57
39R-4, 116-118	368.56	16.86	14.43	2.17	2.27	2.68	2.86	1.86	1.94	30.61	31.97	0.44	0.47
40R-1, 113-115	373.53	27.41	21.51	2.07	2.04	2.88	2.81	1.63	1.60	43.50	42.88	0.77	0.75
40R-2, 113-115	375.03	28.70	22.30	2.07	2.03	2.94	2.82	1.61	1.58	45.11	44.13	0.82	0.79
40R-3, 114-116	376.54	30.06	23.11	2.02	1.96	2.85	2.69	1.55	1.50	45.51	44.08	0.84	0.79
40R-4, 123-125	378.13	30.14	23.16	2.05	1.99	2.92	2.78	1.57	1.53	46.24	44.94	0.86	0.82
40R-5, 114-116	379.54	26.50	20.95	2.13	2.06	2.99	2.81	1.69	1.63	43.63	42.10	0.77	0.73
40R-6, 112-114	381.02	26.90	21.19	2.09	2.03	2.89	2.76	1.64	1.60	43.14	42.03	0.76	0.72
41R-1, 119-121	383.09	25.99	20.63	2.10	2.05	2.88	2.78	1.67	1.63	42.24	41.32	0.73	0.70
41R-2, 106-108	384.46	27.23	21.40	2.09	2.01	2.92	2.71	1.64	1.58	43.70	41.87	0.78	0.72
41R-3, 117-119	386.07	27.29	21.44	2.06	2.03	2.85	2.76	1.62	1.59	43.15	42.37	0.76	0.74
41R-4, 119-121	387.59	27.47	21.55	2.06	2.01	2.85	2.73	1.62	1.58	43.32	42.22	0.76	0.73
41R-5, 119-121	389.09	22.49	18.36	2.17	2.10	2.90	2.74	1.77	1.71	38.90	37.56	0.64	0.60
41R-6, 119-121	390.59	21.28	17.55	2.14	2.11	2.78	2.72	1.76	1.74	36.61	36.13	0.58	0.57
42R-1, 98-100	392.48	22.91	18.64	2.10	2.05	2.76	2.65	1.71	1.67	38.17	37.24	0.62	0.59
42R-2, 98-100	393.98	23.87	19.27	2.07	2.05	2.74	2.69	1.67	1.65	38.97	38.54	0.64	0.63
42R-3, 98-100	395.48	22.02	18.04	2.15	2.11	2.84	2.75	1.76	1.73	37.88	37.10	0.61	0.59
42R-4, 98-100	396.98	23.14	18.79	2.10	2.05	2.77	2.67	1.70	1.67	38.47	37.61	0.63	0.60
42R-5, 98-100	398.48	23.15	18.80	2.10	2.07	2.77	2.71	1.70	1.68	38.50	38.01	0.63	0.61
42R-6, 98-100	399.98	22.52	18.38	2.10	2.05	2.75	2.64	1.72	1.67	37.70	36.71	0.61	0.58
43R-1, 98-100	402.18	23.96	19.33	2.12	2.06	2.84	2.73	1.71	1.67	39.92	38.93	0.66	0.64
43R-2, 98-100	403.68	21.02	17.37	2.15	2.11	2.80	2.71	1.78	1.74	36.47	35.72	0.57	0.56
43R-3, 98-100	405.18	20.47	16.99	2.20	2.14	2.88	2.75	1.83	1.77	36.54	35.44	0.58	0.55
43R-4, 98-100	406.68	20.73	17.17	2.14	2.10	2.76	2.67	1.77	1.74	35.81	35.11	0.56	0.54
43R-5, 110-112	408.30	24.26	19.52	2.11	2.07	2.83	2.75	1.69	1.67	40.10	39.46	0.67	0.65
43R-6, 98-100	409.68	22.39	18.29	2.13	2.09	2.81	2.72	1.74	1.71	37.99	37.30	0.61	0.59
44R-1, 98-100	411.78	22.30	18.24	2.13	2.07	2.80	2.69	1.74	1.70	37.85	36.91	0.61	0.59
44R-2, 98-100	413.28	21.87	17.94	2.15	2.11	2.83	2.75	1.76	1.73	37.62	36.94	0.60	0.59
44R-3, 98-100	414.78	21.45	17.66	2.20	2.10	2.92	2.71	1.81	1.73	37.95	36.18	0.61	0.57
44R-4, 98-100	416.28	21.98	18.02	2.12	2.08	2.76	2.69	1.73	1.71	37.18	36.60	0.59	0.58
44R-5, 98-100	417.78	22.67	18.48	2.13	2.07	2.81	2.70	1.73	1.69	38.36	37.39	0.62	0.60
44R-6, 98-100	419.28	20.95	17.32	2.15	2.08	2.78	2.66	1.77	1.72	36.26	35.20	0.57	0.54
45R-1, 80-82	421.30	23.60	19.09	2.12	2.05	2.84	2.69	1.72	1.66	39.54	38.22	0.65	0.62
45R-2, 80-82	422.80	25.60	20.38	2.12	2.04	2.91	2.73	1.69	1.62	42.10	40.58	0.73	0.68
45R-3, 80-82	424.30	21.67	17.81	2.14	2.09	2.81	2.69	1.76	1.71	37.24	36.23	0.59	0.57
45R-4, 80-82	425.80	19.81	16.54	2.17	2.12	2.78	2.69	1.81	1.77	34.98	34.22	0.54	0.52
45R-5, 80-82	427.30	20.77	17.20	2.18	2.12	2.84	2.73	1.80	1.76	36.55	35.64	0.58	0.55
45R-6, 80-82	428.80	23.24	18.85	2.19	2.08	2.97	2.73	1.78	1.69	40.26	38.25	0.67	0.62
46R-1, 79-81	430.89	22.40	18.30	2.12	2.07	2.78	2.68	1.73	1.69	37.82	36.95	0.61	0.59
46R-2, 79-81	432.39	25.04	20.03	2.11	2.06	2.88	2.77	1.69	1.65	41.26	40.34	0.70	0.68
46R-3, 79-81	433.89	24.95	19.97	2.11	2.04	2.86	2.71	1.69	1.63	41.02	39.78	0.70	0.66
46R-4, 79-81	435.39	25.16	20.10	2.13	2.05	2.93	2.75	1.70	1.64	41.80	40.28	0.72	0.67
46R-5, 64-66	436.74	24.11	19.42	2.13	2.05	2.87	2.71	1.71	1.65	40.29	38.91	0.67	0.64
47R-1, 73-75	440.43	23.97	19.33	2.13	2.07	2.87	2.74	1.72	1.67	40.14	39.05	0.67	0.64
47R-2, 67-69	441.87	23.49	19.02	2.09	2.04	2.77	2.65	1.69	1.65	38.84	37.82	0.63	0.61
47R-3, 51-53	443.21	20.45	16.98	2.21	2.15	2.89	2.77	1.83	1.78	36.56	35.59	0.58	0.55
47R-4, 66-68	444.86	21.32	17.57	2.16	2.09	2.84	2.69	1.78	1.72	37.10	35.87	0.59	0.56
47R-5, 66-68	446.36	23.08	18.75	2.12	2.08	2.82	2.73	1.72	1.69	38.82	38.06	0.63	0.61
47R-6, 66-68	447.86	22.29	18.23	2.14	2.07	2.82	2.69	1.75	1.70	38.03	36.88	0.61	0.58
47R-7, 20-22	448.90	25.83	20.53	2.08	2.02	2.84	2.69	1.66	1.60	41.71	40.43	0.72	0.68
48R-1, 128-130	450.68	22.81	18.58	2.16	2.10	2.88	2.76	1.76	1.71	39.07	38.08	0.64	0.61
48R-2, 128-130	452.18	20.74	17.18	2.22	2.14	2.93	2.76	1.84	1.77	37.25	35.85	0.59	0.56
48R-3, 128-130	453.68	22.74	18.52	2.13	2.08	2.81	2.71	1.73	1.69	38.44	37.58	0.62	0.60
48R-4, 128-130	455.18	22.57	18.41	2.17	2.11	2.89	2.77	1.77	1.72	38.90	37.88	0.64	0.61
48R-5, 128-130	456.68	22.24	18.19	2.15	2.09	2.85	2.71	1.76	1.71	38.23	37.07	0.62	0.59
48R-6, 70-72	457.60	21.34	17.59	2.16	2.09	2.83	2.69	1.78	1.72	37.06	35.91	0.59	0.56
49R-1, 61-63	459.61	21.64	17.79	2.15	2.10	2.82	2.72	1.77	1.73	37.30	36.47	0.59	0.57
49R-2, 61-63	461.11	30.84	23.57	2.00	1.97	2.82	2.76	1.52	1.51	45.89	45.38	0.85	0.83
49R-3, 61-63	462.61	28.20	22.00	2.06	1.98	2.88	2.69	1.61	1.54	44.19	42.49	0.79	0.74
49R-4, 61-63	464.11	23.07	18.74	2.15	2.08	2.88	2.72	1.75	1.69	39.34	37.96	0.65	0.61
49R-5, 61-63	465.61	24.05	19.38	2.13	2.05	2.89	2.69	1.72	1.65	40.37	38.71	0.68	0.63
49R-6, 61-63	467.11	23.52	19.04	2.15	2.09	2.89	2.76	1.74	1.69	39.87	38.78	0.66	0.63
49R-7, 19-21	468.19	21.55	17.73	2.17	2.11	2.85	2.74	1.78	1.74	37.48	36.57	0.60	0.58
50R-1, 67-69	469.37	21.25	17.52	2.17	2.10	2.84	2.70	1.79	1.73	37.06	35.88	0.59	0.56
50R-2, 67-69	470.87	22.05	18										

Table 11 (continued).

Core, section, interval (cm)	Depth (mbsf)	WC-d (%)	WC-w (%)	WBD ^a (g/cm ³)	WBD ^b (g/cm ³)	GD ^a (g/cm ³)	GD ^b (g/cm ³)	DBD ^a (g/cm ³)	DBD ^b (g/cm ³)	Por ^a (%)	Por ^b (%)	VR ^a	VR ^b
51R-4, 60-62	483.50	22.33	18.25	2.15	2.07	2.85	2.68	1.76	1.69	38.33	36.88	0.62	0.58
51R-5, 19-21	484.59	21.31	17.56	2.23	2.14	2.98	2.79	1.84	1.76	38.29	36.69	0.62	0.58
52R-1, 66-68	488.66	21.21	17.50	2.15	2.10	2.80	2.70	1.77	1.73	36.65	35.87	0.58	0.56
52R-2, 66-68	490.16	22.13	18.12	2.14	2.10	2.82	2.74	1.75	1.72	37.88	37.13	0.61	0.59
52R-3, 66-68	491.66	20.17	16.78	2.18	1.79	2.82	2.11	1.81	1.49	35.67	29.29	0.55	0.41
52R-4, 66-68	493.16	21.40	17.63	2.17	2.11	2.84	2.72	1.78	1.73	37.26	36.22	0.59	0.57
52R-5, 66-68	494.66	20.16	16.77	2.18	2.12	2.82	2.70	1.81	1.76	35.67	34.66	0.55	0.53
52R-6, 66-68	496.16	20.99	17.34	2.19	2.14	2.88	2.77	1.81	1.77	37.05	36.15	0.59	0.57
52R-7, 19-21	497.19	23.94	19.32	2.12	2.08	2.85	2.76	1.71	1.68	39.96	39.16	0.67	0.64
53R-1, 69-71	498.39	20.85	17.25	2.15	2.07	2.79	2.64	1.78	1.72	36.23	34.91	0.57	0.54
53R-2, 69-71	499.89	20.26	16.85	2.20	2.14	2.86	2.74	1.83	1.78	36.12	35.15	0.57	0.54
53R-3, 69-71	501.39	20.10	16.74	2.14	2.14	2.74	2.73	1.78	1.78	34.92	34.89	0.54	0.54
53R-4, 69-71	502.89	20.14	16.76	2.16	2.12	2.79	2.70	1.80	1.77	35.36	34.68	0.55	0.53
53R-5, 69-71	503.92	22.29	18.23	2.16	2.10	2.87	2.74	1.77	1.72	38.43	37.37	0.62	0.60

Notes: WC-w = wet water content (% wet sample weight); WC-d = dry water content (% dry sample weight); WBD = wet-bulk density; DBD = dry-bulk density; GD = grain density; Por = porosity; VR = void ratio.

^aValue calculated using Method B.

^bValue calculated using Method C.

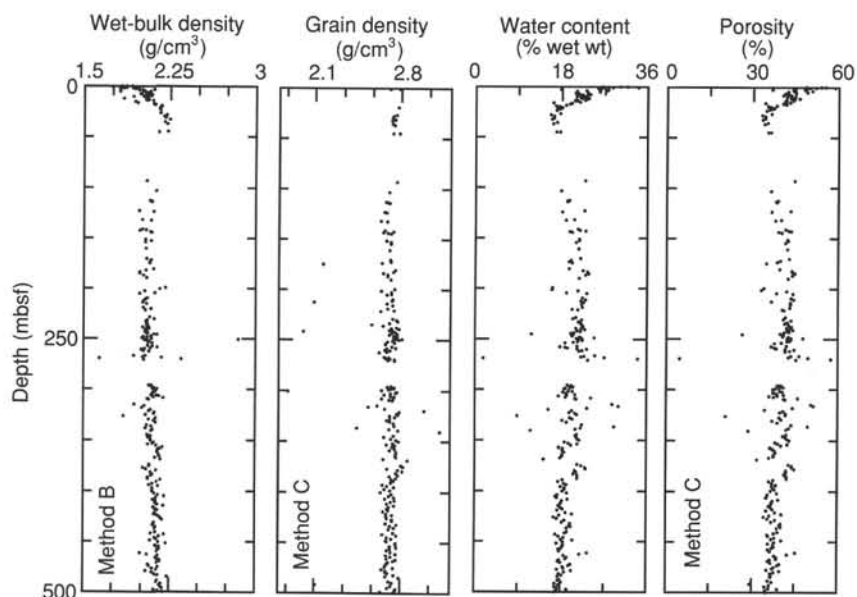


Figure 31. Wet-bulk density, grain density, wet water content, and porosity from Holes 910A, 910B, and 910C.

160.6 mbsf to 59.8% of the advanced length of pipe. GRAPE density, magnetic susceptibility, natural gamma activity, and compressional-wave velocity shipboard measurements were performed on whole-core sections using the multi-sensor track (Fig. 35).

The primary objective of the planned geotechnical study is to estimate the extent of glacial loading and erosion of overburden at this locality off the coast of northwestern Svalbard. These estimates can then be used to constrain and/or test different hypotheses relating to the potential advances and retreats of the Eurasian Ice Sheet in this area during the Quaternary. The objectives of the proposed post-cruise research are: (1) to determine the in-situ strength, pre-consolidation stress, and state of consolidation of the various glaciomarine sedimentary facies encountered in Hole 910D; (2) to determine experimental values of geotechnical and geoacoustic parameters for use in developing improved models of glaciomarine sediments, and thus improve our ability to interpret and utilize seismic and geophysical data collected from high latitude regions; and (3) to use the geoacoustic and geotechnical determinations in conjunction with other available data to infer the extent of glacial loading on the Yermak Plateau during the Quaternary.

DOWNHOLE MEASUREMENTS Logging Operations

Two Schlumberger tool strings were run at Hole 910C: the seismic stratigraphic and the quad combination. The wireline heave compensator (WHC) was used to counter mild ship heave (0.1–0.3 m of motion). The base of the drill pipe was set at 98.9 mbsf. A summary of the logging tool strings used during Leg 151 is presented in the “Explanatory Notes” chapter (this volume). A summary of the logging operations at Hole 910C is given in Table 13.

The seismic stratigraphic tool string comprising sonic (SDT), induction (DIT), and natural gamma-ray (NGT) tools, along with the Lamont-Doherty temperature tool (TLT), was run first. Total penetration in Hole 910C was 507.6 mbsf, but hole fill or possibly a bridge prevented the tool string from getting below 359 mbsf. Data were recorded at a logging speed of 1200 ft/hr from this depth to the mud line. Within the pipe, the sonic and induction data are invalid and the natural gamma-ray data are highly attenuated. In an attempt to log beneath the obstruction at 359 mbsf the conical sidewall entry sub (CSES) was attached to the drill string (see “Explanatory Notes”

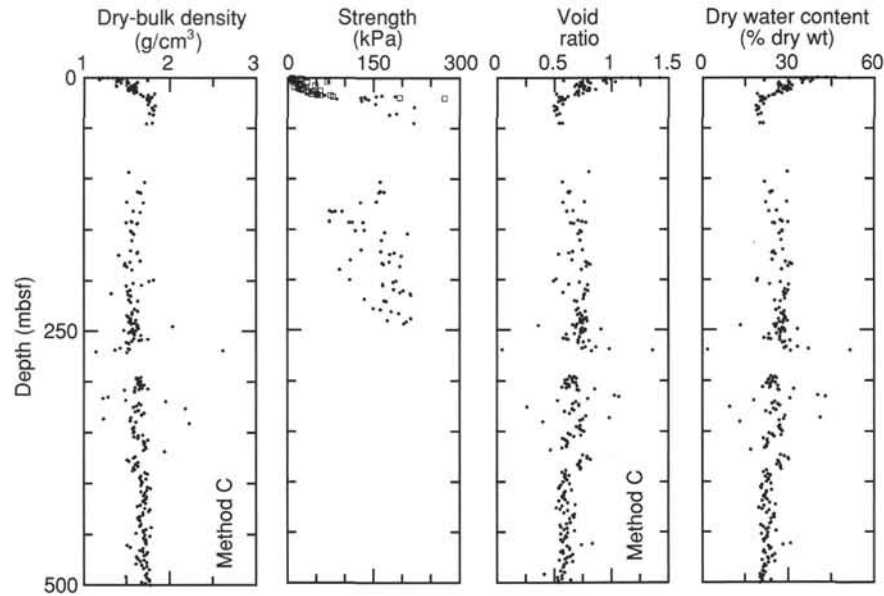


Figure 32. Dry-bulk density, strength (closed circles = penetrometer; open squares = vane shear), void ratio, and dry water content from Holes 910A, 910B, and 910C.

Table 12. Index properties of lithologic units, geotechnical units, and surficial sediments at Site 910.

Unit		WC-w (%)	WC-d (%)	WBD ^a (g/cm ³)	DBD ^b (g/cm ³)	GD ^b (g/cm ³)	Por ^a (%)	VR ^a
I (0–507.4 mbsf)	N(275)	20.37	25.76	2.09	1.62	2.72	41.24	0.71
	Min	11.65	13.19	1.74	1.17	2.09	23.77	0.31
	Max	33.91	51.30	2.25	2.22	3.12	59.92	1.50
	SE	0.18	0.30	0.01	0.01	0.01	0.29	0.01
IA (0–208.7 mbsf)	N(89)	21.28	27.32	2.05	1.59	2.71	42.21	0.75
	Min	15.69	18.62	1.74	1.17	2.10	30.86	0.45
	Max	33.91	51.30	2.25	1.83	2.99	59.92	1.50
	SE	0.39	0.66	0.01	0.02	0.01	0.56	0.02
IB (208.7–391.5 mbsf)	N(113)	20.90	26.56	2.08	1.61	2.72	42.33	0.75
	Min	11.65	13.19	1.94	1.23	2.09	23.77	0.31
	Max	30.10	43.06	2.20	2.22	3.12	59.68	1.48
	SE	0.25	0.40	0.01	0.01	0.01	0.46	0.02
IC (391.5–507.4 mbsf)	N(73)	18.43	22.62	2.14	1.69	2.70	38.39	0.63
	Min	16.54	19.81	2.00	1.49	2.11	34.92	0.54
	Max	23.57	30.84	2.23	1.78	2.79	45.89	0.85
	SE	0.15	0.22	0.01	0.01	0.01	0.24	0.01
G-I (0–19 mbsf)	N(39)	23.61	31.23	1.98	1.50	2.73	45.34	0.85
	Min	16.11	19.21	1.74	1.17	2.10	30.86	0.45
	Max	33.91	51.30	2.12	1.83	2.99	59.92	1.50
	SE	0.60	1.07	0.17	0.02	0.02	0.85	0.31
G-II (19–190 mbsf)	N(45)	19.49	24.31	2.10	1.65	2.70	39.83	0.67
	Min	15.69	18.62	1.98	1.40	2.16	33.92	0.51
	Max	23.78	31.19	2.25	1.83	2.78	46.11	0.86
	SE	0.36	0.56	0.01	0.02	0.01	0.54	0.02
G-III A (190–317 mbsf)	N(74)	21.21	27.05	2.07	1.59	2.70	42.74	0.76
	Min	11.80	13.38	1.94	1.23	2.09	24.33	0.32
	Max	30.10	43.06	2.21	2.03	2.81	59.68	1.48
	SE	0.30	0.49	0.01	0.01	0.01	0.55	0.02
G-III B (317–507 mbsf)	N(117)	19.09	23.68	2.12	1.68	2.72	39.48	0.66
	Min	11.65	13.19	2.00	1.23	2.11	23.77	0.31
	Max	29.22	41.29	2.23	2.22	3.12	59.64	1.48
	SE	0.20	0.31	0.00	0.01	0.01	0.35	0.01
Surface (0–1 mbsf)	N(6)	29.55	42.16	1.84	1.30	2.77	52.91	1.14
	Min	26.40	35.88	1.74	1.17	2.69	48.04	0.92
	Max	33.91	51.30	1.91	1.39	2.84	59.92	1.50
	SE	1.22	2.49	0.23	0.36	0.02	2.00	0.10
APC end (15–20 mbsf)	N(7)	18.62	22.95	2.08	1.72	2.80	37.78	0.61
	Min	16.11	19.21	1.94	1.58	2.73	30.86	0.45
	Max	21.74	27.78	2.17	1.83	2.99	41.25	0.70
	SE	0.76	1.16	0.04	0.03	0.03	1.43	0.04

Notes: WC-w = wet water content (% wet sample weight); WC-d = dry water content (% dry sample weight); WBD = wet-bulk density; DBD = dry-bulk density; GD = grain density; Por = porosity; VR = void ratio; SE = standard error. I to IC = lithologic subunits; G-I to G-III B = geotechnical units.

^aValue calculated using Method B.

^bValue calculated using Method C.

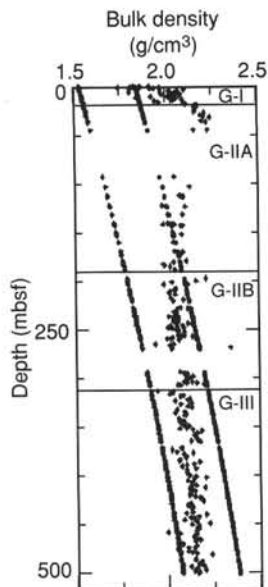


Figure 33. Geotechnical units and bulk density gradient for Site 910.

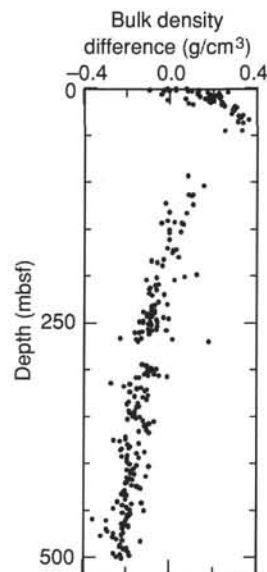


Figure 34. Difference between measured and predicted bulk density for Site 910.

chapter, this volume). The density tool (HLDT) was then rigged up with the sonic (SDT) and resistivity (DIT) tools along with an NGT to form the quad combination tool string. With the aid of the CSES, the quad combination was deployed to a depth of 446.6 mbsf. A main upgoing log was obtained from this depth to the end of pipe (now at 120 mbsf) and a repeat section from 218 to 120 mbsf was made both at a logging speed of 1000 ft/hr. The HLDT was run in high-resolution mode, recording data at 1.2 in. increments. A combination of the large borehole diameter and insufficient logging time precluded the deployment of the Formation MicroScanner and geochemical tool strings in this hole.

Log Quality

The logs from Hole 910C are shown in Figures 36 and 37. As Hole 910C is wide and rugose, shown by the hole caliper in Figure 37, many of the logs have suffered in quality. The white area in the

center of the figure shows the diameter of a gauge hole drilled with the rotary coring bit, and the shaded areas show how much wider the hole is than originally drilled. Flat sections in the log mark where the caliper on the HLDT density tool reached its maximum extension and where the eccentric tool could drift away from the borehole wall. These sections are also areas where the density data are of poor quality because borehole fluids partly occupied the measurement path. The resistivity data are similarly affected by the large borehole diameter but to a much less severe degree.

For the most part, the velocity data from the logs are of good quality. A modicum of cycle skipping and other noise is present in the raw log data, but shipboard processing of the traveltimes eliminated most of these excursions. The sonic velocity presented in Figure 37 is the processed data. It still contains two suspect intervals that could not be eliminated by the simple shipboard processing, ~340–360 mbsf (the location of the bridge that stopped the first logging pass) and ~390–420 mbsf. Rugosity in the hole resulted in poor sonic measurements

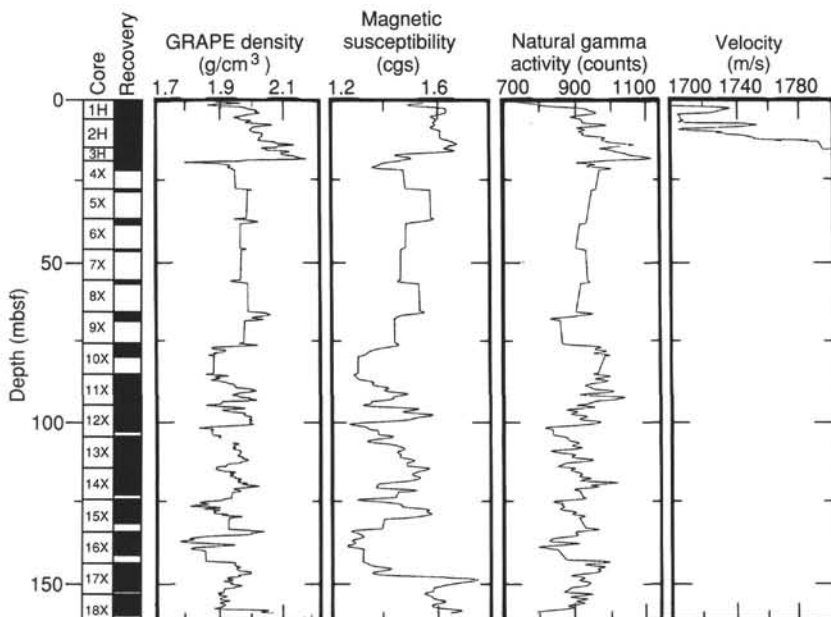


Figure 35. Multi-sensor track results for Hole 910D.

Table 13. Summary of logging operations at Hole 910A.

20 Aug. 1993 22:30	Last core on deck; prepare hole for logging. Drop RCB bit. Pipe set at 99 mbsf.
21 Aug. 1993 05:15	Rig up NGT-SDT-DIT (+TLT).
06:25	RIH with NGT-SDT-DIT (+TLT).
06:58	Start downgoing log from EOP to 358.6 mbsf, where tool unable to pass obstruction.
07:45	Start main upgoing log from 358 mbsf to mud line. POOH. Decision made to rig up conical sidewall entry sub (CSES) to attempt to log basal section of hole.
09:30	Rig up CSES.
13:30	Rig up NGT-SDT-HLDT-DIT.
14:15	Problem with HLDT sonde, tool swapped out.
16:00	RIH with NGT-SDT-HLDT-DIT.
17:20	Drill pipe run down to 435 mbsf. Tool pumped out of end of pipe.
18:32	Main upgoing log from 447 mbsf to 118 mbsf.
19:45	Repeat section to 118 mbsf. POOH.
21:20	Rig down NGT-SDT-HLDT-DIT.
21:50	Rig down CSES (2 hr). End of logging operations.

Notes: Times given in Universal Coordinated Time (UTC). Drillers TD (total depth) = 507.4 mbsf; WD (water depth) = 567.4 mbrf; EOP (end of pipe) = 99 mbsf; RIH = run in hole; POOH = pull out of hole. For further explanation, see "Explanatory Notes" chapter (this volume).

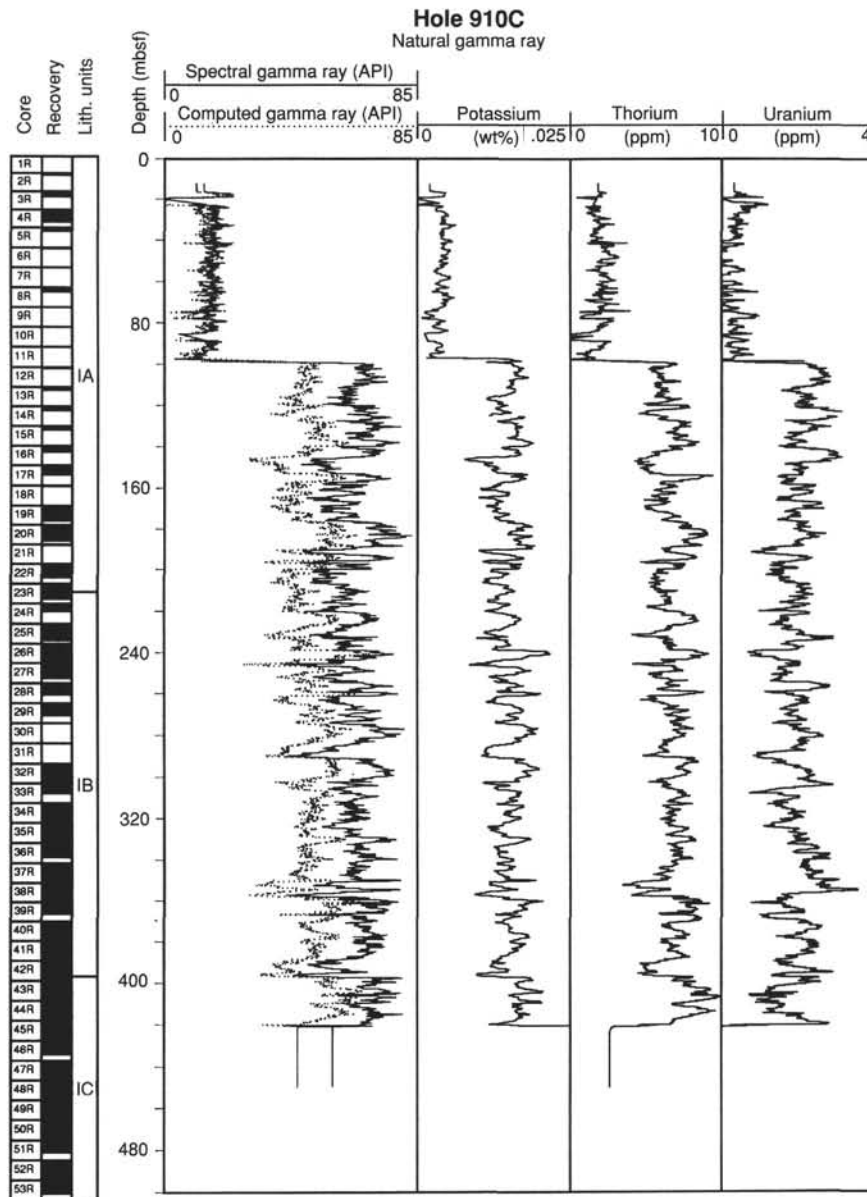


Figure 36. Data from the natural gamma-ray spectrometry tool (NGT) recorded on the seismic stratigraphy and quad combination tool strings. The two runs were spliced at 125 mbsf.

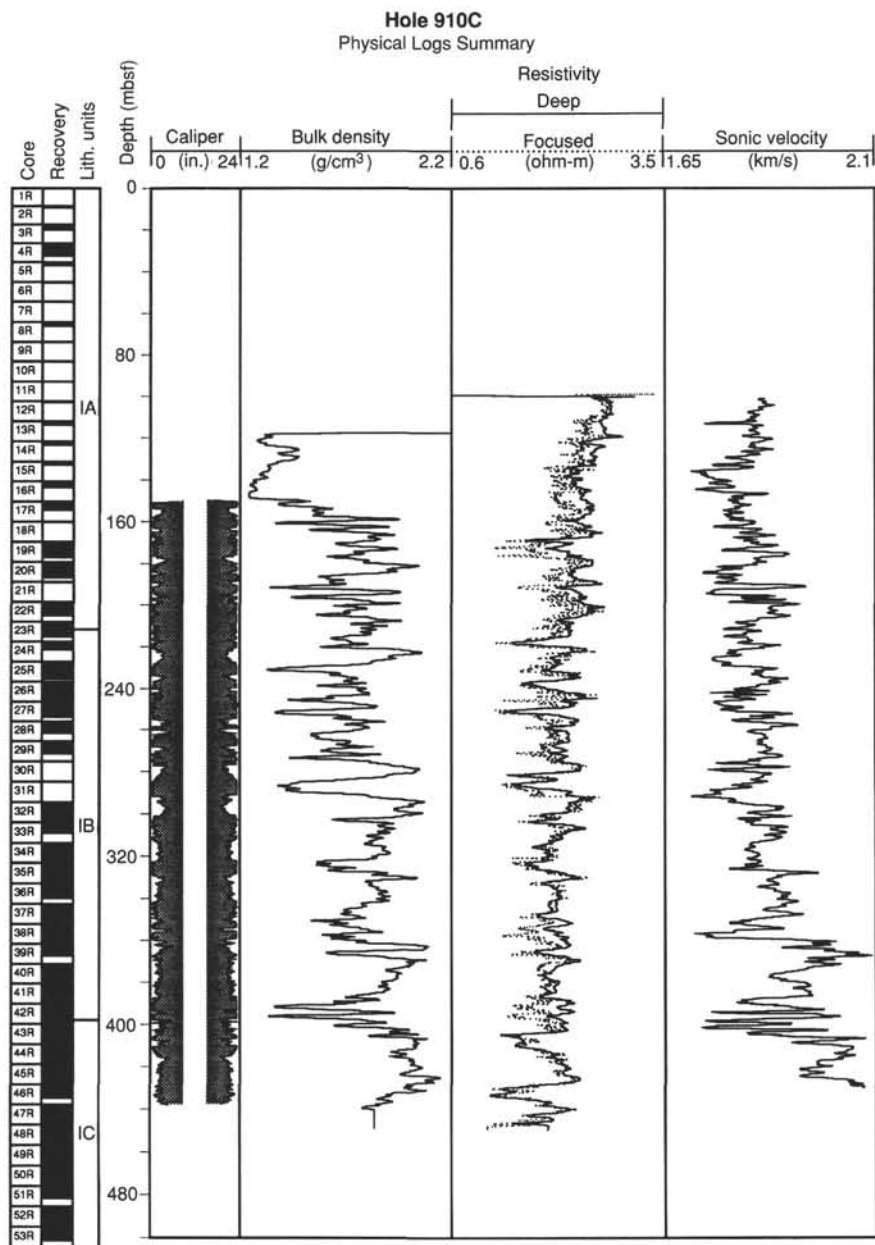


Figure 37. Caliper data from the high-temperature lithodensity tool (HLDT) shown with: bulk density data from the HLDT; deep phasor induction and spherically focused resistivity from the phasor dual induction tool (DIT); sonic velocity data from the long-spaced digital sonic tool (SDT). The central white area in the caliper log represents the RCB bit size (9 7/8 in.), and the shading represents the “washed out” portion of the hole from the bit size to actual measured diameter. The bulk density and velocity data have undergone a linear 7-point (1.07 m) moving average filter for presentation clarity.

at these intervals, and many of the rapid velocity shifts in these intervals are probably artifacts. Waveform analysis could eliminate these artifacts.

Hole width also affected the natural gamma-ray activity log by artificially raising the count rate where the hole is narrow and lowering it where it is wide. This type of artifact is most obvious in the interval 340–370 mbsf (Fig. 38). Standard shore-based processing will correct this artifact.

Results

Borehole Temperature

The TLT was deployed on only one tool string in Hole 910C, as we were concerned about catching the top of the temperature tool on the flapper valve in the side-entry sub assembly. Data were success-

fully recorded only on the seismic stratigraphic tool string, giving a mud line temperature of 1.26°C and a bottom-hole (359 mbsf) temperature of 11.16°C. An accurate thermal gradient cannot be obtained from this single measurement because cold seawater is circulated in the hole during drilling, thus cooling the adjacent formation; a minimum of three bottom-hole temperature measurements over a period of time are required to extrapolate the true bottom-hole temperature and hence calculate the true thermal gradient. Nevertheless, the temperature gradient must have been greater than 30°C/km.

Lithology

The interval logged in Hole 910C (~99–447 mbsf) covers lithostratigraphic Subunits IA through IC (see “Lithostratigraphy” section, this chapter). The Quaternary and Pliocene sequence that this

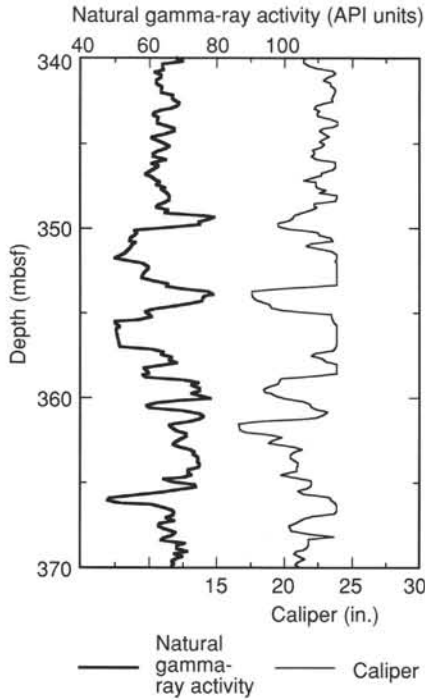


Figure 38. Comparison of the total gamma-ray (SGR) and the caliper logs over the interval 370–340 mbsf in Hole 910C. The negative correlation indicates the influence on the SGR measurement of the borehole diameter.

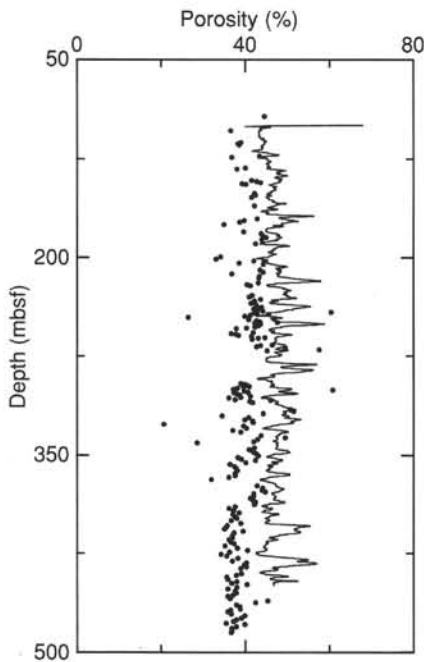


Figure 39. Porosity derived from the deep phasor induction of the dual induction tool compared with porosity measurements on discrete core samples from Hole 910C. The input resistivity data and the final porosity log are unsmoothed.

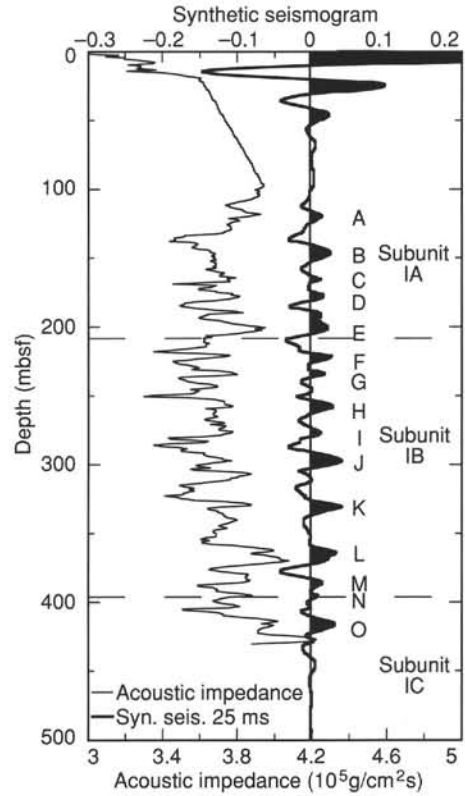


Figure 40. Acoustic impedance compared to the synthetic seismogram at Hole 910A. Also shown are the lithostratigraphic unit boundaries from the “Lithostratigraphy” section (this chapter). The seismogram has been converted from two-way traveltime into equivalent depth (mbsf).

represents is dominantly a dark gray silty clay. There are no major lithologic variations downhole, a feature reflected in the downhole natural gamma-ray activity log. It, too, has cyclicality but no major trends (Fig. 36).

A distinct drop in sonic velocities occurs in the interval from 360 to ~330 mbsf (Fig. 37). The deeper interval averages ~1950 m/s, whereas the sediments above average ~1800 m/s. This main velocity change, however, is separated from the lithostratigraphic Subunit IB/IC boundary (391.5 mbsf) by more than 35 m. We think that the velocity signal comes from diagenetic lithification of the sediment column and not from any primary sedimentary signature.

The lithostratigraphic Subunit IB/IC boundary is apparent as a more subtle increase in baseline velocity at ~400 mbsf. This boundary is more prominent in the density log, which shows a fairly distinct increase to bulk densities of 2.0 g/cm³ in Subunit IC. Subunit IC also is characterized by a more in-gauge borehole diameter than Subunit IB above.

Porosity Estimates from Resistivity

Porosity can be determined from the resistivity logs by using the Archie equation (Archie, 1942):

$$S_w^a = (a/f^m)(R_w/R_t) \tag{2}$$

where S_w is the water saturation, equal to 1 for these virtually hydrocarbon-free sediments, R_w is the resistivity of the formation water, f is the fractional porosity, R_f is the measured formation resistivity, and both a and m are constants depending on lithology and pore space geometry. In this case we calculated porosity using the deep phasor induction resistivity log (IDPH) from the dual induction tool with set values of $a = 1$ and $m = 2.4$. R_w is calculated based on its known relationships to temperature and salinity (Keller, 1982). Temperature was taken from the TLT, and interstitial salinities from core measurements (see "Inorganic Geochemistry" section, this chapter). At low temperatures such as encountered at this hole, R_w varies significantly downhole; therefore, a profile of R_w was calculated as a function of depth.

The calculated porosities have only a fair correlation with those determined from discrete core samples (Fig. 39). The discrepancy may be because of errors in both core and log data: The discrete core measurements undoubtedly were adversely affected by the considerable disturbance caused by sediment degassing.

SEISMIC STRATIGRAPHY

Introduction

A synthetic seismogram was generated from the velocity and density profiles at Site 910 to correlate reflectors in the seismic section to stratigraphic changes. The acoustic impedance profile (the product of density and velocity) and the profile of reflection coefficients (the rate of change of acoustic impedance) were determined both as a function of depth and of two-way acoustic traveltime. Convolution of the reflection coefficient profile with an assumed source acoustic wavelet resulted in a synthetic seismogram to compare with the measured seismic section.

The seismic section used for correlation is the line AWI-91130, collected by the Alfred Wegener Institute for Polar and Marine Research, Bremerhaven. Site 910 is located at shotpoint 100.

Acoustic Wavelet

We did not have a record of the acoustic wavelet from the AWI-91130 line and therefore created a wavelet based upon the strong doublet exhibited at the seafloor. The wavelet used has a 25-ms period with an e-folding attenuation of 14 ms.

Reflection Coefficients

Discrete measurements of density and compressional velocity on the recovered cores (see "Physical Properties" section, this chapter) were combined with logging data (see "Downhole Measurements" section, this chapter) to form a profile of reflection coefficients for Site 910. The logs provided detailed velocity data on the interval 99–430 mbsf. Discrete laboratory measurements added another data set from 0 to 23 mbsf; no valid measurements were collected between 23 and 99 mbsf, and the gap was filled by linear interpolation between the two data sets. The composite velocity profile can be used to convert between mbsf and two-way traveltime in the seismic section. A quicker but still accurate conversion can be made by the following 2nd-order equation:

$$Z = 0.846(\text{TWT}) + 0.000114(\text{TWT})^2, \quad (3)$$

where Z is mbsf, and TWT is two-way traveltime in milliseconds.

Density measurements from the logs were poor because of bad hole conditions (see "Downhole Measurements" section, this chapter) and were not used to create the density profile at Site 910. In-

stead, the deep phasor resistivity log (IDPH) was inverted to create a pseudo-density log. The inversion process consisted of creating a porosity profile by applying a simple Archie law (Archie, 1942) relationship:

$$\phi = \sqrt{R_w/R_f} \quad (4)$$

where ϕ is the porosity, and R_f and R_w are the resistivities measured by the logging tool and that of the pore water, respectively. Because the grain density was essentially constant at 2.7 g/cm³, an estimated wet-bulk density could be calculated from:

$$\rho_b = \rho_w(\phi) + \rho_g(1 - \phi), \quad (5)$$

where ρ is density and the subscripts b , w , and g refer to that of bulk, water, and grains, respectively. The estimated densities from the logs were combined with measured bulk density on cores from the upper 23 m of the site. As with the velocity measurements, there are no valid density measurements from either data set in the interval 23–99 mbsf (29–114 ms below the seafloor). For this reason, no reflectors in this interval will be discussed.

The resulting data were interpolated to a 1-m sample spacing and were used to generate an acoustic impedance profile for Site 910 (Fig. 40). Also shown on the figure are the lithostratigraphic units (see "Lithostratigraphy" section, this chapter) and the synthetic seismogram. The unit boundaries are marked by impedance contrasts that give rise to relatively strong seismic reflectors.

The Synthetic Seismogram

Figure 40 shows the synthetic seismogram resulting from the convolution of the seismic wavelet with the reflection coefficient profile, whereas Figure 41 compares the synthetic seismogram to the recorded seismic section through Site 910. The synthetic seismogram matches the recorded seismic profile well.

The strong increase in impedance near the seafloor due to the very rapid increases in density and velocity is not easily visible in the seismic record (Fig. 41). It occurs shallow enough to lie within the doublet reflector at the seafloor. Nevertheless, the second reflector in the doublet appears stronger than at other sites, perhaps because of its amplification by the shallow impedance contrast.

The first set of reflectors in the synthetic seismogram (A–E) appears to be faint and discontinuous in the seismic section. All, however, are in the seismic record. The base of reflector E marks the lithostratigraphic Subunit IA/IB boundary (208.7 mbsf). Below this boundary the reflectors become more continuous within the seismic section and are easily matched with the synthetic profile. Lithostratigraphic Subunit IB also is characterized by a series of reflectors becoming stronger and more separated toward its base (391.5 mbsf).

No strong seismic expression is present in either the seismic section or the synthetic seismogram for the lithostratigraphic Subunit IB/IC transition at 391 mbsf. It is equivalent to reflector N in the seismic section (Fig. 41). Just above this boundary is the relatively strong reflector L, but it is distinctly shallower in the section. Reflector L could possibly mark a diagenetic cementation horizon in the section (see "Downhole Measurements" section, this chapter).

The base of the data used to construct the synthetic seismogram occurs at 430 mbsf (479 ms two-way traveltime). The base of the hole (507 mbsf) should be at about 608 ms in the seismic section by extrapolating the seismic profile.

Interpretation of the Seismic Section

Figure 42 shows the interpreted seismic section based on the drilling at Site 910. Almost the complete AWI-91130 line is shown in the

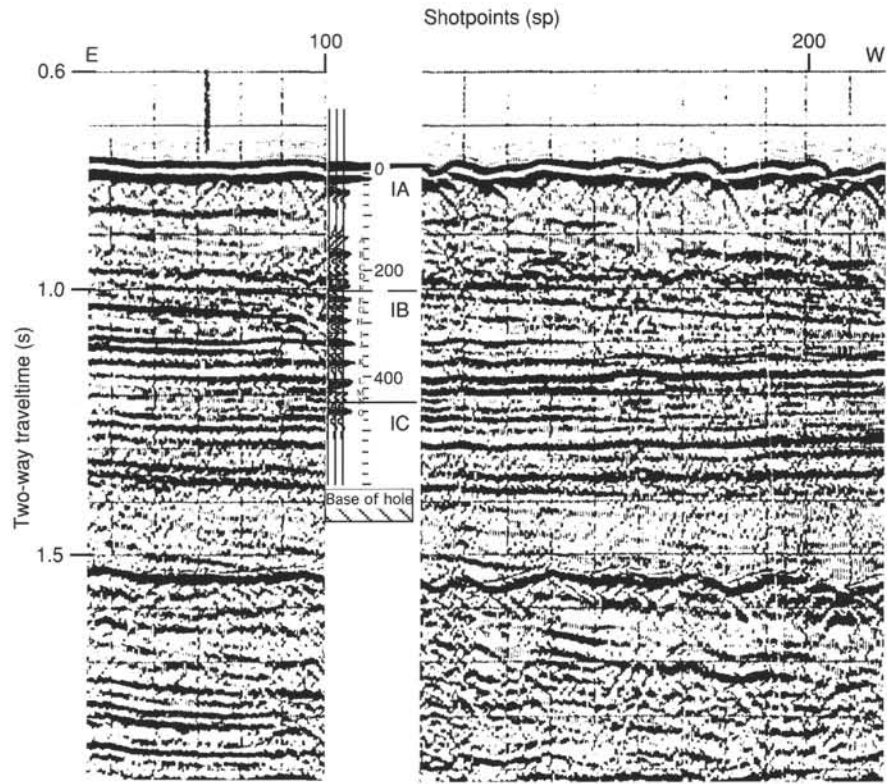


Figure 41. Comparison of synthetic seismogram from Site 910 to seismic line AWI-91130. The base of reflector E marks the lithostratigraphic Subunit IA/IB transition; reflector N marks the IB/IC transition.

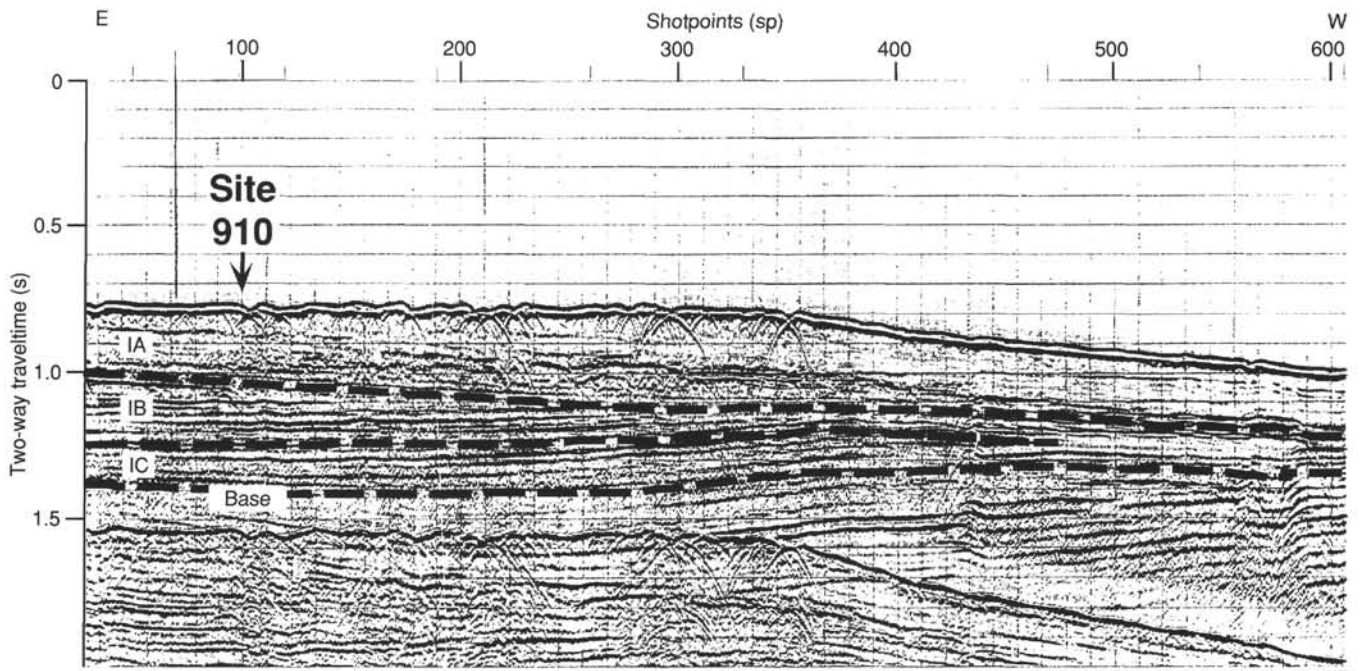


Figure 42. Interpretation of the seismic line AWI-91130 through Site 910. The lower Pliocene lithostratigraphic Subunits IB and IC pinch out to the West in this line, whereas the upper Pliocene/Pleistocene Subunit IA thickens to the shelf edge. "Base" marks the base of the drilled section.

figure, running roughly East-West to the edge of the Yermak Plateau. The older sediments pinch out toward the West and seem to be truncated by the later Subunit IA deposits. The Subunit IA/IB boundary thus marks an unconformity. Subunits IB and IC seem to conform-

ably overlie older sediment packets, and the eastward dip of their bedding is reflected in the bedding below.

Ms 151IR-108

NOTE: For all sites drilled, core-description forms (“barrel sheets”) and core photographs can be found in Section 6, beginning on page 465. Forms containing smear-slide data can be found in Section 7, beginning on page 849. Thin-section descriptions are given in Section 8, beginning on page 885, and sediment thin sections in Section 9, beginning on page 895. Dropstone descriptions are included in Section 10, beginning on page 903.

SHORE-BASED LOG PROCESSING

Hole 910C

Bottom felt: 567.4 mbrf (used for depth shift to seafloor)

Total penetration: 507.4 mbsf

Total core recovered: 293.49 m (57%)

Logging Runs

Logging string 1: DIT/SDT/NGT

Logging string 2: DIT/SDT/HLDT/NGT

Wireline heave compensator was used to counter ship heave resulting from the mild sea state conditions.

Drill Pipe/Bottom-hole Assembly/Casing

The following drill pipe depths are as they appear on the logs after differential depth shift (see **Depth shift** section) and depth shift to the seafloor. As such, there might be a discrepancy with the original depths given by the drillers on board. Possible reasons for depth discrepancies are ship heave, use of wireline heave compensator, and drill-string and/or wireline stretch.

DIT/SDT/NGT: Bottom of drill pipe at 97 mbsf.

DIT/SDT/HLDT/NGT: Bottom of drill pipe at 116 mbsf.

Processing

Depth shift: All logs have been interactively depth shifted with reference to NGT from DIT/SDT/NGT run, and to the seafloor

(-567.4 m). A list of the amount of differential depth shifts applied at this hole is available upon request.

Gamma-ray processing: NGT data were processed to correct for borehole size and type of drilling fluid.

Acoustic data processing: The sonic logs have been processed to eliminate some of the noise and cycle skipping experienced during recording.

Quality Control

Hole diameter was recorded by the 3-arm mechanical caliper, and by the hydraulic caliper on the HLDT tool (CALI). Only the latter, however, is a valid measurement at this hole.

Invalid gamma-ray readings were detected at 20, 86, and 97 mbsf (DIT/SDT/NGT string) and at 105 mbsf (DIT/SDT/HLDT/NGT string)

Note: Details of standard shore-based processing procedures are found in the "Explanatory Notes" chapter, this volume. For further information about the logs, please contact:

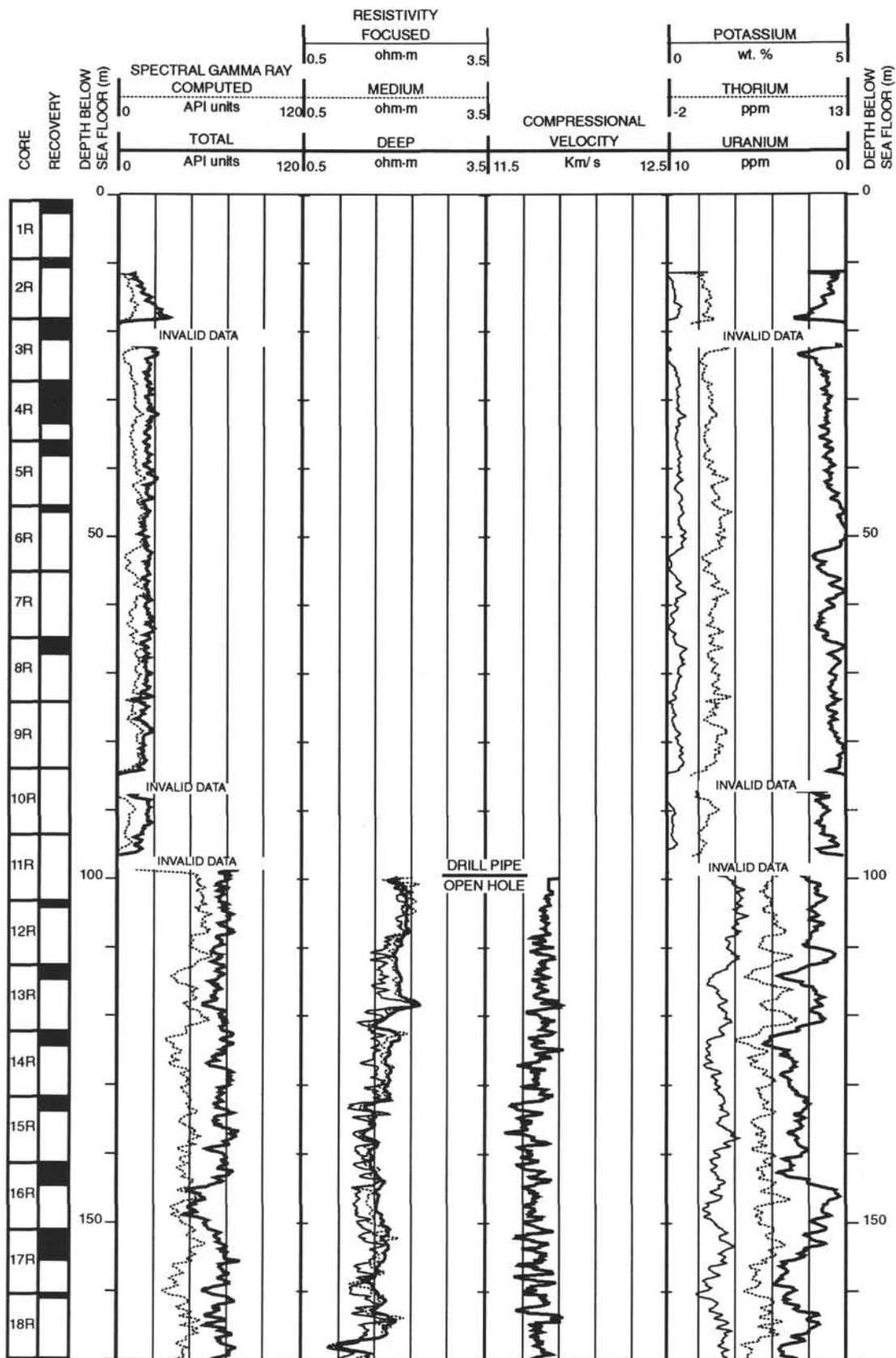
Cristina Broglia
Phone: 914-365-8343
Fax: 914-365-3182

E-mail: chris@ldeo.columbia.edu

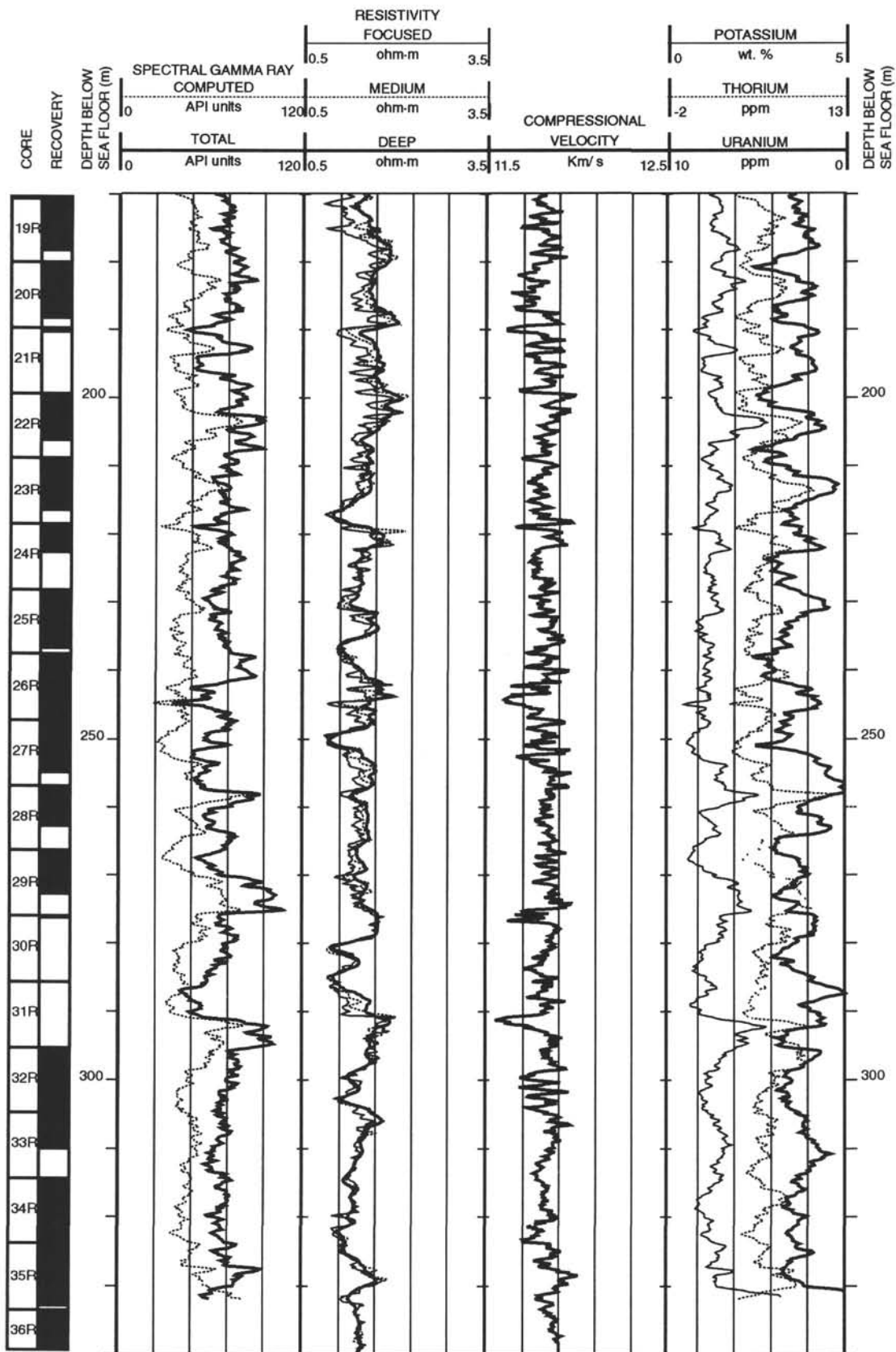
Elizabeth Pratson
Phone: 914-365-8313
Fax: 914-365-3182

E-mail: beth@ldeo.columbia.edu

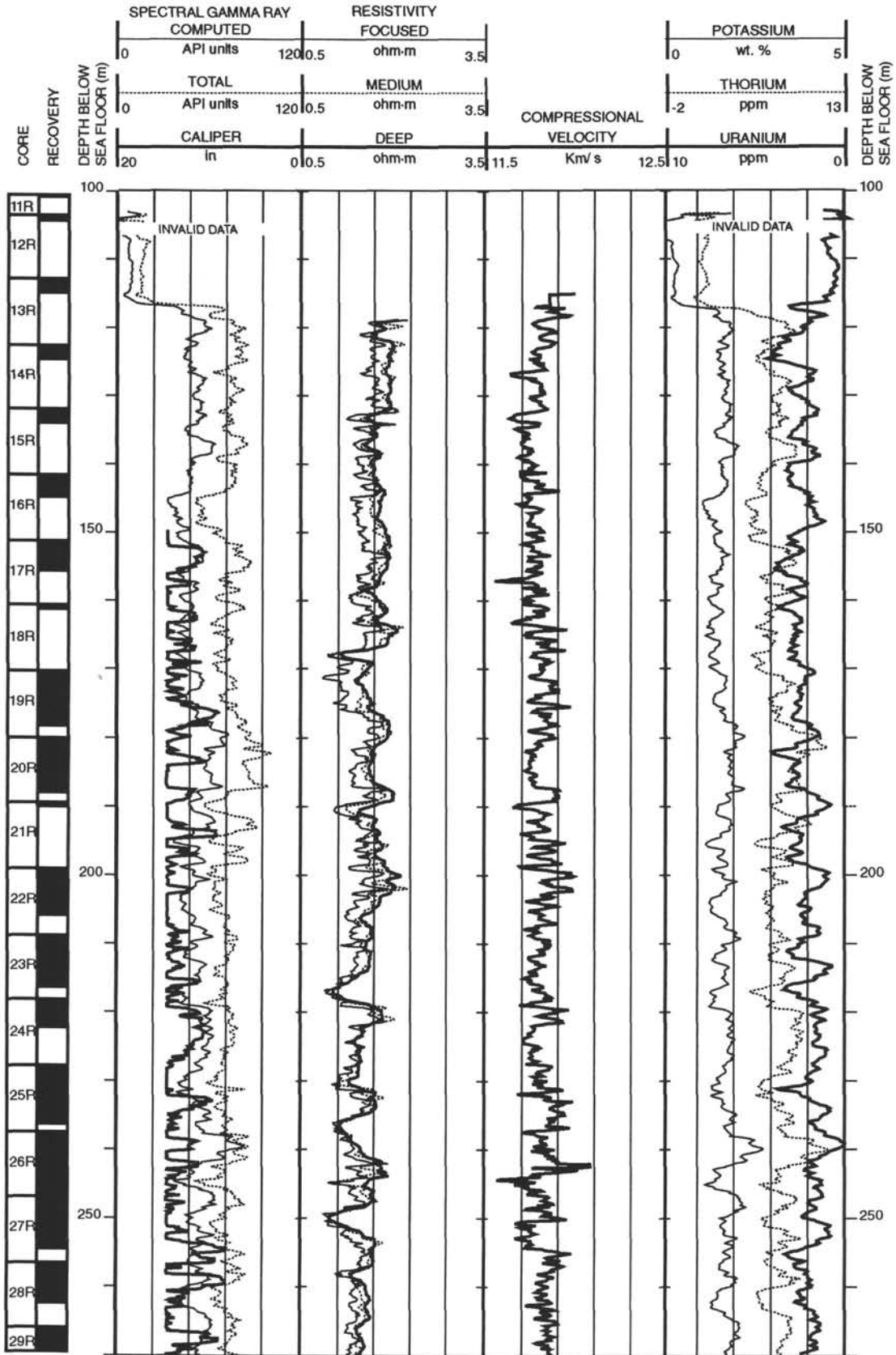
Hole 910C: Resistivity-Velocity-Natural Gamma Ray Log Summary (Pass 1)



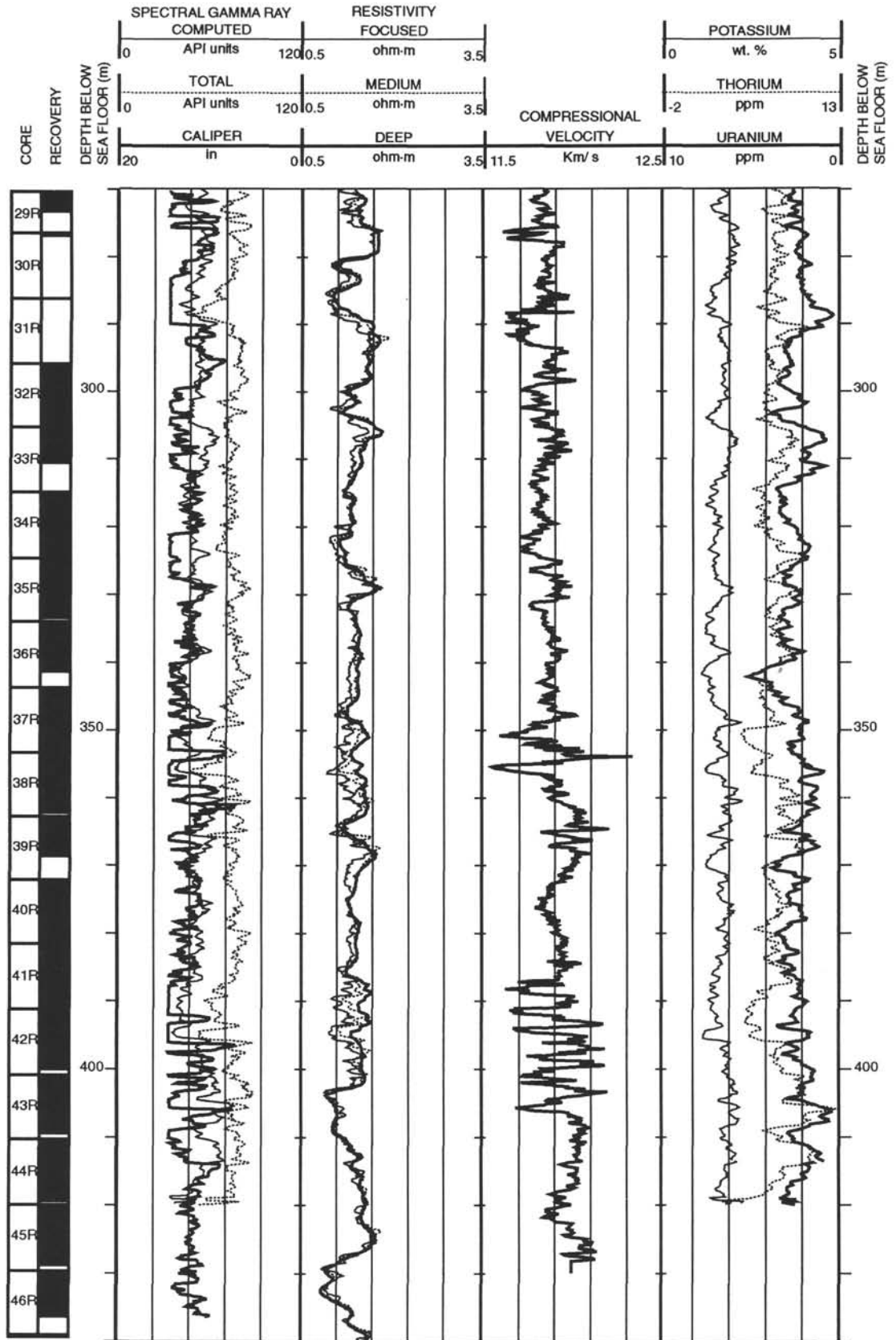
Hole 910C: Resistivity-Velocity-Natural Gamma Ray Log Summary (Pass 1)



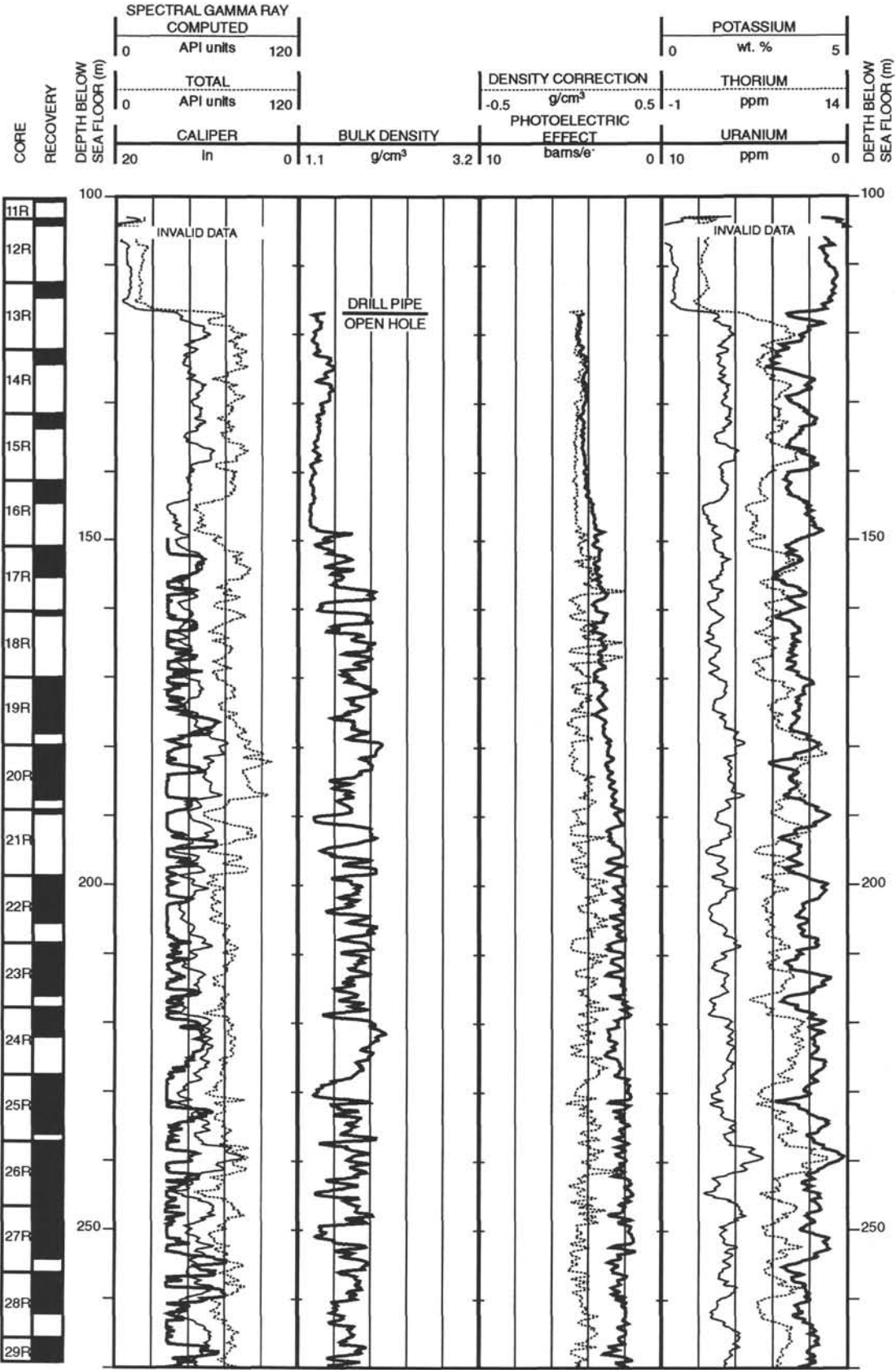
Hole 910C: Resistivity-Velocity-Natural Gamma Ray Log Summary (Pass 2)



Hole 910C: Resistivity-Velocity-Natural Gamma Ray Log Summary (Pass 2)



Hole 910C: Density-Natural Gamma Ray Log Summary



Hole 910C: Density-Natural Gamma Ray Log Summary

